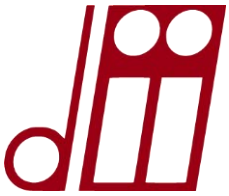

UNIVERSITA' DEGLI STUDI DI PADOVA

Dipartimento di Ingegneria Industriale DII

Corso di Laurea Magistrale in Ingegneria dell'Energia Elettrica

Impact Analysis of Photovoltaic Distributed Generation and Plug-in Electric Vehicles in a LV Distribution Network through the evaluation and application of the Non-Synthetic European LV Test System

Relatore

Prof. Roberto Turri

Correlatore

Dr. Keith Sunderland

Laureando

Marco Bertoncin

1205434

Anno Accademico 2020/2021

Alla mia famiglia, che mi ha sempre
sostenuto durante questo mio
lungo percorso di studi.

Index

Acronyms

3W3P	Three-Wire Three-Phase
4W3P	Four-Wire Three-Phase
AC	Alternated Current
BEV	Battery Electric Vehicle
DC	Direct Current
DG	Distributed Generation
DNR	Distribution Network Reconfiguration
DSO	Distribution System Operator
EPRI	Electric Power Research Institute
EV	Electric Vehicle
GHG	Greenhouse Gas
GIS	Geographic Information System
GOCT	GIS to OpenDSS Conversion Tool
HEV	Hybrid Electric Vehicle
HV	High Voltage
ICE	Internal Combustion Engine
IEC	International Electrotechnical Commission
IEEE	Institute of Electrical and Electronics Engineers
LSPV	Large-Scale Photovoltaic
LV	Low Voltage
LVN	Low Voltage Network
MV	Medium Voltage
NEV	Neutral-to-Earth Voltage
NZEB	Net Zero Energy Building
OLTC	On-Load Tap Changer
PES	Power & Energy Society
PEV	Plug-in Electric Vehicle
PF	Power Factor
PHEV	Plug-in Hybrid Electric Vehicle
PNNL	Pacific Northwest National Laboratory
PV	Photovoltaic
PVDG	Photovoltaic Distributed Generation
RE	Renewable Energy
RES	Renewable Energy Source
TFWG	Test Feeder Working Group
THD	Total Harmonic Distortion
TT	Terré-Terré
V2G	Vehicle-to-Grid

Index of Figures

Index of Tables

Abstract

The new energy paradigm, outlined in the low voltage (LV) distribution network by the implementation of renewable distributed generation (DG), is forcing a major change in the grid structure. Ever higher penetration of micro photovoltaic (PV) plants cannot easily counterbalance the strong increment in electricity demand caused by, among others, the shift toward plug-in electric vehicles (PEVs) of the transportation sector.

In this work, the reasons behind the necessity for accurate and reliable test systems for network analysis are faced, and the almost total absence of representative models for the European LV network is established. Then, the possibility to exploit non-synthetic electric and geographical data to build real networks is debated, and a thorough evaluation of the inspiring work made by Koirala *et al.* is done. In fact, the tool they developed is able to convert Distribution System Operators' data to obtain a functional test model solvable by OpenDSS network simulator. To prove the versatility of the tool – which allows also to modularly implement synthetic data and modify existing elements – an altered version of the Non-Synthetic European Low Voltage Test System is built. Distributed PV generation and PEV representative loads are implemented and simulated in a daily time series power flow analysis for different penetration levels.

The results obtained from the stress test comply with the assertions of prior studies, with some exceptions. A moderated PV implementation – up to around 40% of the base energy absorption – widely improves the grid conditions, even though it is not able to consistently affect the PEV contribution to the load due to mismatch. However, to accommodate a higher penetration of DG while preserving network standard limits, the implementation of coordinated control within the grid is mandatory. Finally, concerns regarding power and voltage rate of change (slope) during the day – as well as neutral-to-earth voltage behavior – in presence of high PV and PEV penetration are raised.

1 Introduction

In a society that is trying to move towards a greener economy, the electric energy vector is one of the main actors in such a revolution. Many fossil-based consumption is being converted or transduced so that it can be used by means of electricity. The transportation sector, which currently contributes to a quarter of the global Greenhouse Gas (GHG) emissions, is every year more penetrated by Plug-in Electric Vehicles (PEVs) [1, 2], which are recharged by plug to the grid. As a matter of fact, a sharp increase in the total electric energy consumption during the next years is expected. Simultaneously, many fossil-based power plants for the production of electricity are being substituted by Renewable Energy Source (RES) plant. The ever-growing implementation of these RES-based plant within the Distribution Network, especially photovoltaic and wind-turbine plants, is causing a deep transformation of the network itself. In fact, the traditional power supply model is no longer representative of the actual situation, and Distributed Generation (DG) is connected throughout the Low Voltage (LV) network such that it is reshaping the concept of electrical system as a whole [3, 4].

Benefits from Photovoltaic (PV) penetration, as DG within the LV Network, are widely proven among researchers [5–9]. Photovoltaic Distributed Generation (PVDG) can compensate the fast-increasing demand, providing incremental capacity and peak load relief, but it also improves voltage profile and reduces power transmission losses. As the PV penetration increases, drawbacks offset these benefits due to the intrinsic uncertainty and unprogrammable nature of PV technology. Because of the heavy mismatch with the load curve, PV plants inject unneeded active power into the grid, causing unwanted effects such as bidirectional power flow with consequent malfunctions in directional protection systems, overvoltage and overload of the lines, augmented transmission losses and power imbalances, as well as unintentional islanding [3, 7, 10–12]. With the actual global energy challenges, researchers are aiming to accommodate as much PV penetration as possible through the implementation of different penetration facilitation methods, which are often based on complex algorithms that require a highly receptive and automatized grid with fully integrated communications [13–15].

While PVDG implementation provides an increment in the network capacity, it is expected that PEV charging will increase the demand by reaching 5-8% of the entire energy consumption within the European LV Distribution Network by 2030, with an increasing trend [16]. PEV load consists of a strong current flow during a relatively long period of charge, that can cause line congestion during peak hours, which are simultaneous with other high energy absorbing human activities [2]. The main consequences of a high PEV penetration on the LV load are voltage drops and unbalance, voltage and frequency deviations, rise in power losses, degradation in power factor (PF) and line current power quality. The consequent electrical and thermal overload in substation transformers will directly affect stability and reliability of the power grid [1, 16–18]. Research [19] asserts that the stability of the network is particularly affected by fast-charge technologies connected to the LV network, which – if not regulated through centralized or decentralized algorithms – will be unbearable in the long run.

Therefore, the management of the electrical network – in the role of Distribution System Operators (DSOs) – is facing new emerging challenges, whose solutions accuracy are closely related to the reliability of the tools used for their study. Test feeders and systems accredited in literature are not as many as one might expect and are often been employed outside of their original scope of intended use [20]. Furthermore, critical issues have been brought to attention from researchers and major actors – including the Institute of Electrical and Electronics Engineers (IEEE) – regarding the reliability of such models in contexts of high Photovoltaic Distributed Generation (PVDG) penetration and unregulated PEV charging within the LV network [21].

Within the wave of new test models published in recent years, the *Non-Synthetic European Low Voltage Test System* published by Koirala *et al.* [22] – on which this work is focused – seems to satisfy (extremely well) the need for scalability, flexibility, and accuracy. The network model is an actual existing grid of a typical European town within northern Spain consisting of 10,289 buses. In the analyses, 8,087 load with time series hourly data are considered, whose data has been recorded by real smart meters over 20 days. The tool created by the researchers to generate this large-scale test system has the potential to represent any existing real network with low effort if the Geographic Information System (GIS) data from the DSOs is accessible. Within the tool process, GIS data are converted through

a MATLAB algorithm to be legible by the power flow simulation software OpenDSS. The simulation results are then exported once again to MATLAB, through which they can be elaborated and represented as needed.

This thesis examines the potential assessment of the GIS to OpenDSS Conversion Tool (GOCT) through its in-depth analysis and evaluation. To prove its flexibility and modularity, the model has been modified by implementing PEV loads representing slow and quick charges, and PVDG homogeneously distributed through the system. The new elements have been implemented through the insertion of a new MATLAB algorithm within the GOCT process, which creates synthetic PV and PEV curves homogenously distributed in the OpenDSS model. Further power flow simulations have been made at increased load absorption, and at different PEV and PVDG penetration levels to test the network in a heavily stressed condition.

In Chapter 2 the characteristic aspects of the European LV Distribution Network, which are of interest for this work, are presented. Following, a thorough bibliographic review of PVDG and PEV drivers, benefits, and issues – and also some of their mitigation methods – are debated. Then, in the same chapter the most accredited test systems of literature are described, pointing out the necessity for new simulation models. The *Non-Synthetic European Low Voltage Test System* and its conversion tool are accurately presented in Chapter 3. Results published on Koirala's paper are validated, and discrepancies are listed, whilst anomalies on the GOCT are corrected. Chapter 4 describes the implementation of PVDG and PEV loads within the test model at different penetration levels. PVDG is simulated from 0% to 100% penetration on the base energy absorption of the grid, whilst PEV load just at 0% and 15%. Then, results of the ten simulations are debated and subsequently, the flexibility of the tool is demonstrated. At last, Chapter 5 summarizes the conclusions reached and presents future works for the covered subjects.

2 A Review of Developments concerning LV European Distribution Networks and the Availability of Test Models

2.1 Network Characteristics

The LV Distribution Networks that supply residential and commercial buildings all over the world were once designed as one-way energy networks with branched structures. With the spread of Distributed Generation (DG) systems – usually wind turbines in MV and photovoltaics in LV – the Distribution Networks gradually and massively changed to an active bidirectional power grid [3, 4].

With the opportunities brought by Renewable Energy Sources (RES), many new drawbacks and challenges emerged, which were not considered when the network was first built. In other words, the cumulative power, as a consequence of the RES, can result in overloading and other potential power quality compliance issues as well as network protection concerns [23].

Historically, Distribution Networks were demand-driven, which means that production of energy was planned to suit the consumers' needs at every time. This was easily viable due to the programmable nature of the energy sources used such as oil, carbon, gas and in large part also hydroelectric. With the installation of widely distributed generation systems throughout the LV – and part of the MV – Distribution Network, it is expected that networks in the near future will have a more supply-driven structure, based on the availability of intermittent and non-programmable RESs with special concern for wind turbines and photovoltaics [22]. In fact, voltage and frequency stability of the demand-driven network is heavily at risk in areas where the high penetration of this kind of DG is forcing engineers to carefully plan how to act to comply with network terms and avoid instability.

These RESs can be installed with dimensions suitable for every kind of costumer and are economically affordable to private investors. Therefore – and in accordance with financial incentives provided by Governments to push towards a more 'green' economy – small power sources that spread very fast in the last decades will keep growing, allowing the birth of a new kind of user, the so called 'prosumer' [24].

The increment in absorbed energy that took place in the last years must also be highlighted, and this will increase further in the coming years. The choice for an economy based on green energy shifted many domestic and commercial users to an electric based consumption, usually renouncing their combustion heating and hob for electric alternatives. In this way, users improve their energy conversion efficiency factor, reducing the total amount of energy consumed, though increasing the total amount of electrical energy absorbed from the network. Still, one of the most influencing factors is the increasing request for Electrical Vehicles (EVs) with network plug-in charging systems. These energivorous vehicles need to be charged as fast as possible, even if connected to the LV distribution network, causing a very high energy demand. The absorption results especially strong during evening hours [2] – in which PV systems are not producing energy – and can cause overload into LV Distribution Networks already stressed.

Then, Distribution Networks will face a very strong increment in energy demand and a shift in load shape in the near future. This challenge can only be solved with new and innovative techniques that will evolve the distribution network to be more intelligent and controllable. Photovoltaic Distributed Generation (PVDG) will be essential, as well as new devices like smart meters, new generation inverters, LV/MV on-load tap changer (OLTC) transformers, which will play a main role on the smart-grid based Distribution Network.

Before deepening the study into models that are used as reliable sources to simulate distribution networks, it is important to define the cardinal characteristics of the LV European Distribution Network. In this section a brief view of these characteristics is presented, followed in the next sections by an accurate review of the influence that PVDG and EVs – as said, the two most significant changes on the LV distribution network – will have in the future power grid. In the last part of the Chapter, a review of the most important test models is made.

In this section, the main characteristics, features and limitations of the European LV Distribution Network are examined. An understanding in this regard is required to comprehend how RES and EVs

will influence the network. Furthermore, this will be of comparison later in this Chapter to understand which test systems can appropriately simulate their real counterpart and then could be reliable tools in planning future modifications and innovations.

The conventional power system, shown in *Figure 2-1*, is designed as a one-direction power system that supplies loads – most of them connected to the LV/MV Distribution Network – from huge central power stations connected to the HV Transmission Network. These power stations have outputs of more than 100 MW – the largest can reach outputs of a dozen of GW – and produce energy mainly from fossil-fuel, nuclear or hydric sources, supplying very wide areas.

***Figure 2-1**. Traditional power network.*

2.1.1 Frequency and Voltage

The European power frequency is set to 50 Hz and, as imposed in the European Standard EN 50160 [3], has allowed band limits of ±1% (49.5 - 50.5 Hz) for 99.5% of the week and -6%/+4% (47 - 52 Hz) for 100% of the week.

Nominal voltage in the European LV Distribution Network is set to 400 V rms phase-to-phase and 230 V rms phase-to-neutral (obtained dividing by $\sqrt{3}$ the phase-to-phase value), with an allowed band of ±10% for 95% of the week. This means that the voltage cannot drop below 360/207 V nor can increase above 440/253 V. However, depending on substation tap arrangements, simulations around these values are possible (416/240 V).

Another important requirement is the voltage Total Harmonic Distortion THD_V, defined as

$$THD_V = 100 * \frac{\sqrt{\sum_{h=2}^{N} \left(V_{h,rms}{}^2\right)}}{V_{1,rms}}, \quad N \to \infty .$$

In the equation, h is the harmonic number, $V_{h,rms}$ is the rms voltage value of the h-th harmonic and $V_{1,rms}$ is the rms voltage value of the first harmonic. As standard, THD_V must be kept under 8%.

At last, here is considered the supply voltage unbalance Ψ_V, which is the ratio between the zero-sequence component and the positive sequence component. It can be estimated as the maximum deviation from the average voltage divided by the average voltage itself.

$$\Psi_V = 100 * \frac{|V_{\max\_dev} - V_{avg}|}{V_{avg}}.$$

V_{avg} is the average voltage value of the line, which should be 400/230 in a LV European network, and $V_{\max\_dev}$ is the farther voltage value from the average reached during the time analysed. As for the European standard, voltage unbalance cannot exceed the value 2%.

2.1.2 Distribution approach

The European Distribution Network is characterized as consisting of few large three-phases MV/LV transformers that feed many residential and commercial consumers distributed in a wide area connected through long LV lines. The median number of LV consumers per MV/LV substation is around 90 in European Union, with a maximum of 278 [25]. Every LV branch is fully functional and is relatively long compared to the North American Distribution System, which is mainly constituted by MV lines and many smaller single-phase transformers that supply usually 1 to 10 consumers [20, 22]. In *Figure*

2-2 schematic representations of the two approaches are shown. On the left is represented the American system, on the right the European.

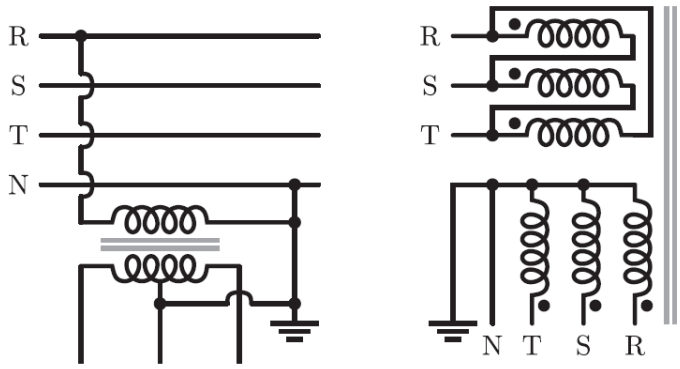

***Figure 2-2**. American (left) and European (right) distribution schemes [22].*

Furthermore, if secondary transformers of the European Network have ratings of between 100 kVA and 1'000 kVA, in North America a secondary transformer is between 10 kVA and 50 kVA, in agreement with the number of the supplied customers [20].

2.1.3 Neutral Conductor and Earthing

Neutral conductor is only present in the LV side of the Distribution Network and due to the structure explained above, it could be very long and have a visible voltage gap with ground potential.

The gap depends on the length and characteristics of the conductor but is especially affected by the earthing system chosen by every country. In Europe historically a terré-terré (TT) earthing system was employed for the LV Distribution Network. This means that the transformer neutral is grounded, as well as the frames of the electrical loads. More recently countries are employing the TN-C(S) earthing, which involves grounding of the transformer neutral and connecting the electrical loads frames to the neutral [26], as shown in *Figure 2-3*.

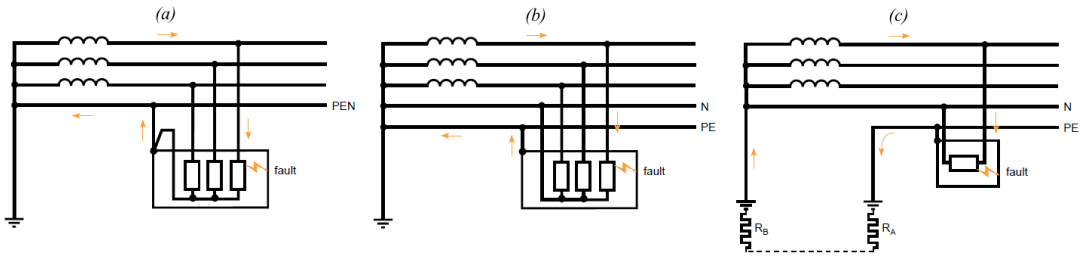

***Figure 2-3**. European earthing systems. (a) TN-C; (b) TN-S; (c) TT [9].*

Sometimes centre-tapping of transformers is implemented so that earth fault voltages are retained within (relatively) safe margins. This only applies for specialized installations such as construction sites.

2.1.4 Transformers and Loads

The LV Distribution Network loads can be divided into residential and commercial groupings. Both could be connected as a single-phase load between one phase and the neutral conductor, or as a three-phase load if the power absorption is high.

On average there are 40 to 60 loads per LV feeder in Europe, and these loads can be residential or commercial installations, 1-phase or 3-phases [22]. The difference between residential and commercial loads consists not only in the absorption but especially in their load characteristics. Commercial loads

often reach their peak during day, whereas residential load profiles achieve it after the sunset as shown in *Figure 2-4*, taken from [27].

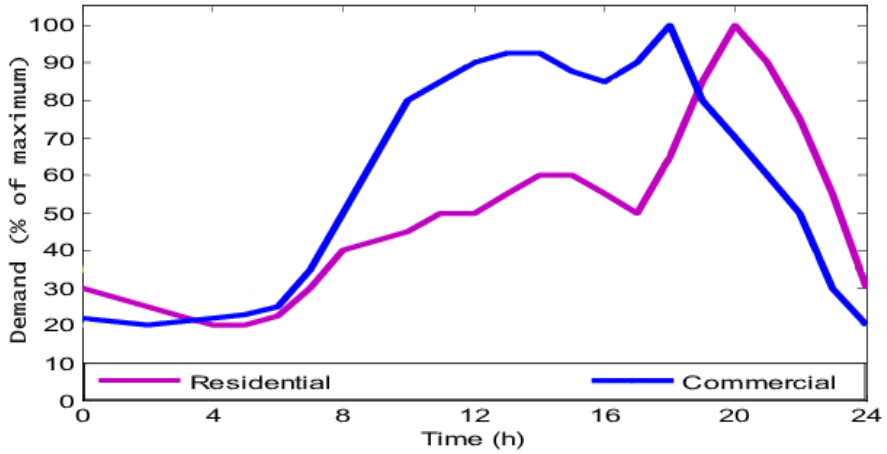

***Figure 2-4**. Qualitative comparation of residential and commercial typical daily load curves [27].*

This highlights how the commercial loads are more suited for a high PV penetrated distribution network rather than the residential customers, that have on average a match factor of just 40% (according to [5, 10]) if no shadowing effect is considered.

2.2 Distributed Energy Generation from Photovoltaics

In recent decades many new technologies emerged thanks to the global aim of reducing the greenhouse gases (GHG) and developing a sustainable economy not based on fossil-fuel products. These clean alternative technologies – like fuel cells, micro-turbines, biomass and solar cell systems – are efficient supply sources that can positively affect the Network. With the decrease in their manufacturing costs, these sources are exponentially spreading all around the globe, with the RESs leading the transformation. In *Figure 2-5* the global growth of wind-turbine and photovoltaic installed capacities is shown. At the end of 2018 the global installed capacity from PV electricity sources was around 500 GW, with Europe and China as leading regions [3, 28].

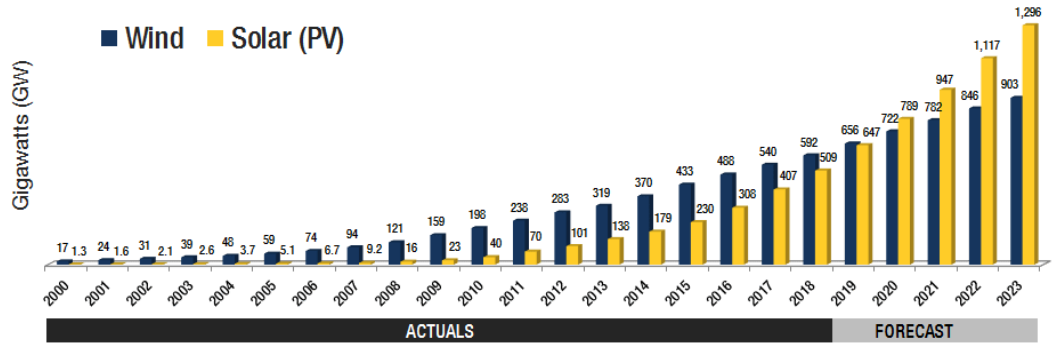

***Figure 2-5**. Global photovoltaic and wind turbine cumulative installed capacity during time [28].*

Large-Scale Photovoltaic (LSPV) and wind-turbine plants with installed capacity of 1 MW or more, have been installed widely across the World and they are known to have volatile and non-programmable characteristics. Previous studies [29–31] analysed how these new technologies are not very advantageous if designed as traditional large power stations connected to the HV Transmission Network. In fact, they can cause highly localized instability in the network voltage, as a consequence of shadowing (for PV parks) or absence of wind (for wind-turbine parks). In [31] the authors consider how the Photovoltaic Distributed Generation (PVDG) structure is economically and environmentally

more affordable if compared to a centralized grid-connected structure, bringing further attention to the DG strategy and taking distance from the large-scale plants. Therefore, the conventional network structure will face a major change with the insertion of DG into the MV/LV Distribution Network, as illustrated in *Figure 2-6*. This evolution, however, will bring important and necessary benefits to the Network. A balanced DG penetration will decrease transmission losses and overall voltage drops in load connection points, but the more the DG penetration – particularly single-phase connections – the more drawbacks will emerge, and the overall stability of the Network will decrease.

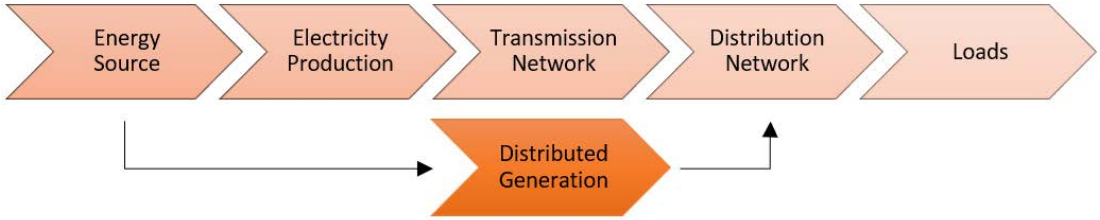

***Figure 2-6**. Power network with the integration of distributed generation.*

The sequent part of the section will focus on the benefits and drawbacks of the implementation of DG based on small-scale PV plants into the LV Distribution Network. Even though one might argue for the inclusion of small-scale wind-turbine plants as another example of DG, they are not taken into account because they are less widespread (especially into the LV network) due to their major investment cost and installation requirements. In fact, PV systems with few kW capacity are commonly installed from residential and commercial users for an investment cost around 1.000€ per kilowatt.

The possibility for private consumers to become micro producers – commonly called 'prosumers' – can facilitate the Network development into a bidirectional power-grid, with all the consequences and ramifications that this may involve and that will be faced below.

2.2.1 Drivers of PVDG

Before deepening the study on benefits and drawbacks of PVDG, it should be understood what drives the researcher's interest towards this technical development of the grid. In fact, PVDG has strongly environmental, economical and structural drivers.

Renewable Energy Distributed Generation (RE-DG) underwent a large environmental-driven boost due to the global fight against fossil-based energy production and limitation of GHG emissions, with the aim to shift gradually towards low carbon technologies. For the same amount of produced energy, GHG overall emissions produced by PV plants – considering production, transport, disposal and other auxiliary services – are about a quarter of oil-fired steam turbine plants and a half of gas-fired combined cycle plants [4]. The boost is also affected by Government incentives all over the world which aim towards a green and sustainable economy. This choice can also protect non-renewable and limited resources to extend their life through time. DG results in a very low environmental footprint – even when compared to large-scale renewable parks – avoiding also issues of land degradation and habitat loss [3, 32]. Additionally, unlike nuclear, solar energy has no security or military risk and unlike oil and gas, it is available almost everywhere.

From an economical perspective, it is observable that with the decrease in manufacturing costs of alternative and clean technologies, small-scale plants are becoming more and more competitive in the energy market. In the conventional power grid, total energy is supplied through HV transmission lines, which are very expensive and space-occupying components of the Network. With the fast increase in power demand, new transmission lines are being built, implying higher operational and maintenance costs, as well as higher distributed power losses that reduce the overall network efficiency. With its dislocation throughout the territory and its closeness to loads, DG technology strongly reduce transmission losses. As consequence, the Network will be relieved from infructuous Joule's losses – allowing lines to feed more loads before reaching full capacity – and the customers' electricity bills will also be positively affected as a result [32]. This can reduce the expansion of the Transmission Network, which is even more difficult with the perceptions concerning possible electromagnetic issues caused by

extended exposure to HV overhead lines. This has translated into preventive standards against unknown potential dangers. Direct consequence of this, as well as for space and environmental reasons, the development of the Transmission and Distribution Networks is focusing on underground lines that are even more expensive than overhead lines.

From a structural aspect, the implementation of DG widely connected to the Distribution Network could offset the increase in demand, improving reliability and power quality, making it easier for DSOs to control the system voltage. Additionally, a strong and automatized DG system could correctly supply important users (like hospitals) in any absence of power [32].

2.2.2 Benefits from Low PVDG Penetration

The constant load growth places a strong pressure on utility companies and the expansion of PVDG could compensate the fast-increasing demand, providing incremental capacity and peak load relief. In the power grid exists an intrinsic connection between system capacity and system reliability and DG can enhance reliability in different aspects [5].

With a carefully planned evaluation, PVDG can partially cover commercial daily demand, shaving the load curve peak during hours of heaviest conditions. It is widely proven [6–9] that a proper sized PVDG in the MV/LV Distribution Network, with a low penetration index, improves voltage profile due to the decrease in current flowing through transmission lines and strongly reduces power transmission losses due to injection of real power into the electrical grid close to loads.

PVDG is especially efficient in extensive rural areas, where there are few customers supplied by an extensive network and the power transmission losses are high and can therefore, be reduced significantly. DG, connected to proper storage systems, is the optimal technology to supply low populated regions, like African rural and desertic areas, avoiding huge investments in plants and networks [3, 9, 33].

2.2.3 Issues from High PVDG Penetration

The intrinsic characteristics of PVDG causes technical issues in a conventional Distribution Network with high PV penetration. The PV penetration index is the ratio of the total amount of energy from PV plants exported to the network and its total energy consumption. A network is considered high PV penetrated when it reaches an index of 30% or more, but depends on how PV penetration is calculated with time-varying loads [3]. A well-designed power system – incorporating PV technologies in the right locations – could accommodate an estimated 50% of PV penetration. This kind of system needs smart-grid technology as well as additional protection and voltage control systems [34].

PV generation is, in its nature, non-programmable and uncertain. A typical PV production curve during a sunny day is shown in *Figure 2-7* and can be compared to residential and commercial load curves of *Figure 2-4*. It is clear that there is a huge mismatch between load demand profiles and the PV generation curve. In [10] an example of urban residential area in southern Italy is shown, and the calculated mismatch factor is 57.6% during a sunny day without considering shadowing effects, proving once more the high mismatch situation in which a PVDG high penetrated power system is subjected to. The main consequence of mismatch is the injection of unneeded active power into the grid, generating a bidirectional power flow, as well as overvoltage and overload of the LV and MV distribution lines that do not have proper voltage control systems. This means augmented transmission losses into the grid, power imbalances and malfunctions in the selectivity of directional protections, that will need to be redesigned [11]. Additionally, under exceptional conditions, a high PV penetrated district could fall into unintentional islanding from the grid and become unstable [12].

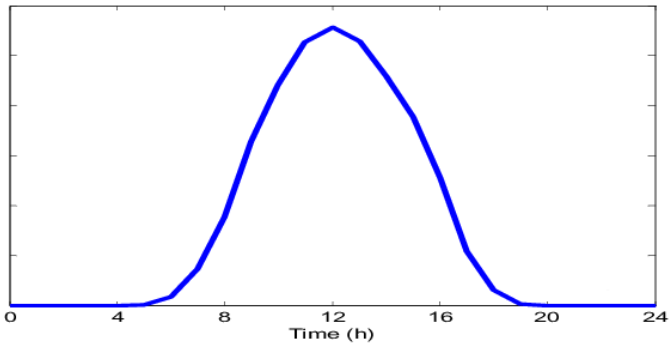

***Figure 2-7**. Qualitative PV generation daily curve during a sunny day [27].*

A PVDG structure is less influenced by local weather and partial shadowing during cloudy days. Through this, high generation spikes are often avoided, overcoming the LSPV high localization problem, but the uncertainty of PV generated energy caused by weather variability is still a detrimental factor. *Figure 2-8* shows the unstable energy production of a PV plant during a partly cloudy day. In fact, this significantly affects network stability and power quality due to frequency fluctuation and flickering problems.

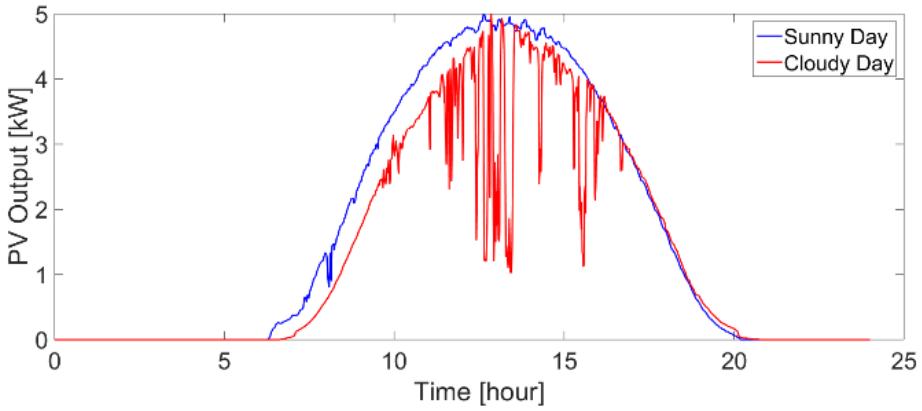

***Figure 2-8**. PV generation of a panel during a sunny day (blue) and a cloudy day (red) [35].*

Power quality is also affected by the utilization of inverters controlling PVDG technologies. In PV panels, energy is produced through DC output and is then converted into AC through power inverters which inject current into the grid with a sine-like shape output with a huge percentage of unwanted harmonics. Harmonics cause power quality degradation by affecting the THD, and can damage modern electronic components that are particularly susceptible to a degraded voltage profile [3, 11]. It should be considered that the quality of small residential inverters cannot be compared to the high efficiency of big plants inverters, and their overall effect on the network is still matter of research.

There are other issues connected to a PVDG structured network. The absence of inertia in PV electricity production – due to the lack of a rotating machine – makes a highly (PV) penetrated network unstable and unsustainable [3]. Furthermore, PVs produces only active power, which causes a unvaried request of reactive power from the HV plants and reduces the network power factor [7]. It should also be considered that a high number of distributed generators causes also an increase in short circuit power [11].

2.2.4 Mitigation Methods

Researchers and DSOs aim to find the best combination of innovative technologies and mitigation strategies to increase as much as possible the PV penetration index without compromising the Distribution Network due to the issues explained above. Many solutions have been studied, but their analysis is not of interest for the purpose of this work. Some of these mitigation methods are briefly

presented below. The solution should not be considered through just one technology, but a sequence of actions must be implemented – together with the new smart-grid technologies – to face this challenge. This includes:

- better weather forecasting tools, to accurately predict solar irradiation and so, when under-generation and over-generation could happen [3];
- Demand-Response economic strategy, to shift electricity demand during hours in which RE-DG supply is cheaper due to higher availability [36, 37];
- installation of smart meter devices at the load connection points that, matched with a good predictive algorithm, can anticipate load profile changes and act accordingly on the network [3];
- utilization of diversified energy supply sources, to increase reliability of the network and shift electricity production curve [32];
- installation of storage systems into the grid, to store excess energy for later use and reduce voltage fluctuations [3];
- installation of intelligent inverters, able to generate reactive power and synthetic inertia [31, 38];
- delocalized PV production, to minimize impact of generation variability due to local cloud cover [3];
- installation of OLTC transformers in MV/LV electrical cabins, to improve control on the LV voltage profile [23, 31];
- active participation of low power generation sources in the grid control [23].

All these strategies and technologies, if applied into a smart-grid implemented Distribution Network – that is a highly communicating and automatized power grid – can strongly reduce PVDG issues. Then, using more sophisticated algorithms, electricity production and consumption can be optimized, achieving a very high level of PV penetration. Many studies (e.g. [13, 14]) are being carried out investigating how to calculate the optimal PV penetration a network can withstand before exceeding the actual frequency and voltage limitations presented in section 2.1.1. Results are different for every power grid, based on its structure.

To accomplish this challenge and create more complex algorithms, the need for strongly accurate test systems is of main importance. As an example, the work of Ren *et al.* [15] combines local distributed control with remote centralized control to have an accurate voltage regulation in order to mitigate PVDG high penetration issues.

2.3 Plug-in Electric Vehicles into the Network

Emissions from the transportation sector currently contribute to a quarter of the global GHG emissions [2] and more than half of the oil extracted every year in the world is consumed in the sector [39]. Consequently, as one of the most influential sectors regarding emission and oil consumption, transportation needs to be addressed assertively to move towards a greener economy. This is mandatory to limit the global temperature increase to 2°C above the pre-industrial level by 2030, as arranged in the Paris Agreement against climate change of 2015.

Electric Vehicles (EVs) will be the main protagonists during the next decades and many industries are producing new car models based on this technology. Both researchers and industries are looking with much interest in road electric vehicles with Plug-in capabilities (PEVs), which allow owners the possibility to charge their vehicle by connecting it to the power grid through small stations or directly at home.

According to the Institute of Electrical and Electronics Engineers (IEEE) definition, PEVs are divided in two subcategories. Battery Electrical Vehicles (BEVs) are full-electrical traction vehicles, Hybrid Electric Vehicles (HEVs) instead combine a conventional Internal Combustion Engine (ICE) with an electric propulsion system. Both, to be categorized as PEVs, must have a battery storage system of at least 4 kWh, a means of recharging the battery from an external source and the ability to drive at least 10 miles in all electric mode [1].

This new technology can strongly lower GHG emissions and dependence from oil, as a function of the energy source mix from which electricity for the power grid is produced. It is supposed that vehicle oil consumption would be reduced by two-thirds with an all-electric driving range of 60 kilometers [40]. EVs have a much higher energy conversion efficiency when compared to traditional vehicles (61% of EVs against very low 12.6% of ICE vehicles), reducing the overall energy consumption [1]. EV technology also improves air quality and public health of citizens, decreases the fuel cost per kilometer, reduce dependence on foreign energy sources, offers flexibility in charging locations, and is unique in the possibility of applying Vehicle-to-Grid (V2G) technology, that could improve network stability and reliability [1, 39, 41].

2.3.1 Issues from High Penetration of PEVs

Plug-in Hybrid Electric Vehicles (PHEVs) reached by 2016 a high market penetration with 1.5 million vehicles sold, which became 3 million by the next year and it's presumed a market penetration of 50 million by 2030, with PHEVs to be 25% of the total new vehicles purchasing [1, 2]. With this penetration in the market, PEVs will have strong impact on the distribution grid because of their high electricity consumption, leading to high power demand by the consumers. As reviewed in [16], it is suggested that in Belgium, by 2030, the electricity consumption from PEVs will be up to 5% to 8% of the total demand, with an incremental trend.

This evolution will lead to several power grid problems, if not coordinated. There will be large power demand during peak hours, that will cause voltage drops and imbalance, voltage and frequency deviations and rise in power losses, making transformers and feeders work in heavy load or overload conditions and destabilizing the network [1, 16–18]. Furthermore, many harmonics will be injected into the grid during conversion from AC to DC by power electronics high frequency switching converters, which degrade line current power quality – increasing THD – and will cause electrical and thermal overload of the distribution transformers, affecting their life expectancy [17, 18]. Fast charging stations connected to the Distribution Network will also stress the utility due to their low input power factor, reducing even more the life of distribution transformers [17].

Cai *et al.* [19], highlight how the operating conditions of the distribution transformers directly affect stability and security of the power grid. They demonstrate how heavy load and overload operational conditions of transformers deeply impacts the power supply reliability, increasing transformer failures.

2.3.2 Approaches to Network Sustainability with PEVs

Researchers agree [16, 18, 42] that an uncontrolled high PEV penetration in the power network would cause the grid to work in maximum capacity condition (or even above), with unsustainable consequences, failure of PEVs charging, unreliability and instability of the network as well as frequent blackouts. Aware of this, many studies have been made both to understand the entity of this problem and to find mitigation methods and strategies to solve it. Here, a brief review of some of the most accredited tests and methods is made.

A commonly accepted way to shift the demand and flatten the load curve is through regulated charging, also called smart or coordinated charging. This means that a centralized or decentralized control system in the network would allow to shift and control the charging process of PEVs, taking advantage of off-peak periods and filling 'valleys' in the load curve. A proper control system would also mitigate fluctuations and imbalances in the network, as well as increase its power factor and hosting capacity [1, 2, 16]. In [18] a deep comparison between different PEVs penetration rates, charging technologies (slow or fast) and modality of charging (regulated or not) is made. Results showed how regulated charging improves just slightly the network performance, and that the fast-charge technology heavily influences the outcome. According to this study, there should be a combination of regulated and only slow-charge technologies to have an optimal mitigation method that can truly lighten the pressure on the LV network, even at high PEVs penetration rates. *Figure 2-9* shows the minimum voltage reached by the network during the simulation they made in different scenarios. In figure, scenarios S4, S5, S8, S9, S12 and S13 are the ones with PEV penetration equal or above 20%. It is observable that only scenarios S12 and S13 – which are the ones with regulated charging and without fast-charge technology – comply with the network standard parameters. To have this system working, the network should be strictly

communicating through a smart grid. Today, decentralized control options are more economically and technically achievable, but in the future a combination of centralized and decentralized control will be needed to sustain a high PEVs penetrated power grid and exploit its full capacity [39]. However, further studies should be made because impact varies depending on the characteristics of the LV network tested.

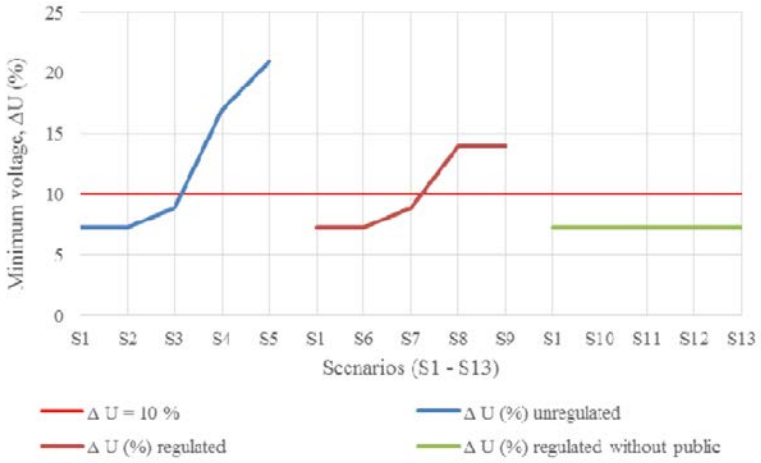

***Figure 2-9**. Minimum voltage in the network during peak load for various scenarios of [18].*

Location of fast-charge stations should be carefully planned, both geographically and within the network connections [18]. These stations have a high impact into the LV Distribution Network due to their high current demand. Then, they should be equally distributed in the territory and connected to independent feeders or transformer stations. Furthermore, authors from [43] suggest that a valuable option in the future is to build a DC power grid coexistent with the AC network. This DC network should be supplied by DC sources – mainly PV generation – and should supply DC loads only, such as LED illumination and EVs. This would solve all the harmonics problems brought from DC loads and generators and would have some other advantages, such as higher transmission efficiency, easier expansion of the grid and better access to RESs.

Another technology that is worth being introduced is the Vehicle-to-Grid (V2G). What make V2G technology unique is the possibility to have high penetration of many small storage systems distributed throughout the LV network. In a strongly communicating network – the smart-grid indeed – storage systems from PEVs can offer ancillary services to DSOs, providing frequency and voltage regulation. While attached to the Distribution Network, PEVs could be used to deliver active and reactive power, as well as filter current harmonics, enhancing system efficiency, stability and reliability [2, 41]. However, V2G would shorten life and storage capacity of the consumers' batteries through extensive charging and discharging cycles [41]. This issue could negatively influence consumers' interest in buying a plug-in electric car.

2.3.3 Compatibility with PV technology

As explained above, PV technology has a very high potential. Then, a high PV penetration could theoretically make up for the heavy burden brought from the increment of PEVs into the network.

The concept of Net Zero Energy Building (NZEB) can be summarized in a building with annual energy balance – between its own production and consumption – equal to zero [2]. Due to the volatile and non-programmable nature of PV technology – which has both seasonal and diurnal mismatch – the NZEB concept is not able to avoid occasional shortage of self-produced electricity, that needs to be supplied from an external power grid.

If the attention is focused on the compatibility between PV energy production and PEV charging demand, a net zero energy balance could be found, but there will be still a high mismatch between offer and demand [2]. In fact, PEVs owners would recharge their vehicles based on their daily mobility patterns and activity schedules. In *Figure 2-10 (a)* and *(b)* are shown respectively the daily electricity

load profile – sum of residential and commercial profiles – of a city and a typical PV daily power production profile averaged over a year. *Figure 2-10 (c)* illustrates a hypothetical PEV unregulated charging profile based on the model proposed in [44]. In this profile there are two demand peaks, one between 6.00 and 10.00 due to charging at workplaces, and the other between 16.00 and 20.00 due to home charging. Both peaks coincide with periods of high electricity demand. As explained in [2], this is caused by the fact that charging starts simultaneously with other human activities (charging upon arrival behavior).

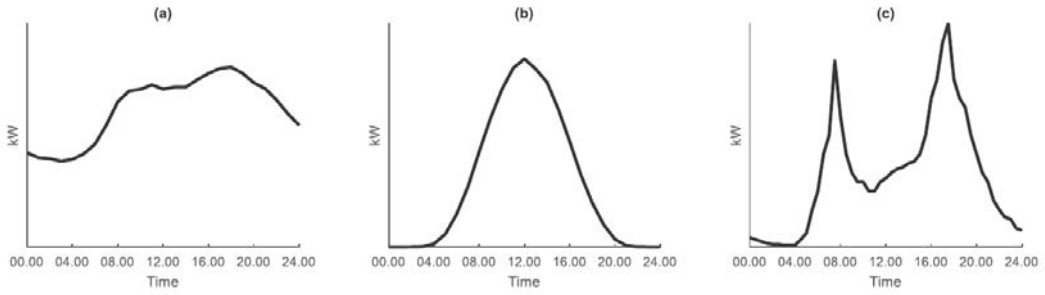

***Figure 2-10**. (a) Electricity load profile in Sweden on a day in January 2019. (b) Typical PV power production profile based on a daily average solar global horizontal irradiance curve for Stockholm. (c) Typical city scale EV charging load shape [2].*

When the PV generation qualitative curve is added to the baseload, the so-called 'duck-curve' appears. This curve is characterized by a large depression during midday hours and two high ramps during morning and evening due to the nature of PV energy production, as shows the red curve of *Figure 2-11*. Then, if the uncontrolled PEV charging curve is also added, the resulting shape would get worse, as shown in the green curve of *Figure 2-11*, with a higher evening ramp and a just small peak shaving.

This explains the importance of having a well-coordinated PEV charging system to reshape the load curve, especially if the aim is to take advantage of the energy intake from PV generation.

According to [45], the challenge for DSOs will be to have an effective management of the Distribution Network imbalance. The Optimal Distributed Generation Placement and Allocation (OPDGA) technique – based on the principles and considerations discussed in section 2.2 – should be implemented along with some Distribution Network Reconfiguration (DNR) techniques. DNR requires the implementation of complex optimization procedures capable of handling large combinatorial problems and power flow analysis, bringing out the necessity for larger and more accurate test models.

Future research should further study the impact of smart charging EVs, including PV and load, in different countries at different latitudes, with various climate and mobility behavior. Attention should be brought also in finding an optimal trade-off between simplicity and performance for practical implementation of smart charging schemes [2].

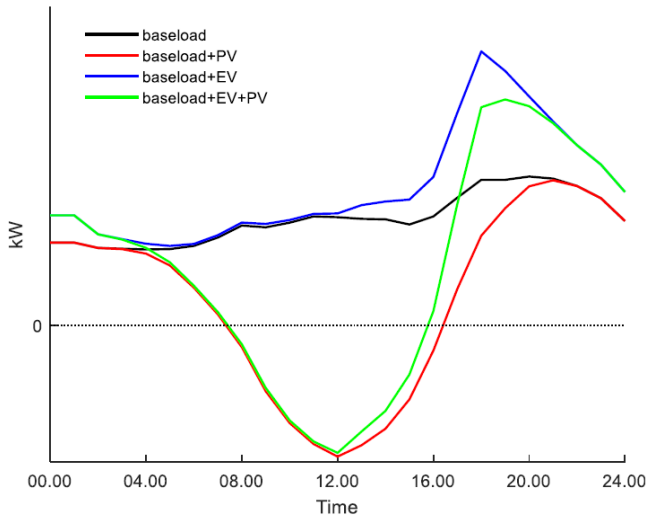

***Figure 2-11**. Typical load curves in several scenarios in residential distribution grids [2].*

2.4 Considerations about actual Test Feeders and Systems

As highlighted in [20], online test feeders and systems have been used for a wide range of researches due to their utility and accessibility and often for purposes outside of their original scope of intended use. Networks throughout the world are very different from each other and the utilization of an inappropriate test model could cause logic errors and misleading solutions. Consequently, the request to simulate more and more large-sized and diversified network situations lead the necessity to create models which simulate networks from different regions with accuracy and precision. Still, the number of openly available models is low, and furthermore, many models are of interest for very specific computational problems or geographic areas, making them not suitable for many researches.

Most accredited test feeders and systems of literature will be presented in this section, and their characteristics will be described. At the end of this section the necessity for new test systems representing the European Distribution Network, in which this work is focusing, will be evident. The main characteristics of the European LV Distribution Network shown in section 2.1 will be used as starting point to evaluate the reliability of the test systems and further deficiencies will be brought to attention.

2.4.1 The Original Test Feeders

Between 1991 and 1992 the IEEE Power & Energy Society's (PES') Test Feeder Working Group (TFWG) published the original set of four test models [46]. These radial test feeders, which provided researchers with models that included unbalanced loads and non-transposed distribution systems, were published for free use and for the purposes of testing new power flow solution methods. Plenty of new computational power flow solvers were being proposed in those years and they needed to be tested with proper models to evaluate their reliability and precision. A fifth test model was added later to test power flow simulations on different transformer primary-secondary connections. So, the original test feeders represented the type of unbalanced radial systems that are common in North America, but they were not designed to represent the size or complexity of full-size distribution feeders.

Every model was constructed to highlight a specific analytic challenge [20]:

- the *13-Node Test Feeder* was provided to test convergence of a program in a very unbalanced system;
- the *34-Node Test Feeder* is a very long feeder, which aimed to test voltage regulators in the power flow simulation software that was being tested;
- the *37-Node Test Feeder* is a three-wire delta ungrounded underground system;

- the *123-Node Test Feeder* is a medium size system with multiple voltage regulators and shunt capacitors;
- at last, the *4-Node Test Feeder* was provided to test the capability of solvers to represent all common three-phase transformer connections.

More than fifteen years went by before the need for new test feeders arose. In 2009 IEEE PES published an article [21] in which the requirement for new test feeders was motivated in seven different areas. The subject areas that were identified as high priority for the development of test cases included Neutral-to-Earth Voltage (NEV) studies, DG effects into the network, large distribution system models, comprehensive and asymmetrical contingencies test systems.

Multiple test models make use of the Kron's reduction in Carson's Equation to reduce the four-wire three-phase (4W3P) model of the European style distribution system to a three-wire three-phase (3W3P) equivalent system. This reduction assumes that the neutral and the ground are coincident, and their voltage difference is zero. This could give the exact result in case of MV or HV lines, or in networks with short and multiple grounded LV lines. Though, European LV Distribution Networks have long lines and neutral earthing at the cabin transformer with highly unbalanced load (see section 2.1) and consequently, it is expected that NEV is always greater than 0 V, with values that cannot be ignored. Because of this, a more realistic four-wire model is necessary.

In 2008 the first *NEV Test Case* [47] was already developed to study the 'stray voltage' phenomena between the ground and the neutral, as explained above. This is a 12.47 kV medium size radial system with both overhead and underground cables. It uses a 4x4 primitive impedance matrix instead of the previous 3x3 impedance matrix, allowing a neutral-to-ground impedance and a NEV higher than zero. Subsequently, LV asymmetric distribution models with isolated earthing should not make use of Kron's reduction to avoid dangerous approximations.

2.4.2 Test Models Over the Years

After the roadmap was presented, from 2010 a number of new IEEE test feeders were developed and published to address the new necessities. The *Comprehensive Distribution Test Feeder* [48] is a complex 42-bus feeder developed to test the ability to model a wide range of distribution system elements, with special attention to transformers and step-voltage regulators. The *8500-Node Test Feeder* [49] represents an unbalanced radial system with a large number of line segments. This second model was specifically developed to simulate an urban full-size distribution system and address the fact that this configuration was therefore not adequately represented.

In 2014 the *IEEE 342-Node Low Voltage Networked Test System* [50] – also called Low Voltage Network (LVN) Test System – was published, representing a small portion of an urban area. In contrast to the previous models, this system includes multiple 13.2 kV feeders supplying a 120/480 V high meshed LV network. This is the first model to consider a small meshed system rather than a single radial feeder, offering new computational challenges and a better (but still small) view of the network. In addition, this is the first IEEE test feeder to consider also unbalanced networked components.

During the same years, some models were developed by researchers of the Pacific Northwest National Laboratory (PNNL) and Electric Power Research Institute (EPRI). The *PNNL Taxonomy Feeder* study [51] proposed a set of 24 representative radial distribution feeder models based upon statistical analysis of 575 distribution feeders. EPRI's researchers, as part of the Green Circuit Project Database, proposed 6 different real feeders sanitized for public use and openly available online [52, 53]. The peculiarity of EPRI models – called *J1*, *K1*, *M1*, *ckt5*, *ckt7* and *ckt24* – is the non-synthetic origin of the feeders modelled, which make them extremely valid for studies made on those areas. PNNL models, due to their statistical build, are also very reliable if applied to a proper network.

In fact, all these test models are based on the North American network configuration and – as previously mentioned – are not representative of the European power grid and other countries as well. In 2015 the TFWG released the *IEEE European Low Voltage Test Feeder* (available online at [54]) which was the first model based on the European network and that will be discussed below. This test feeder is quite close to modelling the real European grid. Still, networks in Europe are diversified from each other and

every country has its own preferences about grid structure as well as different urbanization and population density.

Due to the dissimilarity of networks, few independent works have been made to represent specific regions, such as [55] for Western Australia, [56] for Northwest of England and [57] for Midwest U.S. Furthermore, in 2017 a group of researchers proposed a methodology to build reliable test network models and as an example developed multiple European representative test systems and feeders [58].

Recently (in February 2020), two new IEEE test systems were published for the purpose of voltage stability studies [59]. The *Nordic Test System* is based on an older test system called Nordic32 test system and is a fictitious system with similarities with the Swedish and Nordic network. The *Reliability and Voltage Stability (RVS) Test System* is based on the 1979 IEEE Reliability Test System. Both are made with the intention to be appropriate models for every kind of voltage stability studies rather than to be an exact representation of a real system.

2.4.3 European Test Models

In disagreement with the multitude of different networks that exists, very few models that represent European networks have been developed. Here, their strengths and weaknesses will be explained.

The European model proposed by IEEE, apart from having base frequency of 50 Hz and LV voltage of 416 V, has still some modelling approximations that make it a non-representative source and an unreliable model for the purpose of testing new algorithms. The model is based on a typical United Kingdom network and provided with very accurate one-minute load profiles for time-series simulations. On the other hand, the 4W3P model is reduced, through the Kron's reduction, to a 3W3P equivalent system, causing the inaccuracies explained in section 2.4.1. Furthermore, the model simulates an individual feeder connected to a 0.8 MVA transformer and to the feeders are attached 55 single-phase loads. The impact of multiple feeders in the same transformer has not been considered. According to the characteristics of the European network described in sections 2.1.2 and 2.1.4, transformer nominal power and number of loads are suitable, but having only single-phase loads and just one feeder connected to the transformer is quite unrealistic. In fact, typical loading values of distribution transformers are around 70%, but in the model it is loaded only at 10% of its capacity [22].

The independent Northwest England study [56] proposed 11 new representative feeders to consider the different type of network and load structures of North England. They are obtained through clustering algorithms applied to a set of 232 residential LV feeders, making them statistically accurate. Still, they are based once more on the England distribution network and works as individual feeders, rather than as the combination of them.

In the independent article [58], solid examples of European representative test systems and feeders are developed. The study is based on real data provided from 79 European DSOs, with which 9 representative networks are made. Three of them are large-scale models that include from HV to LV lines and represent urban, semi-urban and rural areas. The other six models are single MV and LV feeders instead. The models are built synthetically by using a large-scale distribution network planning tool, using data previously analysed to characterize the network in a realistic way. Models do not consider any imbalance in the grid structure.

In November 2019 the *Non-Synthetic European Low Voltage Test System* – upon which this work is focused - was developed by *Koirala et al.* and published [22]. This large-scale network is an actual existing grid of a typical European town of northern Spain, whose exact location is not shared for sensible data reasons. The most innovative point of the whole article is not the model itself, but the tool developed to build it, that will be analysed in-depth in Chapter 3.

2.5 The Necessity for New Test Systems

The necessity for new and more accurate test systems was officially brought to attention in 2009 with the IEEE roadmap [21] due to the still uncertain effects that a high PVDG penetration would cause to the networks. During those years, in-depth studies confirmed that DG implementation into the grid was

– and is still – causing a fall in power quality and network stability and reliability (as discussed in section 2.2). More recently, another major criticism arose from preventive studies about high PEV penetrations into the load curve of the LV network. The very high and inconstant load factor brought by the unregulated charging of EVs, with their statistically high-pitched load shape, will place another heavy burden on the already stressed network (see Chapter 2.3), and with the potential for worsening conditions, possibly bringing it to unsustainability.

Almost all the mitigation strategies (sections 2.2.4 and 2.3.2) that have been proposed to prevent the inevitable collapse of the network are based on new smart technologies and algorithms that can work with real-time data of the network. To evaluate these algorithms, having accurate test models is mandatory. Furthermore, to maintain accuracy, considered the variety of network structures existing, a multitude of representative models should be developed. Alternatively, a tool to easily build representative test systems could be planned to allow researchers to build their own models, based on their necessities.

Test models are basically created in 4 different ways:

- the first method consist in the manual design of the distribution network, like in the Original Test Feeders [46], but also [47–49];
- the second method consists of taking the data from the real distribution network, removing private information and sanitizing it with new names, like in EPRI models [52, 53];
- the third method uses clustering algorithms to analyse several networks to build a synthetic representation of them and obtaining a statistically accurate model, [51, 56];
- the fourth method is based on planning tools using economic and technical criteria in order to create a realistic distribution network, like what have been made in [58].

Many of the developed test feeders and systems discussed have intrinsic deficiencies that prevent them to be representative of the European LV Distribution Network. For a clear overview, *Table 2-1* summarizes the test models described in the previous section, highlighting their scope of intended use and their building methodology.

Instead, this work focuses on the work published by Koirala *et al.* [22] and the test system they developed, with special care for the tool they used to build it. The tool they developed make use of the second method to build test models from real GIS data of the network (owned by DSOs) and load data collection from smart meter. Considering that DSOs will play a very important role in the future grid management, this tool was developed to allow any DSO to build and simulate their own models easily. These models would prove very useful because of their scalability, accuracy (they are non-synthetic) and flexibility. In the next Chapter, an in-depth analysis and evaluation of the network and the tool proposed by *Koirala et al.* is done.

***Table 2-1**. Test models through years.*

Test System Name	Publication Year	Intended use	Building method
4-Node Test Feeder	1991	Simulation software development	Synthetic design
13-Node Test Feeder	1992	Simulation software development	Synthetic design
34-Node Test Feeder	1992	Simulation software development	Synthetic design
37-Node Test Feeder	1992	Simulation software development	Synthetic design
123-Node Test Feeder	1992	Simulation software development	Synthetic design
IEEE NEV Test Case	2008	NEV study	Synthetic design
PNNL Taxonomy Feeders	2009	Representative study	Clustering
IEEE Comprehensive Distribution Test Feeder	2010	Simulation software development	Synthetic design
IEEE 8500-Node Test Feeder	2010	Simulation software development	Synthetic design
EPRI Representative Feeders	2010	Representative study	Real network data
Western Australia Taxonomy Feeders	2013	Representative study	Clustering and Discriminant analysis
IEEE 342-Node LV Networked Test System	2014	Simulation software development	Synthetic design
IEEE European LV Test Feeder	2015	Representative study	Synthetic design
Representative Feeders for North West of England	2016	Representative study	Clustering
European Representative Distribution Networks	2018	Representative study	Clustering and Discriminant analysis
Midwest U.S. Test System	2019	Representative study	Real network data
Nordic Test System	2020	Voltage stability study	Synthetic design
Reliability and Voltage Stability Test System	2020	Voltage stability study	Synthetic design
Non-Synthetic European LV Test System	2019	Representative study	Real Network data

3 The Non-synthetic European Low Voltage Test System

3.1 The Test Network

Koirala et al. [22] presented a large-scaled test network as an example of what their tool is capable of. In fact, the MATLAB tool they created is able to convert GIS data of a real network – owned by DSOs – to an actual OpenDSS code, with which it is possible to make very accurate power flow analysis. The test network is intended for representative studies that need highly accurate and flexible models. Then, in the context of algorithm evaluation and forecasting, it is a reliable source for researchers. The main features of the system are the following:

- It is based on the European voltage and frequency standards.
- There is no Kron's reduction, with a 4W3P structure and earthing only at the transformers.
- It is a very large-scale radial test system, with multiple feeders connected to each of the 30 substation transformers.
- It is an existing network of a small town in northern Spain, from which has been taken real data and sanitized it to avoid the sharing of private information.
- Load is time series format with hourly data collection from real smart meters.
- It is highly adaptable through GIS data, MATLAB and OpenDSS software. The presence of substation and network embedded circuit-breakers that can be opened and closed allows testing in multiple network conditions. Also, different load curves and PV distributed generation can easily be implemented by the user (as done in Chapter 4).

Following, every characteristic of the network is accurately analysed.

3.1.1 Network Features and Description

The network represents a small suburban town located in the north of Spain and it is based on the European standards presented in the previous Chapter.

It has distribution transformer secondary voltages set to 420 V (with LV loads rated 400 V) rms phase-to-phase and a rated frequency of 50 Hz. Kron's reduction is not applied, permitting a voltage gap between neutral and ground. The LV network is then designed as a 4W3P system with neutral grounded only at the substations and isolated from consumer ground, as in the TT Earthing.

The total amount of buses is 10,289 of which 2,673 of them being monitored[1]. The buses not monitored are used for geographical shaping of the network and not of electrical interest. Is then provided a total of 8'087 loads with real load curves taken from smart meters with an hourly data collection of 20 days.

The network consists in 30 MV/LV distribution transformers to which multiple LV feeders are connected. During normal conditions, there is no mesh in the network and every transformer supplies energy in a branched way. The whole system is shown in *Figure 3-1*, with red circles representing the distribution MV/LV substations, and black segments representing the LV network lines. It is assumed that all substations are supplied by a single infinite source. Below, the different components of the system are accurately descripted, with reference to the unmodified test system and the files attached to the article.

[1] An anomaly has been found in the article, with these numbers being respectively of 10,290 and 2,681. A list of all the anomalies can be found at the end of the Chapter, in section 3.5.

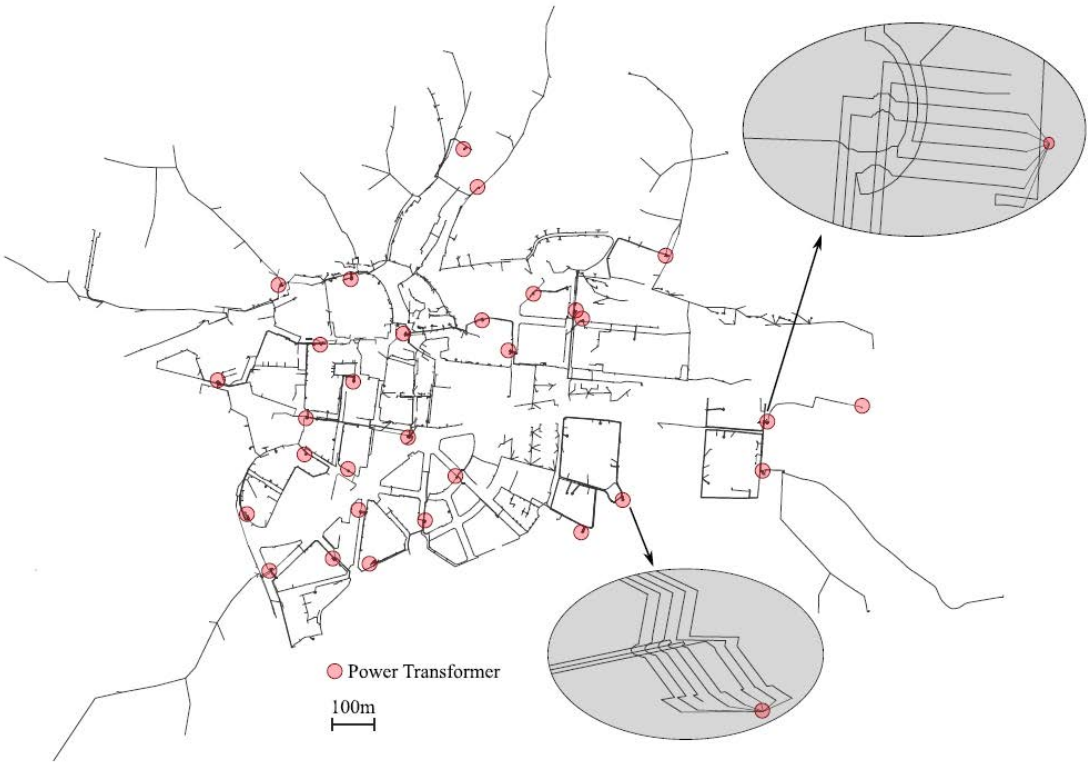

***Figure 3-1**. The Non-synthetic European Low Voltage Test System as a single line diagram [22].*

3.1.1.1 Source

The source is defined as a MV voltage source with a base voltage of 22 kV, a 3-phase short circuit current of 9 kA and a 1-phase short circuit current of 5 kA, similar to the *IEEE European LV Test Feeder*. This can be considered as a nearly infinite source to which the whole network is connected.

3.1.1.2 MV Lines

The source is connected to the substation transformers through virtual 3W3P MV lines with a length of 5 m each. The 30 MV lines are chosen to be of low impact to the network, and resistance and reactance of each conductor is 250 μΩ, represented by the 3x3 matrices shown below in "per kilometer" format[2]. Mutual resistance and mutual reactance have not been considered.

$$Rmatrix_{101} = \begin{bmatrix} 0.05 & 0 & 0 \\ 0 & 0.05 & 0 \\ 0 & 0 & 0.05 \end{bmatrix};\ Xmatrix_{101} = \begin{bmatrix} 0.05 & 0 & 0 \\ 0 & 0.05 & 0 \\ 0 & 0 & 0.05 \end{bmatrix}.\ \ (^{\Omega}/_{km})$$

They are indexed with the name *mv1*, *mv2*, … *mv30* in the *source2txline_ind.txt* file (see *Table 3-1*) and assigned the line code 101 as an identifier, related to the *linecode.txt* file.

***Table 3-1**. Examples of MV lines in the test network.*

MV Line name	Bus 1	Bus 2	N. of phases	Line code	Length (m)
mv1	Source	1	3	101	5
mv7	Source	7	3	101	5
mv18	Source	18	3	101	5

[2] In the article was denoted a value of 25 μΩ. This work follows the parameters denoted in the code, which presents a value of 250 μΩ.

3.1.1.3 Distribution Transformers

30 distribution transformers are connected at the end of the MV lines, all of them configurated with a delta-wye connection and group 11 (Dy11). The voltage rating is 22/0.420 kV and the power rating of almost every transformer is 630 kVA, except for one at 250 kVA and one at 1,000 kVA[3]. Each transformer has an impedance of 4% and is grounded at the LV side. If needed, OpenDSS allows the editing of the provided model with multiple other parameters.

Transformers are named with their original names from GIS data and are indexed in *Transformer_ind.txt* file, of which examples are shown in *Table 3-2*.

***Table 3-2**. Examples of distribution transformers in the test network.*

Transformer name	Bus1	Bus2	Connection	Power Rating (kVA)	Voltage Ratings (kVs)	XHL (%)
TD401346	1	31	Dy11	630	22 / 0.420	4.0
TD006563	7	37	Dy11	630	22 / 0.420	4.0
TD004454	30	60	Dy11	250	22 / 0.420	4.0

3.1.1.4 Feeders

For feeder is intended the element that connect the transformer secondary winding with the circuit-breaker of the substation. Of the 252 feeders, only the 160 with a closed circuit-breaker are transposed from GIS data into OpenDSS[4]. Feeders with an open circuit-breaker are not considered into the test system.

All of them are modeled as 4W3P lines with the same conductors and with aerial configuration. These values are represented by the following 4x4 impedance matrices and described by line code 205:

$$Rmatrix_{205} = \begin{bmatrix} 0.160 & 0 & 0 & 0 \\ 0 & 0.160 & 0 & 0 \\ 0 & 0 & 0.160 & 0 \\ 0 & 0 & 0 & 0.231 \end{bmatrix};\ Xmatrix_{205} = \begin{bmatrix} 0.079 & 0 & 0 & 0 \\ 0 & 0.079 & 0 & 0 \\ 0 & 0 & 0.079 & 0 \\ 0 & 0 & 0 & 0.085 \end{bmatrix}. \quad (^{\Omega}/_{km})$$

Feeders are named *feeder1*, *feeder2*, … *feeder160* and are indexed in the first rows of *Line_indexed_check.txt* file. Examples are shown in *Table 3-3*.

***Table 3-3**. Examples of LV feeders in the test network.*

Feeder name	Bus 1	Bus 2	N. of phases	Line code	Length (m)
feeder1	31	31_1	4	205	4.340
feeder34	37	37_1	4	205	2.550
feeder35	37	37_3	4	205	1.401

3.1.1.5 Substation Circuit-breakers

Substation circuit-breakers connect feeders to the LV network lines. As for the feeders, only closed circuit-breakers are represented in the OpenDSS system. They are modelled as short lines (0.5 m) with self-resistance and reactance of 25 μΩ. Their line code is 102, and their impedance matrices are the following:

[3] An anomaly has been observed between the code and the article. The second suggests a transformer of 100 kVA instead of 1,000kVA.
[4] The article mentions a total of 161 transposed feeders instead.

$$Rmatrix_{102} = \begin{bmatrix} 0.05 & 0 & 0 & 0 \\ 0 & 0.05 & 0 & 0 \\ 0 & 0 & 0.05 & 0 \\ 0 & 0 & 0 & 0.05 \end{bmatrix};\ Xmatrix_{102} = \begin{bmatrix} 0.05 & 0 & 0 & 0 \\ 0 & 0.05 & 0 & 0 \\ 0 & 0 & 0.05 & 0 \\ 0 & 0 & 0 & 0.05 \end{bmatrix}.\ (^{\Omega}/_{km})$$

As for feeders, circuit-breaker elements are indexed in *Line_indexed_check.txt* file too, and are called *cktbk1*, *cktbk2*, … *cktbk160* (see *Table 3-4*).

***Table 3-4**. Examples of substation circuit-breakers in the test network.*

Substation circuit-breaker name	Bus 1	Bus 2	N. of phases	Line code	Length (m)
cktbk1	31_1	2684	4	102	0.5
cktbk34	37_1	2574	4	102	0.5
cktbk35	37_3	2575	4	102	0.5

3.1.1.6 LV Network Lines

The LV lines that form the network connect the substations circuit-breakers to the consumer's loads. The network is modelled by 4W3P lines that start from the substation circuit-breakers. Lines can be overhead or underground, with isolated neutral. Codes and impedance values of the cross-sections of every line conductor are listed in *Table 3-5* and *Table 3-6*. Codes that start with the digit 2 are referred to overhead lines, those that start with the digit 3 to underground lines instead. Codes 250 and 350 are associated to non-recognized cable types. As in previous line elements, only self-resistance and self-reactance have been considered in the 4x4 matrices, while mutual impedances are considered negligible. Examples of LV lines are shown in *Table 3-7*.

***Table 3-5**. Cable types and assigned line codes in the test network.*

Cable Type	Aerial	Underground	Undefined
BT – MANGUERA (hose)	201	301	-
BT – RV 0,6/1 kV 2*16 KAL	202	302	-
BT – RV 0,6/1 kV 2*25 KAL	203	303	-
BT – RV 0,6/1 kV 3(1*150 KAL) + 1*95 KAL	204	304	-
BT – RV 0,6/1 kV 3(1*240 KAL) + 1*150 KAL	205	305	-
BT – RV 0,6/1 kV 3(1*240 KAL) + 1*95 KAL	206	306	-
BT – RV 0,6/1 kV 4*25 KAL	207	307	-
BT – RV 0,6/1 kV 4*50 KAL	208	308	-
BT – RV 0,6/1 kV 4*95 KAL	209	309	-
BT – RX 0,6/1 kV 2*16 Cu	210	310	-
BT – RX 0,6/1 kV 2*2 Cu	211	311	-
BT – RX 0,6/1 kV 2*4 Cu	212	312	-
BT – RX 0,6/1 kV 2*6 Cu	213	313	-
BT – RZ 0,6/1 kV 2*16 AL	214	314	-
BT – RZ 0,6/1 kV 3*150 AL/80 ALM	215	315	-
BT – RZ 0,6/1 kV 3*150 AL/95 ALM	216	316	-
BT – RZ 0,6/1 kV 3*25 AL/54,6 ALM	217	317	-
BT – RZ 0,6/1 kV 3*35 AL/54,6 ALM	218	318	-
BT – RZ 0,6/1 kV 3*50 AL/ 54,6 ALM	219	319	-
BT – RZ 0,6/1 kV 3*70 ALM/ 54,6 AL	220	320	-
BT – RZ 0,6/1 kV 3*95 AL/54,6 ALM	221	321	-
BT – RZ 0,6/1 kV 4*16 AL	222	322	-
BT – Desconocido BT (unknown cable)	250	350	-
MV Line	-	-	101
Circuit-breaker	-	-	102

Table 3-6. Resistance and reactance (in Ω/km) of the cables used in the test network.

Cross-section	R (Aerial)	X (Aerial)	R (Underground)	X (Underground)
2 mm Cu	9.9	0.075	9.9	0.075
4 mm Cu	4.95	0.075	4.95	0.075
6 mm Cu	3.30	0.075	3.30	0.075
16 mm Cu	1.23	0.08	1.23	0.08
16 mm Al	2.14	0.09	2.14	0.09
25 mm Cu	1.34	0.097	1.538	0.095
35 mm Al	0.907	0.095	0.907	0.095
50 mm Al	0.718	0.093	0.718	0.093
54.6 mm Al	0.658	0.09	0.658	0.09
80 mm Al	0.39	0.090	0.450	0.084
95 mm Al	0.3587	0.089	0.410	0.083
150 mm Al	0.231	0.085	0.264	0.082
240 mm Al	0.160	0.079	0.160	0.079
Desconocido (unknown)	0.210	0.075	0.210	0.075

Of the 2,493 non-feeder LV lines, 2,483 of them are transposed in the test system (explained in further section 3.3.3.4), but every line is made of multiple sub-segments which represent the physical shape and topological coordinates of the network[5]. Consequently, 9,819 is the total number of LV line elements indexed in the *Line_indexed_check.txt* file.

Table 3-7. Examples of LV Line segments in the test network.

LV Line (sub-segment) name	Bus 1	Bus 2	N. of phases	Line code	Length (m)
166_0	2574	166_1	4	304	2.422
166_1	166_1	166_2	4	304	8.504
166	166_2	166	4	304	5.765

LV lines are named with ordered numbers, from 61 to 2550, followed by a counter for sub-segments belonging to the same line. The last sub-segment of every line is an integer number and matches with the name of the second bus of the line, for easy monitoring. Integers from 1 to 60 represent buses on MV and LV side of the transformers. An example of bus and line name allocations is shown in *Figure 3-2*.

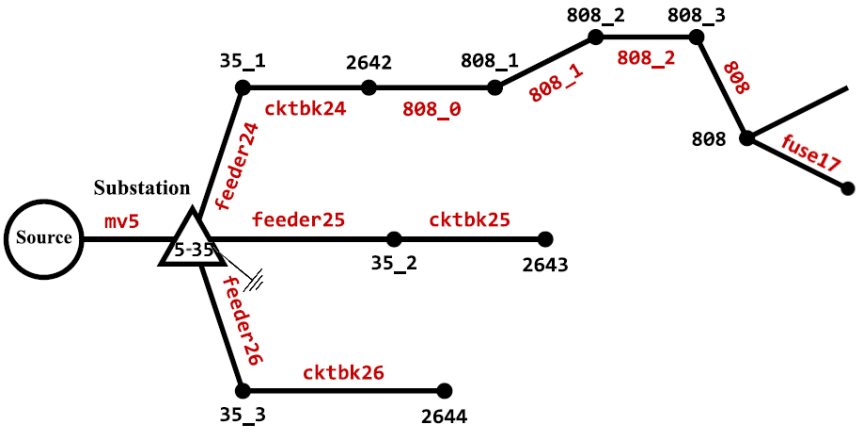

Figure 3-2. Bus and line indexing representation, based on an image from [22].

[5] Anomaly has been found within the article, with non-feeder LV lines being 2,490.

3.1.1.7 Network Circuit-breakers

As in real grids, in this test system there are circuit-breakers embedded in the LV network, between non-feeder LV lines. These 135 breakers are built in the same way of substation circuit-breakers and indexed in *fuse_indexed.txt* file with names *fuse1*, *fuse2*, … *fuse135* (examples in *Table 3-8*). Fuses that are open in standard network conditions are commented (anticipated by an exclamation point) within the text file and their element is not built in OpenDSS.

Thanks to this peculiar feature, the system can be easily reconfigured and tested in multiple conditions. In fact, the switching operation of each substation and network circuit-breaker can be easily implemented by modifying the excel GIS files. In this way, extraordinary conditions of the network (such as maintenance or short-circuit situations) can be considered for alternative scenario studies.

***Table 3-8**. Examples of LV network embedded circuit-breakers in the test network.*

LV Network circuit-breaker name	Condition	Bus 1	Bus 2	N. of phases	Line code	Length (m)
fuse2	Closed (C)	2677	1099	4	102	0.5
fuse45	Open (A)	1683	1681	4	102	0.5
fuse130	Closed (C)	2768	1801	4	102	0.5

3.1.1.8 Reactors

The reactor components indexed in *neutral_ind.txt* represent the earthing of each substation distribution transformer. Every reactor has a resistance of 5 Ω and a reactance of 0.01 Ω connected in series and is connected between the neutral of a transformer LV side (buses number 31 to 60) and ground. Their names are *grnd1*, *grnd2*, … *grnd30* and are defined as in *Table 3-9*.

***Table 3-9**. Examples of reactor elements in the test network.*

Reactor name	Bus 1	Bus 2	N. of phases	R (Ω)	X (Ω)
grnd1	31 (neutral)	Ground	1	5	0.01
grnd7	37 (neutral)	Ground	1	5	0.01
grnd30	60 (neutral)	Ground	1	5	0.01

3.1.1.9 Loads

Loads are provided with information regarding the number of phases and, for single-phase loads, which one supplies the load. In GIS files the load connection points are not coincident with the buses of the LV lines, but are connected to them through a short line. Instead, they are considered coincident in the test system, avoiding further complexity. Consequently, consumers' conductors are connected directly to the network and neutrals are isolated from ground.

Loads are modelled as constant PF loads, collecting just the active power values from smart meters and applying a constant PF of 0.95. They are indexed in the *Load_indexed.txt* file and defined as in *Table 3-10*.

***Table 3-10**. Examples of loads in the test network.*

Load name	Bus 1	N. of phases	Connected phase	kV	Power factor	kW (loadshape)	Data samples
LOAD1	1233	1	1	0.23	0.95	Shape_1	481
LOAD4562	1278	3	123	0.4	0.95	Shape_4562	481
LOAD5104	312	1	2	0.23	0.95	Shape_5105	481

The GIS files provides 8,087 loads grouped in 1,138 power supplies (load connection points) connected to the test network. The simulation is based on 20 days hourly data collection and consequently every load has its proper curve based on 481 data samples taken from real smart meters. However, these values are affected by the following considerations.

- Some bus connection points, in the *Acomeditas* datasheet are connected to a non-existent connection bus, consequently 14 loads have been commented in the OpenDSS code. Two of them are commented manually and this will be discussed in section 3.3.3.11.
- In the GIS files there are 618 loads with a quantity of data samples exceeding or subceeding 481 that, for simplicity, are substituted with a null load shape.
- As in a real network, there are multiple loads not absorbing energy, whose null data are collected from smart meters anyway. In this network, 272 loads are in this condition.
- Due to the simplification explained before, some connection points have been merged into the same LV network bus.

These observations make the total number of loads connected to the test system equal to 8,073. Furthermore, the number of loads affecting the model (loads with non-zero curves) is reduced to 7,188 – almost a thousand loads less – distributed in 1,002 power supplies throughout the network.

Note that these results are made after the correction to the code which is faced in section 3.3.4.1.

Since the model is open and flexible, load elements can be easily modified by changing their values in the MATLAB code, as for every other element of the network. So, the user can implement reactive power data from smart meters, change the shape of load curves, modify load consumption and potentially implement other loads and generators to the grid.

3.2 OpenDSS Solver

The test system is based on the electric power distribution system simulator software OpenDSS freely available online. This tool can perform power flow simulations, as well as fault and harmonic studies, and it is designed to support analyses that meet future needs related to smart grid, renewable energy sources research and grid modernization. OpenDSS is able to run time series power flow simulations and then export its results through an interface with programming platforms such as MATLAB or Python. In this way, the results from OpenDSS simulation can be subsequently elaborated with compatible software.

This is exactly what is done with this test system. The model is run in OpenDSS through a MATLAB interface and monitored results are sent as output back on MATLAB again, which gives plenty of possibilities in their elaboration.

3.2.1 Power Flow Simulation Method

OpenDSS is able to solve both radial and meshed power circuits. It can make use of two power flow solution methods: Iterative and Direct solution. The Direct solution includes nonlinear elements (such as loads and distributed generators) as admittances and are added to the system admittance matrix. In this way the matrix can be solved directly. Instead, the Iterative power flow analysis interpret nonlinear elements as injection sources and the solution is obtained in an iterative way [60].

There are two algorithms employed in the Iterative solver: Normal current injection and Newton mode. The Normal mode is faster, but the Newton mode is more robust and should be applied to circuit that are difficult to solve [60].

The Normal Iterative mode is set by default and – considered the huge size of the network – it has been used in the Non-Synthetic European LV Test System due to its capability to solve time series power flow analysis fast.

3.2.2 Simulation Results: Monitors and Energy Meters

When the time series power flow simulation is completed, the OpenDSS software makes available the sequence of solutions only in the ‘monitor’ elements, as defined by the user. A monitor object saves the complex values of voltage and current, or active and reactive power, of all the bus phases in which is set.

In the Non-Synthetic network, there are a total of 2'673 monitored buses, located as in *Figure 3-3*:

- MV side of each substation distribution transformer, indexed in the *MVmon.txt* file;
- Bus 2 of the 160 active feeders, indexed in the *monitor_feeder.txt* file;
- Last bus of each LV line, corresponding to the 2'483 LV buses with integer numbers. These monitors are indexed in *monitor_line.txt*.

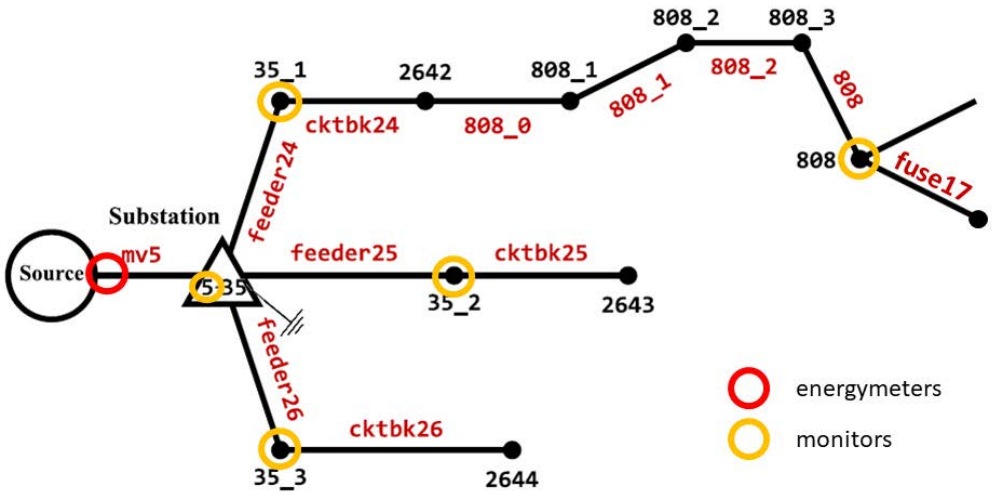

***Figure 3-3**. Monitors (yellow) and energy meters (red) allocation in a circuit representation.*

Note that the neutral voltage and current are directly recorded by monitors, which is useful for result elaboration (and contextualization) purposes.

Furthermore, OpenDSS makes use of the 'energymeter' elements that can simulate an actual energy meter. It measures power values at its location and can integrate them to obtain the energy consumption. It can also provide losses and overload information in a defined region of the circuit.

In the network, energymeter objects are located in the 30 terminals of the MV lines connected to the source and indexed in *energymeter_ind.txt*. Their purpose is to analyse the overall energy absorption of the LV network and to compare the branches consumption in network optimization analysis.

3.3 The Test System building Tool

The MATLAB tool created by *Koirala et al.* is able to convert GIS raw data files from DSOs (in excel format) into OpenDSS code (indexed into text files). This allows researchers with the access to DSOs information to experiment on real (non-synthetic) networks, with all the benefits that this includes. From now on, this tool will be called "GIS to OpenDSS Conversion Tool (GOCT)" for easier understanding.

The GOCT is structured in 5 main parts processed as in *Figure 3-4*:

- The GIS data files in excel format, with also the electrical information of the network elements, provided from the DSOs.
- A standard OpenDSS master file, which sets the base frequency and the MV source. Then calls for the text files that will be created by the GOCT.
- The *A_MakeNet.m* script file, that builds the entire network to be read into OpenDSS.
- The *B_MakeLoad.m* script file, that defines the time series and builds every single load curve of the network.
- The *C_Run.m* script file, that runs the power flow analysis and export the monitored results to MATLAB, from which the data can be easily elaborated.

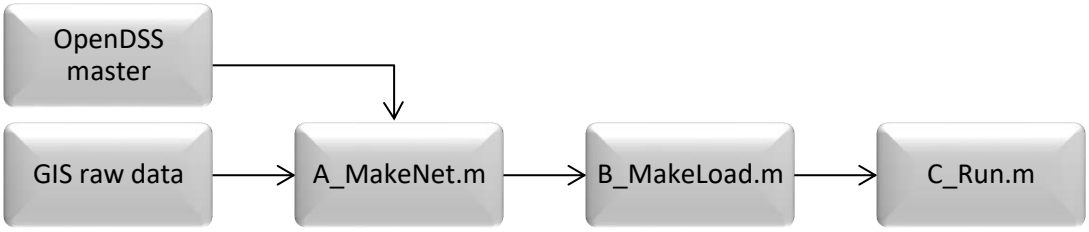

***Figure 3-4**. GIS to OpenDSS Conversion Tool (GOCT) working process.*

To make the conversion and the simulation work, the user must run the '*A*', '*B*', and '*C*' MATLAB scripts in the proper order. The first two scripts are strictly connected and represent the true conversion tool. The third script instead runs the power flow analysis and provides results. The division has been made to simplify researchers' modifications to the process.

In the following section, an in-depth analysis of each part – as provided in *Figure 3-4* – is carried out to describe how the GOCT works, which will facilitate subsequent opportunities to build non-synthetic networks with this tool.

Furthermore, in the script some potential anomalies were identified, and corrections subsequently applied. This section will explain in detail what has been amended and what optimization opportunities are available.

3.3.1 GIS Excel Data Files

The GIS raw data files provided by *Koirala et al.* in their article are contained in the *GIS_data* folder and divided into 10 files (*master.xlsx*, *load.xlsx*, *phase meters.xlsx* and *file1.xlsx* to *file7.xlsx*). Note that these files contain the whole network and load information. Therefore, their size of 218 Mb, is significant.

In the excel files there are some columns which are not used by the GOCT. Only the excel columns that are meant to be converted are explained in this section. Columns not converted by the GOCT are referred in here only if their data are useful to the understanding of the process or give further development opportunities. These columns are referred under parenthesis.

The *master.xlsx* file contains all the network raw information, and it is divided into six data sheets, representing the different network elements. The *load.xlsx* file links the loads to their connection points and the *phase meters.xlsx* file describes which phases are connected to them. Then, files from *file1.xlsx* to *file7.xlsx* record every single meter data sample taken in every load connection point.

3.3.1.1 Master File: Substation Transformers Datasheet

All the data regarding the transformers are indexed in the *CT – TRAFO* sheet and summarized in *Table 3-11*. Column A represents the transformer Mslink univocal code number. Similarly, transformer names are uniquely represented in column H, which are used as transformer names also in the test model. In column J the power rating in kVA of the transformers is provided. Columns F and K respectively present the MV and LV side through which the transformer is connected to the network. Column D and E define the X-Y coordinates of the transformer, while considering MV and LV buses located in the same geographical point[6].

[6] It must be denoted that the real GIS coordinates has been encrypted into a X-Y cartesian coordinate system. This system still allows to completely appreciate the test network and it is also necessary to calculate the length of the lines through Pythagoras' theorem.

***Table 3-11**. Raw transformer data example, located in "CT – Trafo" subfile.*

Transf. Mslink **A**	X coord. **D**	Y coord. **E**	Bus 1 MV side **F**	Transf. name **H**	Power rating (kVA) **J**	Bus 2 feeder side **K**
65043	5704.11	102361.92	65045	**TD401346**	630	3865289
65079	5597.29	102217.67	65081	**TD400291**	1000	3864018

3.3.1.2 Master File: LV Feeders Datasheet

The *Linea BT* excel sheet gives all the information regarding LV substation feeders and the status of their circuit-breakers. From this sheet, only feeders with a circuit-breaker Current status set to 'Closed' are transposed in OpenDSS code.

As *Table 3-12* summarizes, column A of the datasheet is reserved to the feeder univocal Mslink code number. Columns E and F denote, respectively, the transformer LV side bus and the circuit-breaker side bus of the feeder. The coordinates in columns G and H refers to the bus 2 of the feeder. Column I and J represent the Normal and Current status of the circuit-breaker that link the feeder with the LV network. The status of a circuit-breaker can be Closed ('C') or Open ('A'). The GOCT makes use only of the Current status. Of the 252 feeders in the network, only the 160 with circuit-breakers with current Closed status are transposed into the OpenDSS model.

***Table 3-12**. Raw LV feeder data example, located in "Linea BT" subfile.*

Feeder Mslink **A**	Feeder number **B**	Bus 1 Transf. side **E**	Bus 2 breaker side **F**	X coord. **G**	Y coord. **H**	Normal Status **(I)**	Current Status **J**
775431	1	3865289	108023	5703.39	102366.2	C	C
775431	2	3865289	108024	5703.31	102365.51	C	C

The OpenDSS software does not have an easy interface for network reconfiguration purposes. Therefore, modifications to the excel files are required to test different network configurations through successive iterations of the GOCT coding structure. In this case it is crucial to detect the corresponding breakers embedded in the network to be operated accordingly, avoiding islanding of any part of the network.

3.3.1.3 Master File: LV Lines Datasheet

The third sheet, named *Segmento BT*, concern the LV network lines. In the sheet there is a total of 2'493 LV lines with the information shown in *Table 3-13*.

The Mslink unique code number of each line is shown in column A. In column D instead are listed the Mslink numbers proper of the feeders at the head of the LV lines. First and last bus of the LV line are represented respectively in columns F and G. Column C describe if the line is developed underground ('Subterráneo') or overhead ('Aéreo') and, at last, column H express the cable of which the line is made (the cable impedance values have been summarized previously in *Table 3-5*).

***Table 3-13**. Raw LV line data example, located in "Segmento BT" subfile.*

LV line Mslink **A**	Typology of line **C**	Feeder Mslink **D**	Line first bus **F**	Line last bus **G**	Cable Type **H**
74437	Subterráneo	73796	41291	3225463	BT - RZ 0,6/1 KV 3*150 AL/95 ALM
1374735	Subterráneo	73796	1169197	2528898	BT - RV 0,6/1 KV 3(1*150 KAL) + 1*95 KAL

3.3.1.4 Master File: Coordinates of the LV Line buses Datasheet

In the datasheet called *Coordenadas Segmentos* the buses that shape the geographical structure of every LV line are specified. The LV lines are split into sub-segments with the same electrical characteristics

to obtain the network shape illustrated in *Figure 3-1*. Column A represents the Mslink code number of the LV line to which the bus belongs. In column F, the order of the buses – in which the number zero correspond to the first bus of the line – is listed. Columns G and H describe the coordinates of the bus. Examples are made in *Table 3-14*.

***Table 3-14**. Raw LV line buses coordinates data example, located in "Coordenadas Segmentos" subfile.*

LV line Mslink **A**	Bus sequence number **F**	X coord. **G**	Y coord. **H**
74437	0	5238.27	101965.38
74437	1	5240.86	101965.23

Note that in the model the first and last buses of every line are named with integer numbers. Instead, the mid-line buses are not-integer numbers and will not be monitored because not of electrical interest.

3.3.1.5 Master File: Network-to-Load Lines

As already said, loads are not connected directly to the LV lines. Between the network and the load connection points there are short electrical lines that for simplicity are not implemented in the model. Consequently, the two buses of these lines have been merged and the load have been directly connected to the bus of the LV network.

Table 3-15 has been exported from the datasheet *Acometidas*. The only two columns of interest for the purpose of GOCT are column B and C, representing respectively the bus of the load connection point and the bus of the network LV line[7].

***Table 3-15**. Raw network-to-load lines data example, located in "Acometidas" subfile.*

Load line Mslink (**A**)	Load connection point bus **B**	LV Network side bus **C**
1220006	3790730	954350
80007	3774374	2573500

3.3.1.6 Master File: LV Network Circuit-Breakers

The last datasheet, named *Fusible* contains the information regarding the 135 circuit-breakers embedded in the LV network. *Table 3-16* shows that column A represents the circuit-breaker Mslink code number. Columns D and E define which buses are connected by the element. Normal and Current status are represented respectively in columns F and G by the terms 'C' and 'A', and – as for substation circuit-breakers – only elements that are Closed are represented in the model. The open elements are instead transposed as commented code into the same OpenDSS file.

***Table 3-16**. Raw network embedded circuit-breakers data example, located in "Fusible" subfile.*

Fusible Mslink **A**	Bus 1 **D**	Bus 2 **E**	Normal Status (**F**)	Current Status **G**
80034	44257	1402524	A	A
2360167	2509198	2509208	C	C

3.3.1.7 Load Connection File

Table 3-17 refers to the load data located in *load.xlsx* excel file. Column A expresses the load identification code assigned by the DSOs. In column K is then represented the connection type of each

[7] An anomaly has been found both in the article and in the column labels within the GIS *master.xlsx* file. In those, columns referred as buses 1 and 2 are respectively asserted to be columns C and D instead. It has been verified according to the code that the columns used by the GOCT are columns B and C.

load to the network. The letter 'M' defines single-phase loads, while the letter 'U' defines three-phase loads. The load connection point is referred in column R, and the label of the load group in column T.

***Table 3-17**. Raw load connection data example, located in 'load.xlsx' excel file.*

Load ID code **A**	Type of connection (1-phase or 3-phases) **K**	Load connection point bus **R**	Load group label **T**
SAG0145432047	M	36767901	C000601
SAG0145443412	M	4285302	C000601

3.3.1.8 Phase Meters File

The *phase meters.xlsx* excel file contains data regarding load phase connection and the status of phase meters, as summarized in *Table 3-18*. Column A refers to the load identification code which the meter is monitoring. Column B expands the information about phase connection, explaining which phase of the network the load is connected to. The letters R, S and T represent the three different phases of the network, and are converted respectively into phases 1, 2 and 3 in the OpenDSS model. Where a phase is missing (due to data inconsistency), the allocation is set randomly. A three-phase load is represented by the code RST in the datasheet.

It is necessary to observe that there are often multiple phase meters monitoring the same load in the datasheet. These phase meters seem to be duplicates. However, it is verifiable from columns D and E that every load has only one phase meter with 'ACTIVE' status and data collection set to 'OK'.

***Table 3-18**. Raw phase meters data examples, located in 'phase meters.xlsx' file.*

Load ID code **A**	Phases connected **B**	Data Collection (**D**)	Operational status (**E**)
ZIV0034678234	R	OK	ACTIVE
ZIV0049973140	RST	OK	ACTIVE

3.3.1.9 Load Data Samples Files

This set of 7 files – named from *file1.xlsx* to *file7.xlsx* – contains the data samples of every load, taken from actual meters that monitor active and reactive power values. The samples have been taken hourly during a 20-day period (from 1st to 20th of May), representing 481 samples for each load. It is understandable, considering the high number of loads involved, that these data have been divided into 7 files to be more accessible. In fact, there is a total of almost 4 million data rows in the files that will be elaborated by the GOCT.

Referring to *Table 3*-19, only columns C and G are exported. The first refers to the load identification code, the second to the actual active power value absorbed by the load in the moment shown in column D. Column I refers to the reactive power value absorbed at that time but is not exported to the model. The model uses a constant PF for every load to speed up the GOCT process, but this column can be easily implemented to improve the accuracy of the test network.

Due to communication problems or failure in detection, load data may be incomplete for some meters, and will not be considered in the OpenDSS model, as observed in section 3.1.1.9.

***Table 3-19**. Examples of raw load data samples, registered in the set of files named 'fileX.xlsx'.*

Load ID code **C**	Sample hour and day of collection (**D**)	Active power value **G**	Reactive power value (**I**)
ZIV0034684831	01/05/2018 00:00	0.052	0,01
ZIV0049973140	01/05/2018 01:00	0.075	0,01

3.3.2 OpenDSS Master File

The OpenDSS *Master.dss* file made available by *Koirala et al.* defines the bones of the simulation process. Through this file, OpenDSS may run and solve the power flow simulation. Note that information regarding transformers, lines and load data are indexed in multiple text files – exemplified in *Figure 3-5* – that will be built by the GOCT and manipulated through this OpenDSS file.

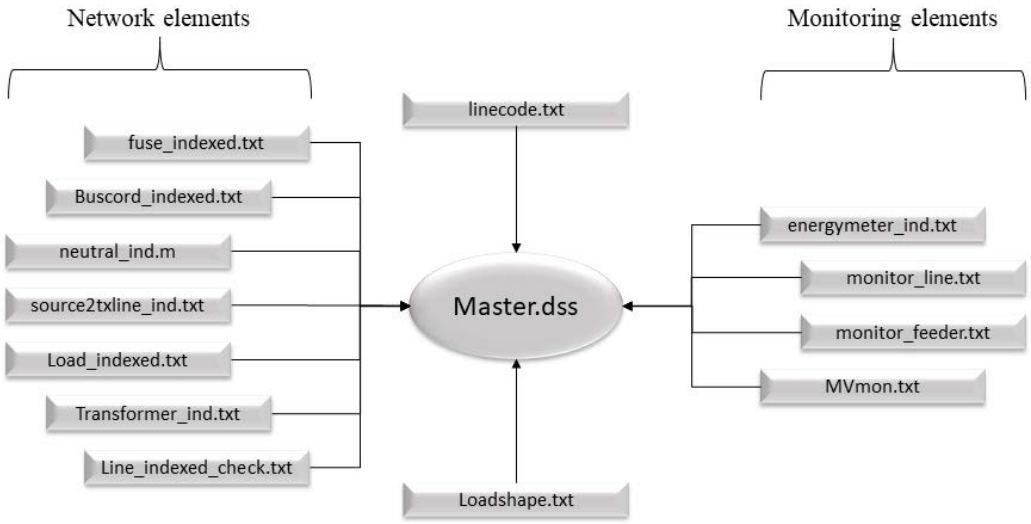

***Figure 3-5**. OpenDSS readable text files required by the Master file to properly work.*

Here, the network frequency is set to 50 Hz and the voltage source element is defined (and from here can be modified). The power flow simulation mode is set to 'daily' with 481 iterations representing 1 hour of time each (20-day hourly simulation). After the simulation, from the master file it is possible to plot the network and have a global view of it (exported in *Figure 3-1*), possibly adding markers, or highlighting other factors of interest.

This file is called at the start of the GOCT process, inside the script *A_MakeNet.m*, but is run only during the model simulation and elaboration process in *C_Run.m*.

3.3.3 Network Building Script: A_MakeNet.m

The first MATLAB process is called *A_MakeNet.m* and, as the name suggest, builds the network starting from the raw GIS data presented above. This script make use only of the first three excel files: *master.xlsx*, *load.xlsx* and *phase meters.xlsx*. The flowchart of the script is shown in *Figure 3-6*.

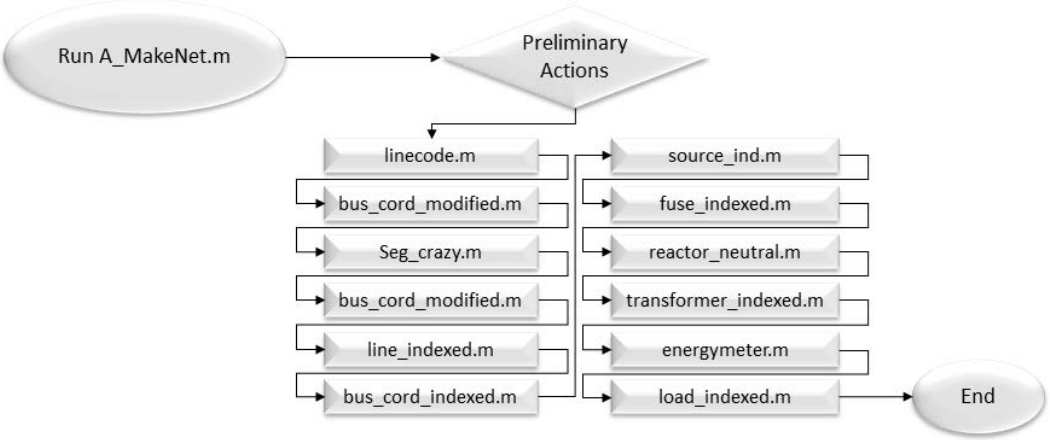

***Figure 3-6**. Process of the algorithm A_MakeNet.m.*

The preliminary actions consist in a series of simple preparatory activities, in particular:

- clear the previous data from MATLAB workspace;
- create the *mat* and *RunDSS* folders and import the *master.dss* file into the second;
- import the three GIS excel files as raw data into MATLAB;
- create the *txID* vector with the code names of every transformer.

Then, the process goes through multiple sub-scripts which elaborate, part by part, the GIS raw data and exports the resulting text files – readable by OpenDSS – to the *RunDSS* folder. They are briefly analysed one by one further in this section.

3.3.3.1 linecode.m

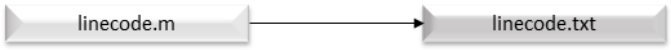

This script calls columns C and H of *Segmento BT* datasheet to elaborate the *linecode.txt* file. The text file prepares the line impedance matrices and number of phases, binding them to their proper line code, with the values anticipated in *Table 3-5* and *Table 3-6*.

3.3.3.2 bus_cord_modified.m

This script is used to index the buses of the raw GIS data and couple them with their own coordinates. It calls for columns D, E, F and K of the subfile *CT – TRAFO*, columns B, E, G, H of *Linea BT*, columns A, G and F of *Segmento BT*, columns A, G and H of *Coordenadas Segmentos*,

The main operation performed by this script is to create the matrix '*busindex*', which contains every bus with integer number. It is decided that these integer buses are the ones at MV and LV sides of the transformers and buses 2 and 1 of every LV line, as in *Figure 3-2*.

After this, the matrix is optimized, removing from it every duplicate, and then renamed '*busindex_new*'. This new matrix has 2,882 rows and the indexing order of this matrix is used to define the number names of buses:

- buses from *1* to *30* represent the MV side of each transformer;
- buses from *31* to *60* represent the LV side of the transformers, indexed with the same order as the previous (transformer number one has buses 1-31, transformer number two has buses 2-32, and so on);
- each bus from *61* to *2553* represent bus 2 of the homonym LV line element of the network;
- buses from *2554* to *2882* represent the remaining buses of LV line elements, which have no homonym line.

This matrix will be called often throughout the whole GOCT process.

3.3.3.3 Seg_crazy.m

This optimization script is meant to re-arrange the wrongly placed buses to have a clearer view of the network. Reversing bus 1 and bus 2 of the LV network lines when needed, with the purpose to have, in each line, the bus 1 upstream in the grid and the bus 2 downstream.

The script calls for columns A, F and J of *Linea BT*, columns F and G of *Segmento BT*, columns G and H of *Coordenadas Segmentos*, columns D, E and G of *Fusible*.

Seg_crazy.m starts by locating every closed feeder and every closed network embedded circuit-breaker. Then, it checks if the LV line bus 1 is the one connected with the substation. If not, it switches bus 1 and bus 2 – and their respective coordinates – and also reverse every sub-segment bus of the lines. Furthermore, the network embedded circuit-breakers are reversed when needed to fit the changings.

After this, the script checks the new LV line allocations, and if there are still badly arranged buses, the process starts all over again by using a converging 'WHILE' process that iterates multiple times.

Finally, the *bus_cord_modified.m* script is run again to fit the new bus allocations in the network. The rows sequence of '*busindex_new*' matrix is rearranged, but other than this, the rows values and quantity are unchanged.

3.3.3.4 Line_indexed.m

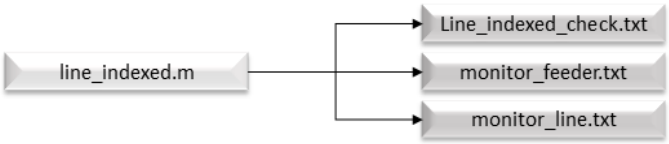

This script converts the raw line data into OpenDSS format, exporting them into the *Line_indexed_check.txt* readable file. Furthermore, it defines which buses will be monitored in text files *monitor_feeder.txt* and *monitor_line.txt*. The process can be divided into three parts.

In the first part, the 160 feeder line elements connected to closed circuit-breakers are generated (starting from *Linea BT* columns A, B, E, G, H, J and from *CT – TRAFO* columns D and E). They are exported to *Line_indexed_check.txt* with the conductor matrices described in section 3.1.1.4. Then, PQ (active-reactive power) and VI (voltage-current) monitors are defined for bus 2 of every feeder in the *monitor_feeder.txt* file. The '*Openlineattx*' vector collect every open (disconnected) feeder Mslink.

The second part builds and exports the substation circuit-breaker line elements connected to the feeders. Starting from the same excel datasheets, it exports only the closed circuit-breakers to the same text file with the parameters exposed in section 3.1.1.5.

The third and last part of the script elaborates and exports every LV line element – corresponding to each sub-segment of every LV line – for a total of 9,819 OpenDSS line elements. The process makes use of the values from columns A, D, F and G of the *Segmento BT* subfile, and columns F, G, H of the *Coordenadas Segmentos* (see also section 3.1.1.6). PQ and VI monitors are defined for every LV line bus 2 (as shown in the example *Figure 3-3)* and exported in *monitor_line.txt* file.

In the script, two important vectors are defined.

The '*notmonitored*' vector lists every LV line which is floating, without any connection to the source. These, in a normal condition, are the lines *462*, *463*, *464*, *465*, *1085*, *2551*, *2552*, *2553*, which are also memorized in *notmonitored.txt*, present between the given files.

The '*SkipNum*' vector list the lines which are chosen to be not transposed into the OpenDSS model due to various reasons. In the test model presented, lines *1505* and *2482* are removed because they are floating and could not be found by the algorithm.

This explains why, of the 2,493 LV lines listed in the raw GIS datasheet, 10 of them have not been transposed.

Furthermore, the variable '*linecount*' – that express the number of LV lines – is exported to the *mat* folder.

3.3.3.5 bus_cord_indexed.m

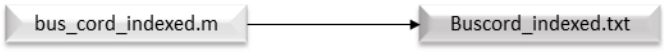

This script uses columns D, E, F, K from *CT – TRAFO* datasheet, columns B, E, G, H from *Linea BT*, columns F, G from *Segmento BT* and columns F, G, H from *Coordenadas Segmentos*.

It exports every bus of the network into the *Buscord_indexed.txt* file, with its proper X-Y coordinates. The file is readable by OpenDSS, which is then able to build the geographical shape of the model as in *Figure 3-1*.

3.3.3.6 source_ind.m

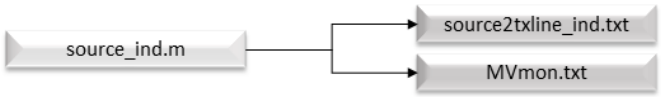

The script uses just columns A and F of the *CT – TRAFO* datasheet to create the *source2txline_ind.txt* file. In this file are built from scratch the 30 virtual MV lines that connect the source to the distribution substation transformers (MV side bus). All information regarding MV lines is described in section 3.1.1.2.

Simultaneously, the *MVmon.txt* file is built. It defines the PQ and VI monitor objects in bus 2 of each MV line, which is the MV side bus of the substation.

3.3.3.7 fuse_indexed.m

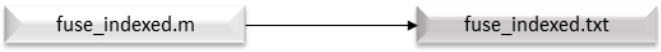

Here, columns A, D, E and G of *Fusible* datasheet are used to build the file *fuse_indexed.txt*, into which are transposed all the network embedded circuit-breakers. Note that every circuit-breaker labelled as 'Open' is commented with a '!' in the text file. In this way, OpenDSS does not implement that element into the model.

3.3.3.8 reactor_neutral.m

This simple script defines the earthing of the network. As explained in section 3.1.1.8, the network is grounded only at the transformer secondary bus with a small impedance of 5+j0.01 Ω.

Thanks to the versatility of OpenDSS and MATLAB, this script could be easily modified to reflect the necessities of the user.

3.3.3.9 transformer_indexed.m

Here, transformer components are defined. As previously said, buses regarding transformers are the ones from *1* to *30* (MV side buses) and from *31* to *60* (LV side buses). The first transformer is made of buses *1-31*, the second is made of buses *2-32*, and so on.

Through columns F, H, J and K of *CT – TRAFO* datasheet, the *Transformer_ind.txt* file is made, in which every information regarding the coupling of the buses is defined (as shown in section 3.1.1.3).

The variable '*txno*', defining the total number of transformers, is saved into *mat* folder for later purposes.

3.3.3.10 energymeter.m

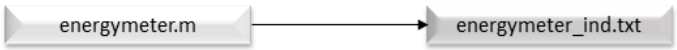

The script defines the energy meters that will calculate the energy consumption during the simulation. These are built on the bus 1 of every MV line, for a total of 30 elements, and exported in the file *energymeter_ind.txt*.

3.3.3.11 load_indexed.m

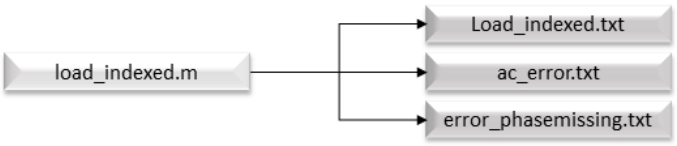

The last sub-script of *A_MakeNet.m* has the purpose of defining and connecting the load objects to the model. It uses columns B, C from *Acometidas* datasheet, columns A, K, R, T from *load.xlsx* file, and columns A, B from *phase meters.xlsx* file.

In here, the simplification anticipated in section 3.3.1.5 is carried out, through which network-to-load lines are removed and loads are directly connected to the main LV lines. Data regarding these new load connection points are all grouped into the '*bus1*' vector. If the required load connection point does not exist in the model, the bus is substituted in the vector with the value '*0*' and the load is exported into the file *ac_error.txt* as a reminder.

Then, proper phase (or phases) – with proper rated voltage (230/400 V) – are assigned to every load. Phases R, S and T from raw data are converted respectively to phases 1, 2 and 3 into the OpenDSS model. In the chance that a phase has not being defined in raw phase meter data (due to data inconsistency), the script assigns one random phase to the load and export its identification name to *error_phasemissing.txt* file as a reminder.

The resulting file – named *Load_indexed.txt* – contains the load elements readable by OpenDSS, from which are commented the 12 loads with bus '*0*'. Note that the values of the power absorbed through the 20-day period are defined in the *loadshape.txt* file, that will be built during the *B_MakeLoad.m* process.

3.3.3.11.1 Observations about 'load_indexed.m'

This script is not run throughout the normal routine even if it creates an essential file for the model. In fact, the file *Load_indexed.txt* is imported (already compiled) from a previous run during the preliminary actions of the *A_MakeNet.m* process. This is done possibly for two reasons:

- As mentioned in the article, two loads have been commented manually inside the text file. The reason has been verified to be the presence of floating loads that where not recognized by the MATLAB code. As a matter of facts, *Load7900* and *Load8070* [8] are connected respectively to buses *2553* and *2552*, which are related to lines that have been removed from the model due to being floating. The problem was not identified within the article, asserting to be a communication failure.
- Due to the random generation of phases of 291 loads, this script should be run just one time to avoid unwanted variation of the power flow results.

In this script a constant PF of 0.95 is chosen for every load. If it is of interest to implement the reactive power samples obtained in the raw GIS data, then it is necessary to convert the load elements to a variable PF format.

3.3.4 Load Curves Building Script: B_MakeLoad.m

The second part of the GOCT process uses the data located in the 7 files of smart meter hourly samples – *load1.xlsx* to *load7.xlsx* – to generate the 20-day period curve of every load. The flowchart of the process is shown in *Figure 3-7*.

The process makes use only of column A of *load.xlsx* and columns C and G of the 7 load samples files and still, the computation time is high due to the size of the raw files. The algorithm can be improved by adding the extraction and implementation of the reactive power, but further slowing down the process.

[8] An anomaly has been found in the article, in which are mentioned *Load7990* and *Load8070* instead. This was verified within the code.

If the user desires to apply its own synthetical load curves to the network, this algorithm can be avoided. In this case, the user should just define the *Loadshape.txt* file and link it to the proper curve values.

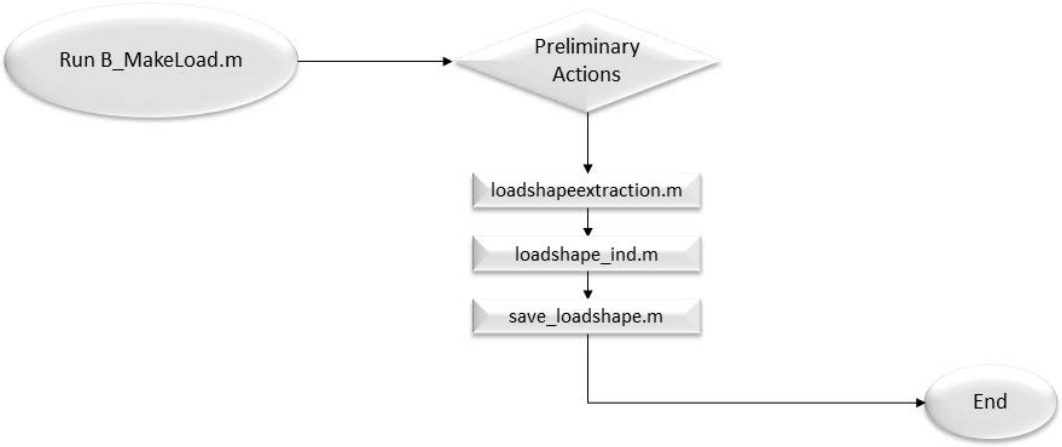

Figure 3-7*. Process of the algorithm B_MakeLoad.m.*

The preliminary actions consist into manually define the number of files to be analysed (that is 7, from *file1.xlsx* to *file7.xlsx*) and the number of days of sampling (20 in normal routine). Remember that this number must agree with the iteration value located in file *Master.dss*.

3.3.4.1 loadshapeextraction.m

This first script extracts every information needed from the raw data files to create the '*shape*' matrix, that contains 8,087 '*shape[#].hrs*' vectors, where # is the load ordered number. In every '*shape[#].hrs*' vector, the 481 hourly values representing the active power samples of that load are saved.

To simplify the process, the algorithm defines the curve only of the loads with exactly 481 data samples. If there are few or more samples, the load curve is replaced with null values. As observed in section 3.1.1.9, almost a thousand loads in the model have null values. For a clearer view of the facts, the user can refer to the '*fulldata*' and '*notfulldata*' vectors. The first lists the loads with exactly 481 samples, the second lists the others.

3.3.4.1.1 Observations and Anomalies on loadshapeextraction.m

It has been observed that during the process of building the '*shape[#].hrs*' vectors, a peculiar artifice has been done. In rows 29 and 30 of the MATLAB script has been found this check:

```
27 -  if (sum(m) == SampleCount)
28 -        LoadShape = pow1(m);
29 -       k = LoadShape > 1e3;
30 -       LoadShape(k) = LoadShape(k) * 1e-3;
31 -        shape(i).hrs(1 : SampleCount) = LoadShape;
```

"If the active power sample has a value higher than 1,000, it has to be divided by 1,000". To make sense out of this, it must be first understood that MATLAB uses the dots to explicit decimal digits of numbers. For some inapprehensible reason, in the raw GIS data files are used commas to explicit decimals, but only when the active power value is higher than 1. When the value is lower, dots are used instead. Therefore, this fix is made to compensate the fact that MATLAB recognizes the commas has indices of thousands. The solution chosen is risky and situational and it is important to be removed if the algorithm will be applied to any other data file.

Through the analysis of this script, two anomalies have been found. The first is located in row 18 of the MATLAB script, as shown:

```
17 - pow1 = xlsread(filename,'G:G');
18 - pow1 = pow1(2:end);
19 - n = length(pow1);
20 - text = text(2 : n + 1, 1);
```

As observable, the first number from the vector '*pow1*' is removed, probably with the purpose to remove the column label (imported from the excel raw file). This action should be deleted from the code because MATLAB already removed the first row autonomously. As consequence of this, the power samples are built misaligned with the loads, having the first sample of each load saved as the last sample of the previous load.

The second anomaly concerns the exportation of the power samples from the files. When defining the load curve, the samples are supposed to be chronologically ordered and no check of this kind is done within the code. However, it appears that in various occasions the samples are not disposed from the oldest to the most recent in the raw data files. Therefore, the user should properly sort the raw datasheets of the 7 samples files before running the process.

These two corrections have been applied in simulation *(c)* during the verification (section 3.4) of the paper.

3.3.4.2 loadshape_ind.m

This script builds the *Loadshape.txt* file which defines the number of samples of which the load curve is made. The active power values of each load shape are indexed in the *shape_#.csv* files (where # is the ordered number of each load), that will be built in the next script.

3.3.4.3 save_loadshape.m

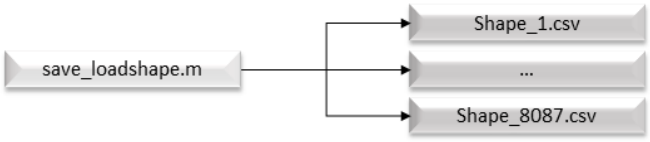

The data previously collected from the raw files are here exported inside the *day_20_profile* directory, into a number of *shape_#.csv* files equal to the number of loads (8,087). In each of these files the 481 samples of a singular load are collected, prepared in a vertical chronological order, from the older to the most recent one.

These files are called by *Loadshape.txt* and defines the active power absorbed by the load during each iteration of the power flow simulation.

3.3.5 Simulation and Elaboration Script: C_Run.m

The last algorithm runs the OpenDSS power flow analysis that elaborates the model built in the previous processes. Then, it elaborates the results obtained from the OpenDSS monitors, as shown in *Figure 3-8*.

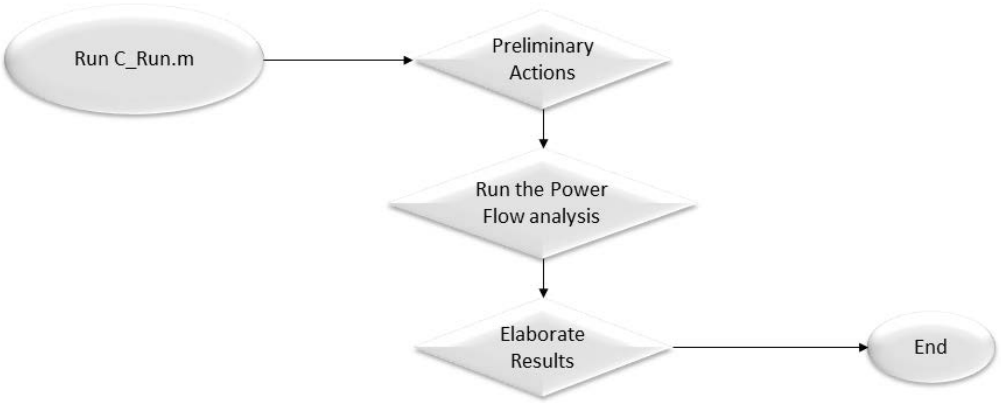

Figure 3-8. *Process of the algorithm C_Run.m.*

With the preliminary actions, the process clears the MATLAB workspace and initializes just the following variables: '*linecount*', '*txno*', '*notmonitored*', '*SkipNum*' [9].

Then, the MATLAB algorithm is connected to OpenDSS through the COM server and the *Master.dss* file is run. Here, OpenDSS software processes the 481 iterations of the power flow analysis, collecting the information of the network from the text files built with the previous algorithms and recording the results into the monitor and energy meter elements previously defined.

In normal routine, the network plot represented in *Figure 3-1* is built.

3.3.5.1 Elaboration of the Results

The results are exported from the OpenDSS monitors into two MATLAB matrices called: '*monitor_VI*' and '*monitor_PQ*'. Each matrix is built on 3 dimensions, representing the hours, the bus names, and the information, as shown in *Figure 3-9*.

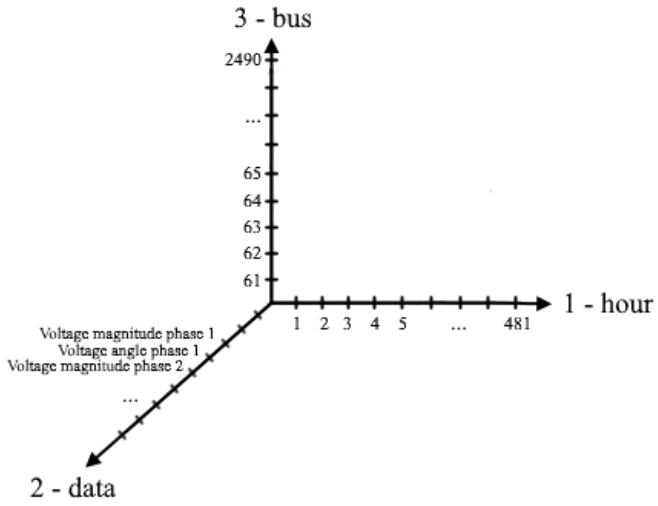

Figure 3-9. *'Monitor-VI' three dimensional matrix.*

The first dimension identifies each hour of the analysis – which are the number of iterations – with values ordered from 1 to 481 for both matrices.

[9] The variables *linecount* and *txno* are located in *mat* directory. The *notmonitored* and *SkipNum* vectors instead are manually written inside the algorithm. These should be made automatic to avoid oversights during tests.

In the second dimension are listed all the information the monitors have collected, which are the data presented in *Table 3-20* and *Table 3-21*, respectively for '*monitor_VI*' and '*monitor_PQ*' matrices.

***Table 3-20**. Data indexing of dimension 2 in 'monitor_VI' matrix.*

1	Hour/iteration number		
2	-		
3	Voltage magnitude (V) of phase 1	**11**	Current magnitude (A) of phase 1
4	Voltage Angle (degrees) of phase 1	**12**	Current Angle (degrees) of phase 1
5	Voltage magnitude (V) of phase 2	**13**	Current magnitude (A) of phase 2
6	Voltage Angle (degrees) of phase 2	**14**	Current Angle (degrees) of phase 2
7	Voltage magnitude (V) of phase 3	**15**	Current magnitude (A) of phase 3
8	Voltage Angle (degrees) of phase 3	**16**	Current Angle (degrees) of phase 3
9	Voltage magnitude (V) neutral-to-ground	**17**	Current magnitude (A) of neutral
10	Voltage Angle (degrees) neutral-to-ground	**18**	Current Angle (degrees) of neutral

***Table 3-21**. Data indexing of dimension 2 in 'monitor_PQ' matrix.*

1	Hour/iteration number		
2	-		
3	Active Power (kW) of phase 1	**7**	Active Power (kW) of phase 3
4	Reactive Power (kvar) of phase 1	**8**	Reactive Power (kvar) of phase 3
5	Active Power (kW) of phase 2	**9**	Active Power (kW) of neutral
6	Reactive Power (kvar) of phase 2	**10**	Reactive Power (kvar) of neutral

The last dimension is reserved to the bus numeration (that coincides with the LV line index). The dimension length is of 2550, equal to the *linecount* value. This comprehends the 60 transformer buses (which values goes from *1* to *60*) and the 2,490 LV line buses (from *61* to *2550*) [10].

At last, the data collected are further elaborated to obtain an ordered database that is exported into the '*mat*' folder with the name *bus.mat*. In the file, data are stocked into multiple sub-directories represented in *Figure 3-10*. Note that voltage and current angles are not exported into this file. After this, the process is completed.

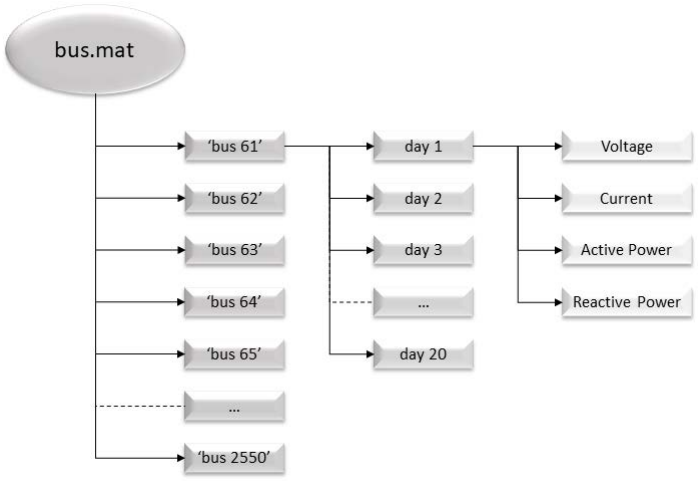

***Figure 3-10**. 'bus.mat' database.*

[10] The lines are in truth 2,493 but the last three LV lines (*2551*, *2552* and *2553*) are open, consequently their monitors are absent.

3.3.5.1.1 Observations on the Elaboration of the results

It is important to mention that the bus numbers are inverted inside the matrices and the *bus.mat* file. The first 2,490 arrays are reserved to the LV line buses, while the last 60 are empty. This is counterintuitive because, as an example, the monitored values of bus (and line) *500* are located in column 440 of the matrices. Therefore, the user must subtract 60 to the bus number of which they want to observe the data, obtaining in this way the right array in which the information is located.

Even though monitor elements have been defined for transformer and feeder buses, these values have not been exported to MATLAB nor elsewhere. This could be done with a code like the one used to build the two monitor MATLAB matrices.

3.4 Verification of the Results

The results presented in the article [22] by Koirala *et al.* is verified in this section, by comparing the graphical results published to those obtained through a new simulation of the same process. Furthermore, another power flow analysis is done after the corrections reported in section 3.3.4.1, id est:

- deletion of row 18 of the sub-script *loadshapeextraction.m*;
- chronological rearrangement of raw sample files (*file1.xlsx* to *file7.xlsx*) from the older to the most recent samples.

To represent the network, the authors chose to chart the values obtained by monitors of transformer 13 and LV bus 2113 – whose locations are highlighted in *Figure 3-11* – during day 1 and during a 20-day time period. The comparison, argued below, shows some anomalies on the results published by the researchers in the article.

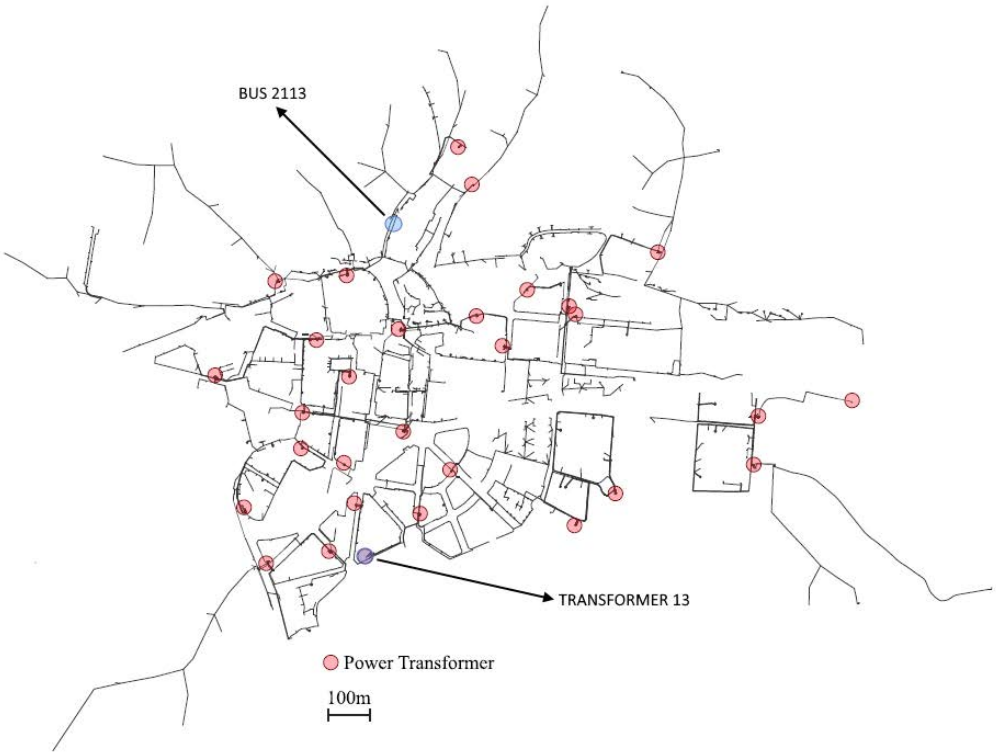

***Figure 3-11**. Locations of Bus 2113 and Transformer 13 in the test system.*

3.4.1 LV Line Monitoring

The terminal that has been chosen by the authors to be a representative example of the test system is bus *2113*, located at the end side of the homonym LV network line. *Figure 3-12* represents the voltages phase-to-ground and phase-to-neutral for each phase during day 1 (from hour 1 to hour 24), followed by the representation of the neutral-to-ground voltage. In this and every other figure of the section, the simulation cases are defined as follows:

- *(a)* displays the graphical results presented in the article;
- *(b)* shows the results of the unmodified power flow simulation;
- *(c)* shows the data after the corrections.

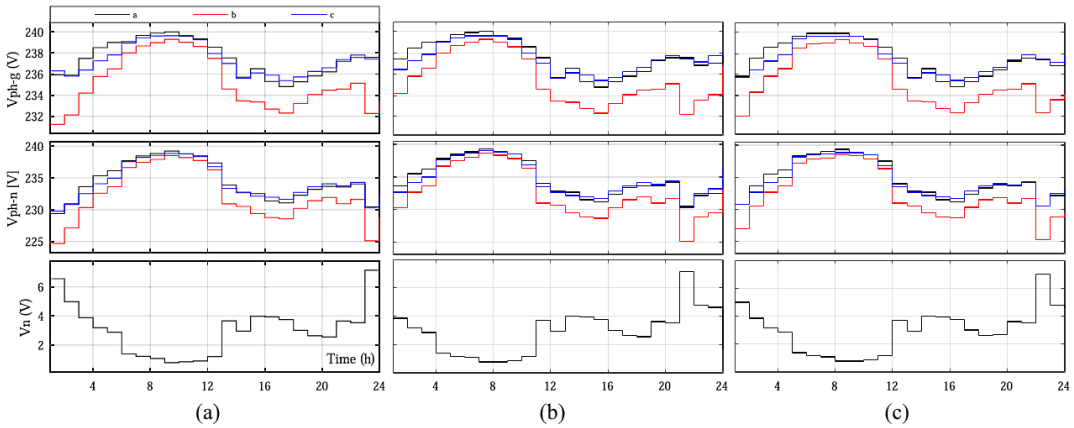

***Figure 3-12**. Voltages of bus 2113, monitored during day 1.*

Results obtained in simulations *(a)* and *(b)* are equal, except for a mismatch in the time axis of 2 hours. After applying the corrections – as illustrated in *(c)* – the mismatch is reduced by one. Furthermore, the voltage values slightly change due to the corrections in the load curves.

In *Figure 3-13* – representing the active power delivered through the LV line – the same observations can be noticed when the three simulations are compared.

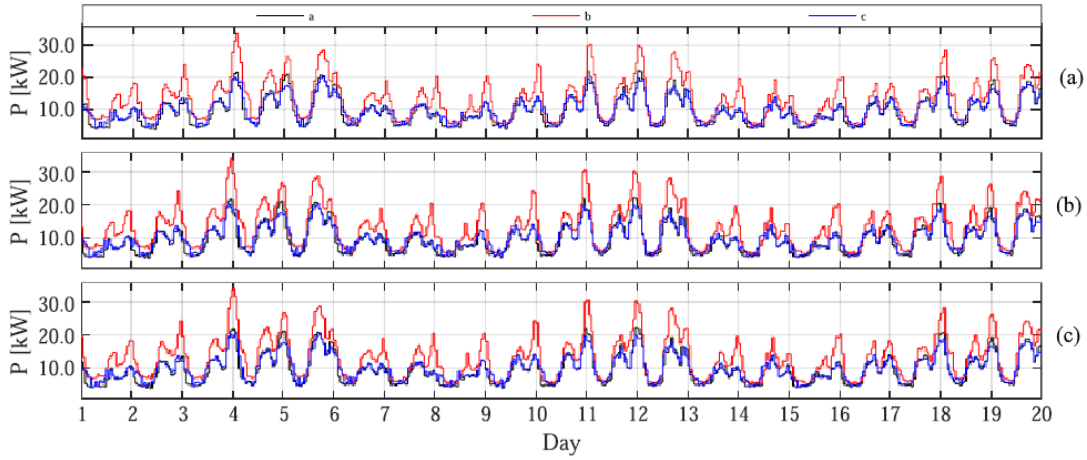

***Figure 3-13**. Active power delivered through bus 2113, monitored during a 20-day period.*

The mismatch is caused by two factors. One of the two is the '*pow*' vector correction (see section 3.3.4.1), which causes a mismatch of one hour. The other is likely due to a misalignment between the time axis values and the voltage values chosen to be represented. Since between simulations *(a)* and *(c)* there is just one hour of mismatch, it follows that the '*pow*' correction was probably already in place within the article simulation.

Altogether, the results obtained in bus *2113* are confirmed in simulations *(b)* and *(c)*.

3.4.2 Transformer Monitoring

The other representative example chosen for the model is the bus at the LV side of the substation transformer number 13. The voltage and power results presented in the article through the first day of power flow analysis – shown in *Figure 3-14 (a)* – are totally inconsistent compared to simulations *(b)* and *(c)*. Voltage ratings are out of expectations and the curves are not compatible.

For the same reasons as before, between simulations *(b)* and *(c)* there is a mismatch of 1 hour.

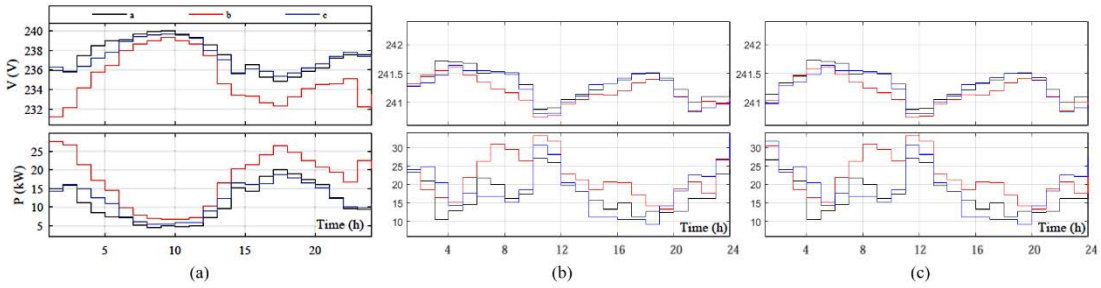

***Figure 3-14**. Phase-to-ground voltages and active power delivered through Transformer 13, during day 1.*

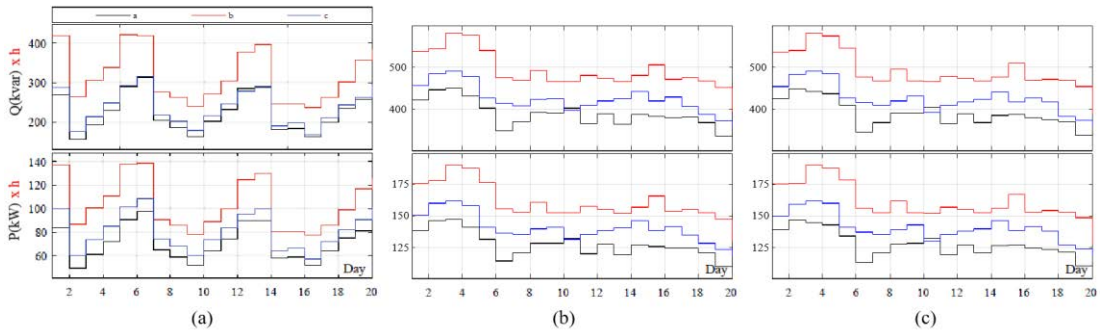

***Figure 3-15**. Active and reactive energy delivered through Transformer 13, during a 20-day period.*

In *Figure 3-15* are represented the active energy absorbed and the reactive energy committed through the transformer during the 20-day period[11]. The results are inconsistent also in this case and it has not been found any other transformer compatible with the results in *Figure 3-15 (a)*.

Then, the proper power flow results of transformer 13 has to be found in simulation *(b)* or – with the corrections – in simulation *(c)* of previous figures.

3.4.3 Total Power Consumption

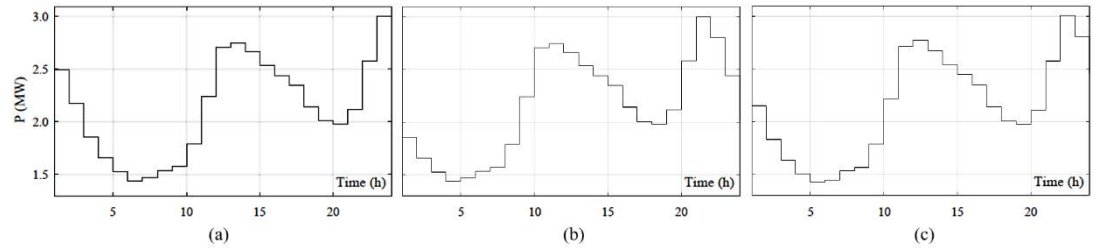

***Figure 3-16**. Total power absorbed by the network, during day 1.*

[11] An anomaly has been found within the article, with the ordinate axis being labelled as powers, but with numerical values suitable only for energy measures.

Lastly, the aggregated power consumption of the thirty substation transformers of the network is represented in *Figure 3-16*. The power values of the graphs refer to the sum of the delivered power during the first day of monitoring through the MV side bus of each transformer, without considering the MV lines power losses.

The compared graphical results have once again just the 2 hours mismatch anomaly, confirming the overall power consumption of the system.

3.4.4 Transformer loading

Results bring to evidence that the system is widely and heavily underloaded compared to what is expected from a typical European distribution network. In fact, in disagreement with the assertion in the article [22] – which states that typical loading values of distribution transformers are around 70% – the average loading of the simulated transformers is widely below expectation.

Figure 3-17 represent the average power delivered through each distribution transformer and its consequent loading factor, which ranges between 5% and 25%, with the highest value being 29% at transformer 12.

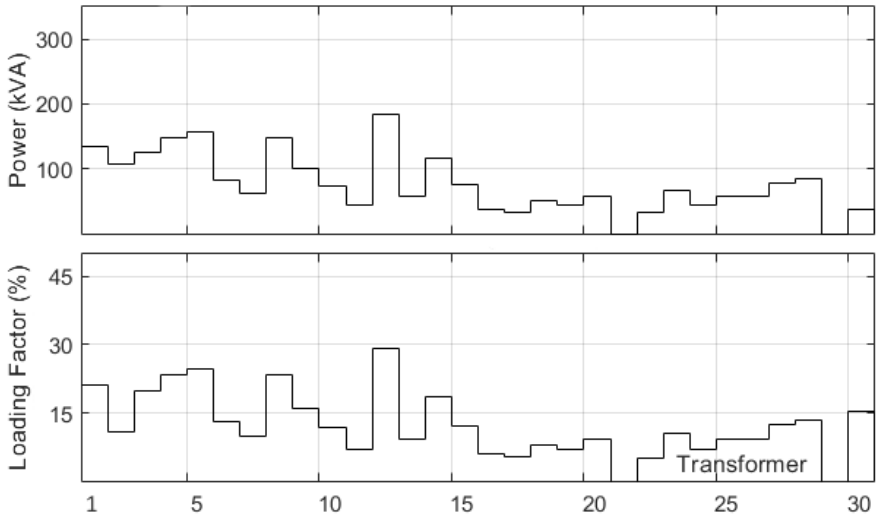

***Figure 3-17**. Average power delivered and loading factor of transformers, during a 20-day period.*

Even when the peak power delivered during the 20-day period and its peak loading factor are considered – as shown in *Figure 3-18* – the transformers result quite well underloaded. The highest loading value is indeed 46%, reached by transformer 1, while the other transformers range between 12% and 40%.

Note that *Figure 3-17* and *Figure 3-18* represent the network case *(c)*, with the corrections applied.

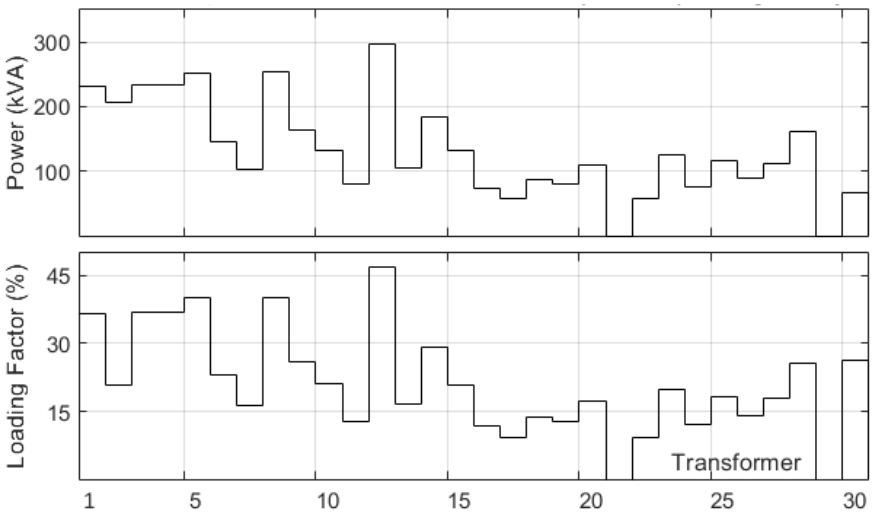

***Figure 3-18**. Peak power delivered and loading factor of transformers, during a 20-day period.*

In conclusion, the transposed network results heavily underloaded, and consequently not representative of the typical European scenario in regard to the power absorbed by loads. Due to this discrepancy, in Chapter 4 the load absorption will be increased to be more aligned to the European network conditions.

3.5 Table of Anomalies

Table 3-22 is a comprehensive list of every anomaly between what was found in the article and what has been observed within the GOCT code. It has been made to allows a fast reference by the user when needed.

It is important to highlight that these anomalies are referred only to what is written within the article and represent just a mismatch between the code published and the article itself. Therefore, they do not compromise the exceptionality and potentiality of the GOCT code and, consequently, of this work.

***Table 3-22**. List of the anomalies identified between the article and the GOCT code.*

Anomalies identified	Values explicated in the article	Values identified within the code
n. of buses transposed into the model	10,290	10,289
n. of monitored buses in the network	2,681	2,673
of which LV lines	-	*2,483*
of which feeders	-	*160*
of which transf. MV side	-	*30*
n. of feeders provided	-	252
of which transposed into the model	*161*	*160*
LV lines provided	-	2,493
of which transposed into the model	*2,490*	*2,483*
Power supplies (load connection points) provided	1,138	1,131
of which transposed into the model	-	*1,106*
Loads provided	8,087	8,087
of which transposed into the model	-	*8,073*
of which with non-null load shape	-	*7,188*
Resistance and inductance of MV lines	25 μΩ	250 μΩ
Transformer power rating values	100, 250, 630 kVA	250, 630, 1000 kVA
Location of bus 1 and 2 in *Acometidas* subfile	Columns C and D	Columns B and C
Loads manually commented in load_indexed.m	Load7990 Load8070	Load7900 Load8070
Article Figure 4 *(Figure 3-15)*	Inconsistent results. Power ratings out of expectation ranges.	
Article Figure 5 *(Figure 3-14)*	Inconsistent results. Voltage ratings out of expectation ranges.	
Article Figure 6 *(Figure 3-13)*	Mismatch of 2 hours in the results.	
Article Figure 7 *(Figure 3-12)*	Mismatch of 2 hours in the results.	
Article Figure 8 *(Figure 3-16)*	Mismatch of 2 hours in the results.	

4 Impact of PEV Loads and PV Distributed Generation in a European Suburban Residential Area

4.1 Fundamentals of the Simulation

This Chapter presents a new power simulation process that features residential photovoltaic (PV) plants and Plug-In Electric Vehicles (PEV) charged through household connections within the grid. The purpose of this simulation is to expose the high adaptability of the GIS to OpenDSS Conversion Tool (GOCT) by implementing synthetic elements to the simulation in a simple way through MATLAB. Furthermore, the implementation of PV distributed generation and loads representing PEV charging operations proves once more that an unplanned approach to the distribution system will inexorably lead to instability and unsustainability of the network as the penetration of the two increases.

In fact, and in accordance with Chapter 2, it is expected that the heavy daily mismatch between PV generation curve and PEV absorbed energy will lead to a daily 'duck-curve' similar to the one shown in *Figure 2-11*, with two very steep power ramps and a high gap between maximum and minimum power absorption. Then, voltage is expected to increase during daylight hours due to PV generation and worsen in the evening because of EV charging load, leading to a breach of the ±10% voltage standard limits. Furthermore, it is expected to have a reduction in power losses thanks to the local PV distributed generation at low penetration. On the contrary, an increase in power losses is expected at high PV penetration due to unnecessity of the power produced.

The next sections explain the modifications that have been made to the power system, and under which assumptions they have been defined. Note that the network is based on the corrected Non-Synthetic European Low Voltage System that has already been introduced in section 3.4, case (c).

This simulation process analyses only day 1 of the native test system, which correspond to 1st of May. The simulation is set on an hourly basis, from hour 0 to hour 24, which means 25 iterations in total. This has been defined because a test of multiple days would result redundant and would not give further interesting information for the purpose of this study.

4.1.1 Incrementation of the Loading Factor

In section 3.4.4 a deep discrepancy between the network loading factor and the typical European values at the distribution transformers was identified. The reasons for the network underload condition should be considered within the development planning of the area. However, this is of no concern for this study, and the residential suburban area under observation is adapted to fit the typical European loading factor values at the distribution transformers buses. The modification is done with the purpose to have a more rational power absorption when compared to the PV and PEV curves and to their penetration levels.

To reflect the typical 70% peak loading factor of European distribution transformers described in [22], a multiplicator factor has been added inside the *B_MakeLoad.m* script. In this way, the load profiles exported will have their power values multiplied by a constant factor that has been chosen to be:

$$MULT = x1.75$$

The multiplicator has been calculated to obtain 70% as maximum peak loading factor within the test network, corresponding to a power of 444.6 kVA. As shown in *Figure 4-1*, this value is reached by transformer 12 at hour 22.00.

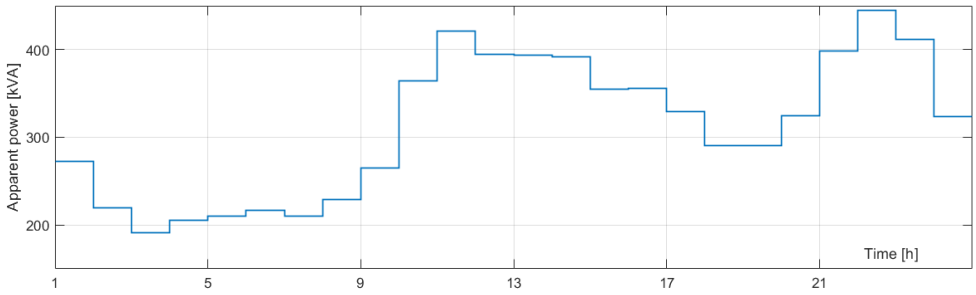

***Figure 4-1**. Apparent power of transformer 12 with multiplier applied during day 1.*

Based on this multiplier, the base energy absorption during day 1 – from hour 1.00 to hour 24.00 – is 90.9 MWh[12].

It should be noted that this operation aims to give a plausible medium-to-heavy loading condition to the network, which applies correctly to the main LV lines and to the distribution transformers. Single loads instead result in unlikely curves which do not accurately reflect real user consumptions in a quantitative way. However, this is of no heavy influence because the analysis focuses on the distribution side and not on the single users.

4.1.2 Implementation of PV Distributed Generation

PVDG has been implemented through a MATLAB script presented in Appendix A. The script is called *B2_Photovoltaics.m* and must be run after *B_MakeLoad.m* script.

First, the process creates an OpenDSS loadshape element (located in file *PV_Loadshape.txt*) that recalls an external file containing the PV daily power curve (*PVshape_3kw.csv*) that has been manually defined as described below. This file represents the hourly power injection of the generator elements.

After making the loadshape element, the script creates the OpenDSS generator elements. These elements are connected to many buses of the network (both 1-phase and 3-phase), where a load already exists, to simulate residential or commercial users with a household PV plant installed.

As referred in *Table 4-1*, the generator elements are indexed with the names *PV2*, *PV5*, … and located within the *PV_indexed.txt* file. For better understanding, the number in each generator name has been built to be correspondent to the load connected to the same bus. Then, every element is defined with a unitary PF (no reactive power is injected) and a generation curve described below.

***Table 4-1**. Examples of generator elements representing 3 kW PV plants, for PV penetration set to 5%.*

Generator name	Bus 1	N. of phases	Connected phase	kV	Power factor	kW (loadshape)	Data samples
PV2	1259	1	3	0.23	1	PVShape_3kw	481
PV5	1267	1	1	0.23	1	PVShape_3kw	481
PV7	1240	3	123	0.40	1	PVShape_3kw	481

An automation has been added to the code to facilitate the evaluation of different quantities of PV plants connected to the grid. By modifying the variable '*PVpen*', the user can choose the PV energy penetration level and the script will create a number of generators as close as possible to satisfy that value (but without exceeding it). The generators are homogeneously distributed through the network. In fact, plants are added regularly every *X* loads, accordingly to the load numeration order. The higher the PV energy penetration level, the lower the value *X* will be.

[12] For *base energy absorption* is intended the energy consumption of the network without considering the contribution part of PEV nor the reduction due to PV energy injection.

This solution considers the fact that the numerical order given to loads has a logical structure which can be exploited to have a homogeneously arranged distribution of PV generators throughout the whole grid. As an example of this, *Figure 4-2* shows the test network with PV plants – marked with red crosses – in a scenario with 5% PV penetration on the base energy absorption. In this case, 313 PV plants are installed, each one injecting a total of 14.5 kWh during a daily cycle.

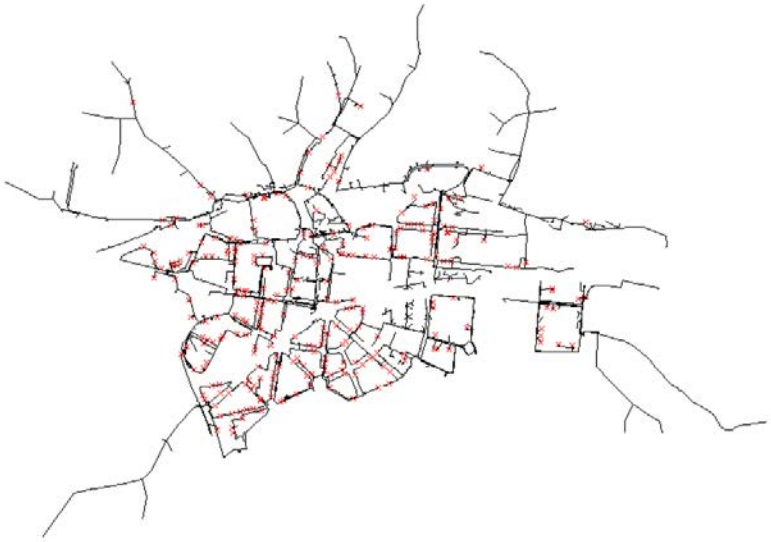

***Figure 4-2**. Network with implemented PV plants for a penetration of 5%.*

It is important to note that through this technique, at the variation of PV energy penetration into the network, the PV plants are connected to different loads. Therefore, their influence in small parts of the network may change slightly. Furthermore, due to the random connection between some loads and the network phases (data inconsistency explained in section 3.3.3), some PV connection phases do not match their own load phases. As a consequence, some LV lines could have an exaltation of their voltage asymmetry, with a slight increase in neutral-to-ground voltage.

4.1.2.1 Photovoltaic Generation Curve

Figure 4-3 shows the daily curve (*PVshape_3kw.csv*) used for generator elements. This shape has been chosen to represent a small household PV plant working during a sunny day of Spring in optimal conditions, with an installed capacity of 3 kW. According to this curve, the total energy injected into the network during a day cycle is 14.5 kWh, starting at 6.00 and becoming null once again at 20.00. The peak power injection happens at 13.00 and is equal to 2.1 kW.

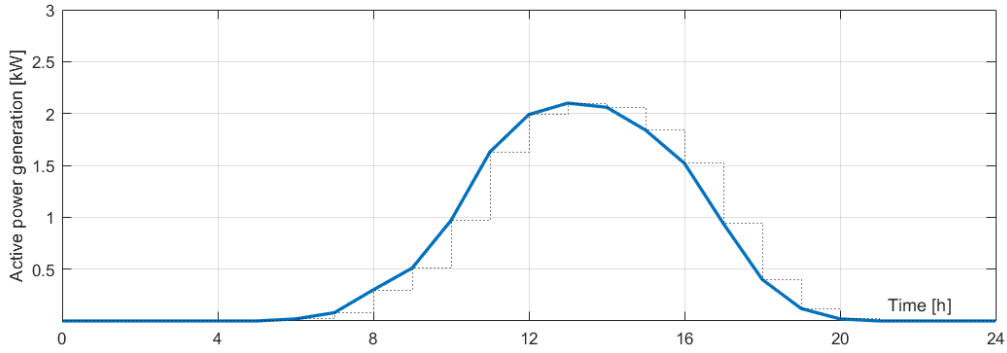

***Figure 4-3**. Daily generation curve of PV plants implemented in the network.*

The curve is based on generation profiles presented in articles [2, 27]. This shape is commonly used as representative solar production during a sunny Spring or Autumn day in central Europe-like climate conditions.

4.1.3 Implementation of PEV charging loads

EVs with plug-in charging system have been implemented with a similar procedure through MATLAB script called *B3_ElectricVehicles.m*, shown in Appendix B.

The process starts by creating two OpenDSS loadshape elements – located in file *EV_Loadshape.txt* – which recall to the two load curves defined manually in files *EVshape_slow.csv* and *EVshape_quick.csv*. They represent respectively the 3.3 kW Slow Charge mode and 11 kW Quick Charge mode, that are explained in the next section.

Then, the script generates the *EV_indexed.txt* OpenDSS readable file, that contains the load elements. EV loads are made to apply on already working load connection points as in a real grid. Therefore, EV are placed where a load already exists. The script checks if the connection is 1-phase or 3-phase and consequently applies the Slow or Quick Charge curve.

As represented in *Table 4-2*, EV load elements are indexed *EV7*, *EV14*, …, with their number correspondent to the base load connected to the same bus. In addition, their connected phase is the same of their base load and their PF is set to 0.98.

***Table 4-2**. Examples of load elements representing the charge of EV battery packs for EV penetration set to 5%.*

EV load name	Bus 1	N. of phases	Connected phase	kV	Power factor	kW (loadshape)	Data samples
EV7	1240	3	123	0.40	0.98	EVshape_quick	481
EV14	1247	1	3	0.23	0.98	EVshape_slow	481
EV21	1247	1	2	0.23	0.98	EVshape_slow	481

As before, an automation has been added to facilitate testing at different EV penetrations through the variable '*EVpen*'. A homogeneous distribution of the EV charging locations is made, at the cost of not having control on how many connection points work at Slow Charge and how many at Quick Charge.

The same weaknesses analysed in the PV script can be observed. Once more, the main interest of this simulation is to demonstrate the potential behind this tool and to have a general verification of the incompatibility between PV plants and unregulated residential EV charging from the distribution transformer point of view. Therefore, their influence on the results is minimal, and it is possible to ignore them.

Figure 4-4 shows the test network with EV charging locations – represented by blue crosses – in a scenario with 5% EV penetration on the base energy absorption. In this case, 113 charging stations are working, of which 14 are set on Quick Charge mode.

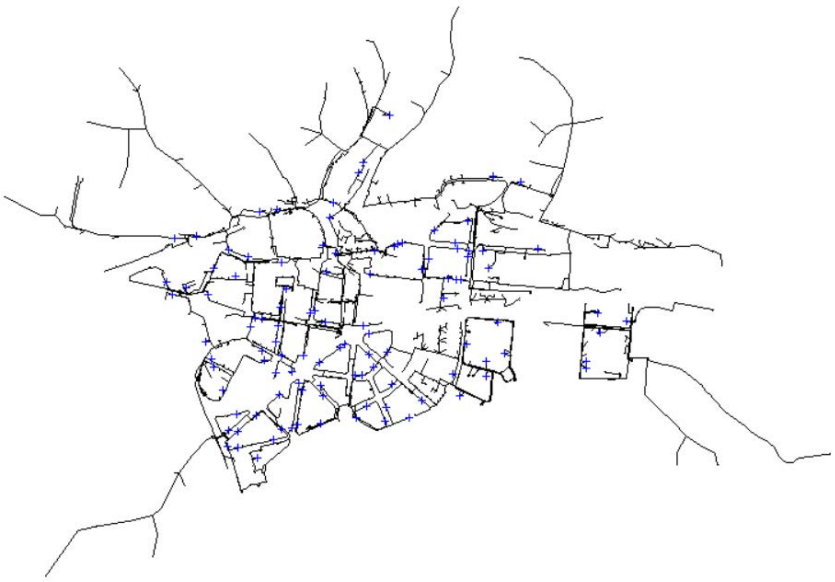

***Figure 4-4**. Network with implemented EV charging connection points for a penetration of 5%.*

4.1.3.1 Electric Vehicles charging curves

Two different load curves – shown in *Figure 4-5* – have been chosen to represent the charging process of the EVs through the grid during the day. Both curves drain the same energy from the network, which represent the charging of a 40-kWh battery pack to full capacity. The battery packs are totally discharged and are plugged to the grid at 18.00, typically when users return to their houses after a working day. The difference between the two concerns the maximum power deliverable. More specifically:

- Curve *(a)* represents a slow household charging point connected as a 1-phase load, which is called Slow Charge. The maximum power deliverable is 3.3 kW, resulting in a power absorption from the network of several hours, that concludes only at hour 8.00 of the next day.
- Curve *(b)* represents a faster charging station connected as a 3-phase load and often called Quick Charge. The maximum power deliverable in this case is 11 kW, that is a considerable power absorption with a shorter charging time of 5 hours (last non-null value of the curve at 22.00).

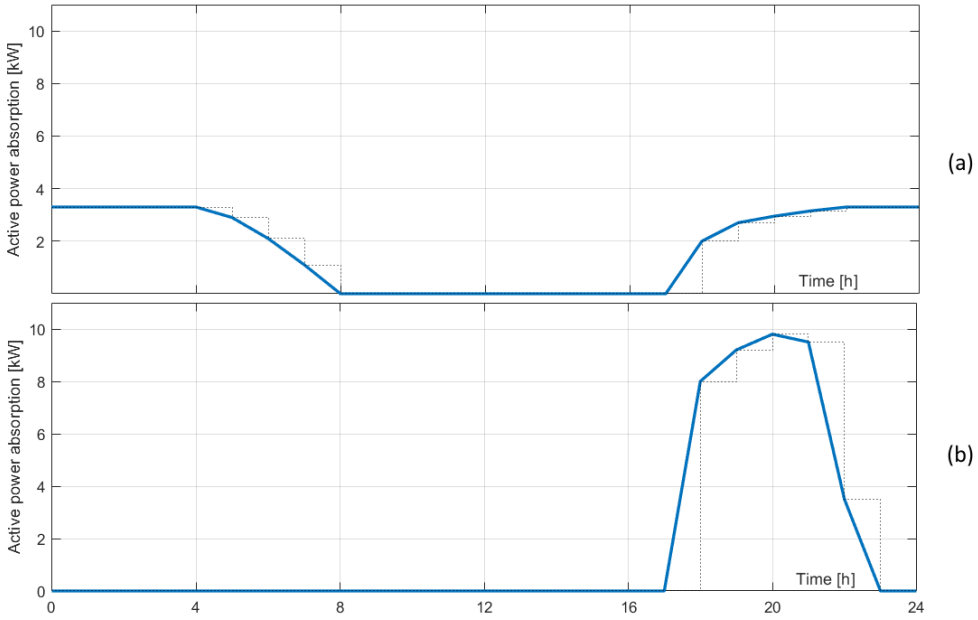

***Figure 4-5**. (a) Slow Charge of a 40-kWh battery pack. (b) Quick Charge of the same battery pack.*

The EV related considerations made in this section are based on the International Electrotechnical Commission (IEC) standards 61851 and 62196, which define the EVs charging modes, connection cases and plug types. Furthermore, the curve shape has been created accordingly to [61], in which is analysed the power absorption as a function of the State of Charge of the battery pack, reported in *Figure 4-6*.

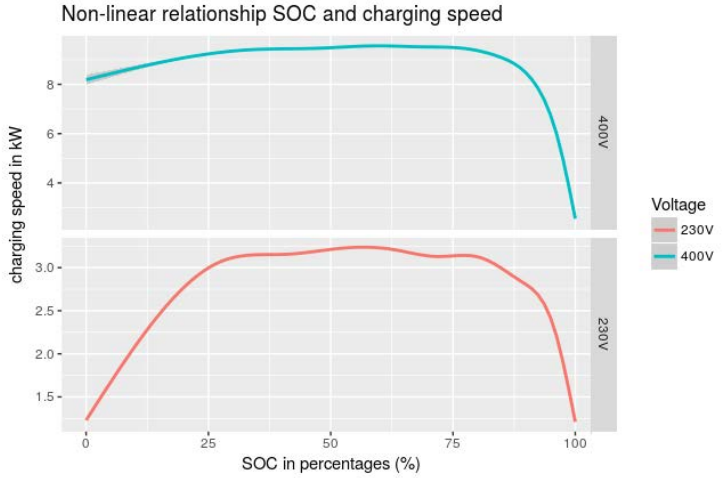

***Figure 4-6**. Charging of a battery pack in relation to its State of Charge (SOC) [61].*

4.1.4 Cases of Study

In the next sections of this Chapter, multiple study cases are analysed. Case A0 represents the network at the base load conditions with the load multiplier described above, but without any PV plant or EV load implemented. Cases from B1 to B5 analyse the network with a progressive increment in PV distributed plants, from 20% to 100% penetration level on the base energy absorption. Cases C1 and C2 retrace respectively simulation A0 and B5 with the addition of distributed loads representing PEV charging operation for a penetration of 15% on the base energy absorption, which consists in a very stressful condition[13]. *Table 4-3* summarizes the cases of study analysed.

***Table 4-3**. Cases of study.*

Case	PV penetration [%]	EV penetration [%]
A0	0	0
B1	20	0
B2	40	0
B3	60	0
B4	80	0
B5	100	0
C1	0	15
C2	100	15

4.2 Case A0: Simulation with Base Energy Consumption

The first simulation is made without implementation of PVDG nor EVs, but only with the multiplier at the base energy consumption explained in section 4.1.1 (and set to *x1.75*). While the PVDG and EVs effects on the network are being analysed, this simulation is referred as the study basis for proper comparison.

[13] This EV penetration value has been chosen to be consistent with what stated in article [16]. In fact, it is asserted that in Belgium, by 2030, around 8% PEV electric penetration will be achieved.

A total of 8,073 loads are connected to the test system, of which 7,188 have a non-null curve as referred in *Table 3-22*. The overall active energy consumption of the network during the first day of analysis, once set the multiplier, is **90.9 MWh** at the MV side of the substation transformers, distributed through the day as shown in *Figure 4-7*.

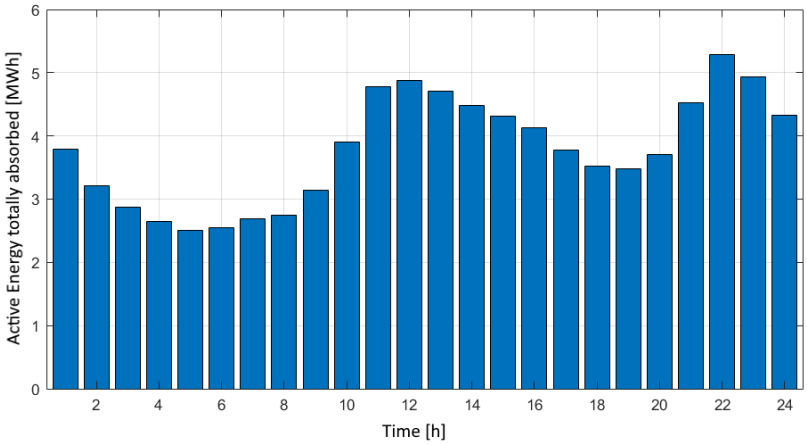

***Figure 4-7**. Cumulative active energy consumption of the network during the day.*

This consumption is inclusive of active energy absorbed by the load and network losses[14]. Then, by a simple aggregation of the power values of the load curves, the active energy absorbed by the users results to be **89.8 MWh**. In this way, the overall energy losses W_{loss} of the network can be obtained through the simple formula:

$$W_{loss} = W_{tot} - W_{load} = 1.16\ MWh\ ,$$

which in percentage results:

$$W_{loss\%} = W_{loss}/W_{tot} * 100 = 1.28\ \%\ .$$

Where W_{tot} is the total active energy absorbed by the network measured at the MV side of transformers and W_{load} is the total active energy absorbed by the load.

4.2.1 Transformers Loading Factor

Figure 4-8 shows the energy consumption at transformers during day 1 – from hour 1.00 to hour 24.00 – in a box and whiskers plot. Each one of the 30 boxes represents its relative substation transformer values. The box is defined by the median value of the day (red line) and the quartiles (blue horizontal lines). The 'whiskers' reach the maximum and minimum values, at the exception of the ones represented by red crosses, which denote outlier values that are exceptionally high or low compared to the others.

[14] Network losses includes both line losses and transformer losses.

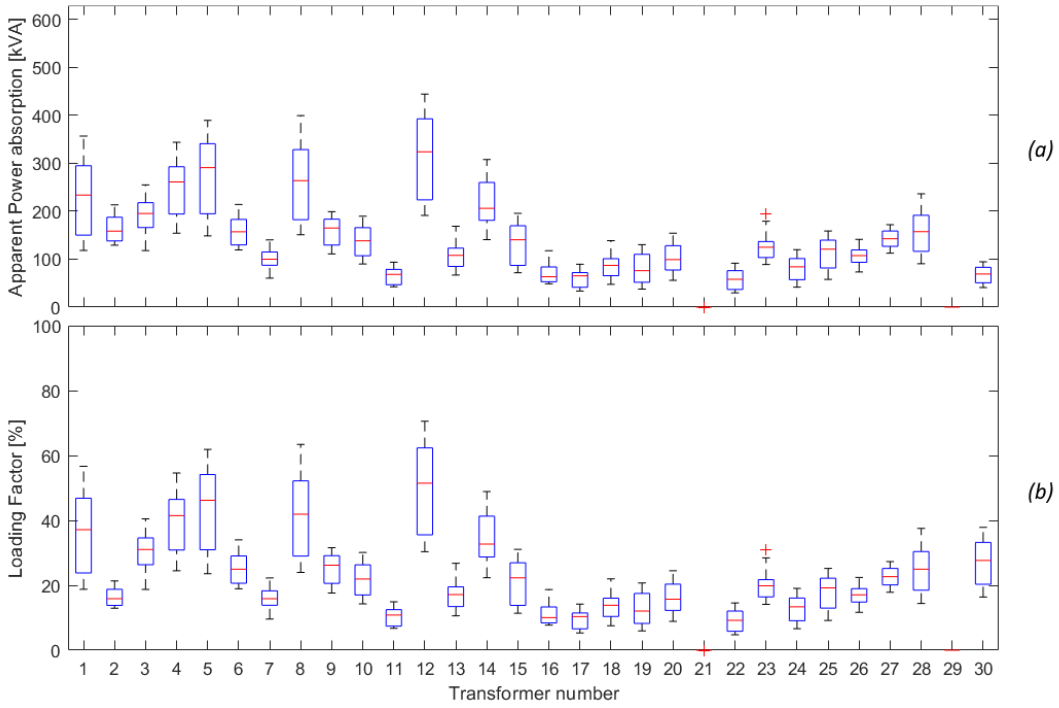

***Figure 4-8**. Apparent power (a) and loading factor (b) of each substation transformer during the day.*

Plot *(a)* represents the apparent power injected in the network at the MV side of the substation transformers. Instead, plot *(b)* shows the transformer loading factor through the day, bringing attention to the ratio between the power injected and the maximum power deliverable, which is defined by the rated value of each transformer. Specifically, transformer number 2 has a rated power of 1'000 kVA, transformer number 30 has a rated power of 250 kVA and the others have all a maximum power deliverable of 630 kVA.

As already anticipated in section 4.1.1, the peak power is 444.6 kVA, reached by Transformer 12 at hour 22.00 and corresponding to a loading factor of 70%. However, power is on average much lower, with maximum values normally between 20% and 40% of their rated power, and median values between 10% and 30%. Transformers that exceed these values are transformer number 1, 4, 5, 8, 12 and 14, which are considered under heavy load condition.

4.2.2 Lines Voltage Drop

The voltage is set to 240 V at the substations, but the rated voltage of the European network is 230 V. This discrepancy is probably due to (On-load or No-Load) Tap Changer transformers that are set to a higher value to compensate the voltage drops that are expected at the furthest buses during heavy load hours. Then, accordingly to the ±10% ranges, the higher voltage limit is 253 V, and the lower limit is 207 V.

The LV bus in heaviest working conditions is bus *2075*, whose voltage is shown in *Figure 4-9*. *(a)* refers to its phase-to-neutral voltage, whilst *(b)* refers to its neutral-to-ground voltage. Phase 1 is represented by the black line, phase 2 by the red one, and phase 3 by the blue one. The thicker line – corresponding to the red one – is the line that reaches the lower value, that is the one with heavier conditions. The minor value reached by phase 2 is 218.7 V at hour 16.00, which is 0.95 per units (pu).

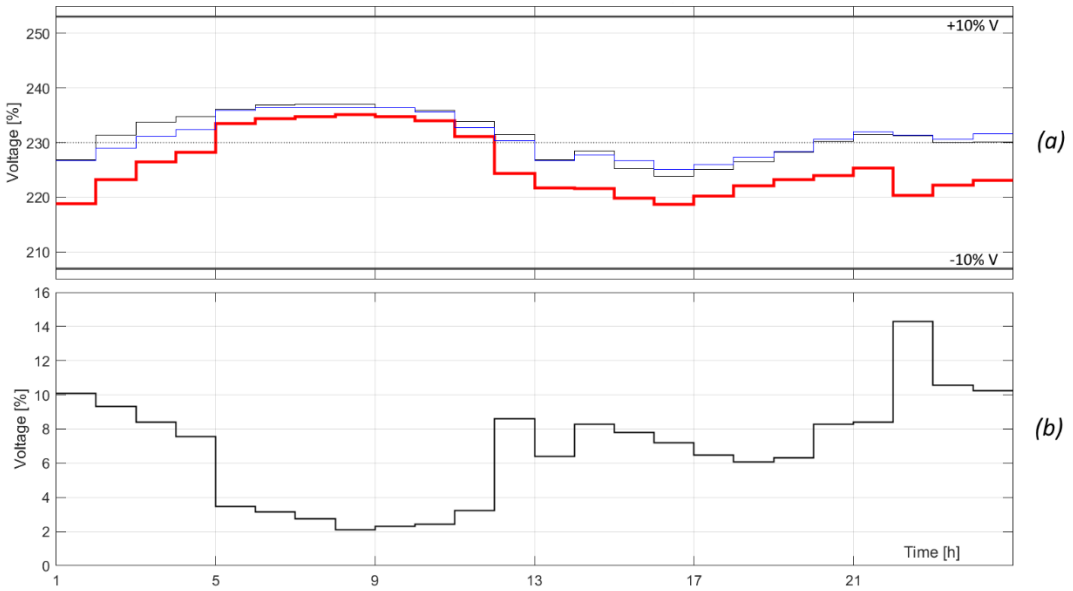

***Figure 4-9**. Bus 2075 voltage daily profile. (a) phase-to-neutral. (b) neutral-to-ground.*

It can be observed that the 3P4W system is quite unbalanced at the bus, directly affecting the neutral-to-ground current. In fact, the highest neutral voltage is reached at 22.00 and it is equal to 14.29 V, an unignorable value.

In conclusion, the voltage against distance profile of every branch of the network is represented in *Figure 4-10*. The measurement of the distance is made starting from the upstream buses of the thirty MV feeders to the furthest ones. The graph shows the network during hour 22.00, which is the worst-case scenario in regard to the maximum voltage drop, that is the heaviest load condition. Each dotted line represents one of the conductors: black for conductor 1, red for conductor 2 and blue for conductor 3. The ordinate axis shows the bus voltages in pu values, where the base voltage is 230 V. Finally, the thicker red horizontal axes represent the maximum and minimum voltage allowed by standards during normal working conditions of the grid.

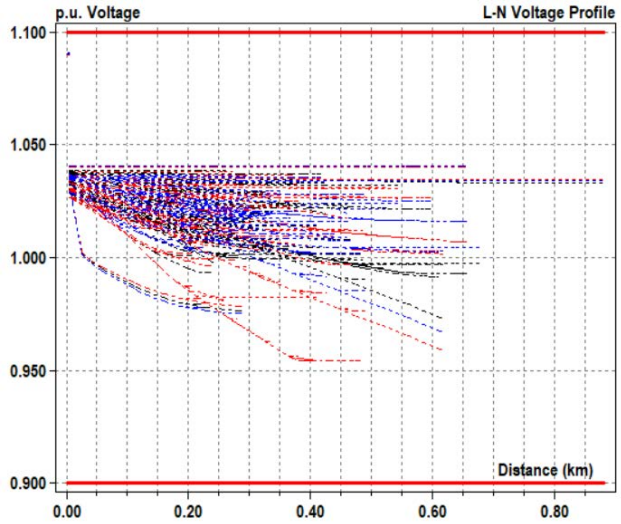

***Figure 4-10**. Voltage drop of network LV lines at hour 22.00.*

From the graph, it is evident that the network can fully withstand the *MULT* load incrementation during every hour of the day. However, it needs to be pointed out that the voltage incrementation at substation level – from 230 V to 240 V – with tap changers is desirable to avoid voltages near the lower limit.

4.3 Cases B1 to B5: Simulations with PV Generation Implementation

In the following simulation cases, small PV plants are implemented progressively with the purpose to exemplify how a distributed generation can influence the distribution LV network. The PV plants are implemented with the criteria explained in section 4.1.2, and the cases chosen to be representative of the network are presented in *Table 4-4*.

***Table 4-4**. PV plants installed for PV study cases.*

	PV Penetration [%]	PV energy generated [MWh]	Number of PV plants installed
Case B1	**20** (20.00)	18.2	1,254
Case B2	**40** (39.98)	36.4	2,507
Case B3	**60** (59.99)	54.6	3’762
Case B4	**80** (79.97)	72.7	5’015
Case B5	**100** (99.97)	90.9	6’269

Cases B1 and B2 represent situations with moderate and high PV penetration levels in respect to the actual definitions [3]. Cases B3 to B5 instead represent ideal situations that could be reached in the future, with a very heavy PVDG implementation in the network. In particular, case B5 refers to the Net Zero Energy condition, where the energy absorbed by the load and produced by PV plants have a daily net sum equal to zero.

The number of PV plants installed varies for each case, with a maximum of more than six thousand plants homogeneously distributed in the network grid in case B5. Each PV plant produces 14.5 kWh per day distributed with an almost parabolical load curve that starts at hour 6.00 and end at 20.00, with production peak at 13.00 (discussed in section 4.1.2). As expected, due to the demand-production discrepancy, from heavy PV penetration cases, multiple undesirable side effects arise. The ones that have been identified through this analysis are:

- inversion of the power flow at transformers;
- increase in transformers loading factors;
- increase in power losses through the lines;
- increase in the daily power and voltage ripple;
- presence of steep power and voltage ramps during the day.

These side effects imply a new and strong factor of instability within the network.

Figure 4-11 illustrates the aggregated energy absorbed by the whole network during day 1 measured at the MV side of the substation transformers, accordingly to the different PV penetration levels simulated. It is observable that in cases B3 to B5 results an incremental excess of energy that flows towards the MV grid and this power inversion can lead to frequency imbalance of the network. Case B2, corresponding to 40% PV penetration, is the optimal case. In fact, the energy absorption of case B2 is almost null during midday hours, making this case an optimal choice to obtain load compensation without having a sustained power inversion during strongly irradiated hours.

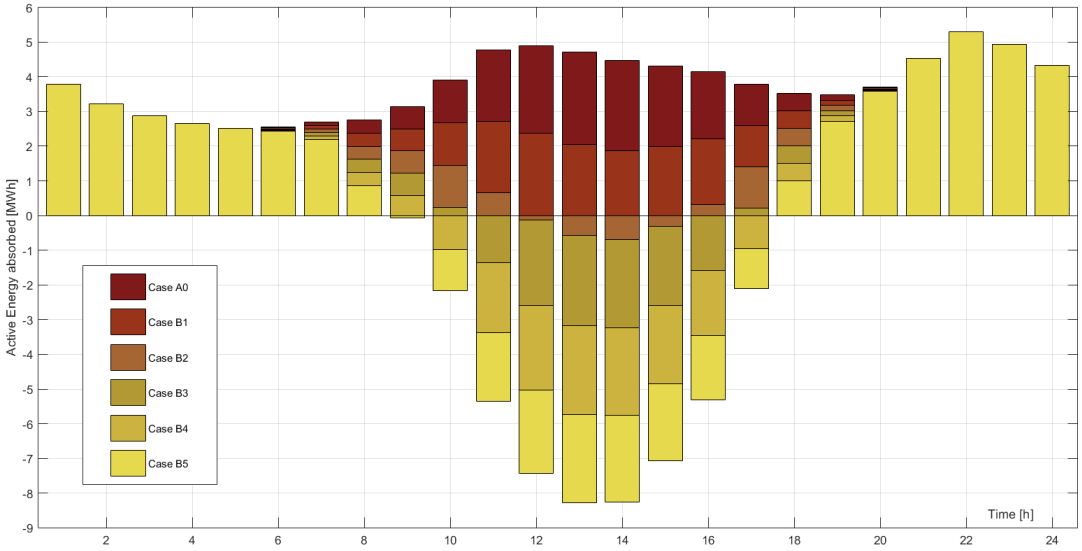

***Figure 4-11**. Aggregated energy consumption of the network during the day. PV implemented cases.*

Furthermore, due to the local power production-absorption cycle, case B2 is also the optimal condition to have minimum network power losses. In *Table 4-5* power losses for each case are calculated. Case A0 has **1.28%** total power losses through lines and transformers, which is reduced to **1.07%** in case B2. It is observable that due to the power inversion, cases B4 and B5 have power losses conditions worse than case A0.

Consequently, case B2 is an optimal condition to avoid sustained power inversion, but also to reduce line power losses within the LV grid.

***Table 4-5**. Power production, absorption, and losses for each PV case of study.*

	W_{tr} [MWh]	W_{PV} [MWh]	W_{tot} [MWh]	W_{base} [MWh]	W_{EV} [MWh]	W_{load} [MWh]	W_{loss} [MWh]	$W_{loss\%}$ [%]
Case A0	90.9	0	90.9	89.8	0	89.8	1.16	**1.28**
Case B1	72.6	18.2	90.8	89.8	0	89.8	1.00	**1.10**
Case B2	54.4	36.4	90.7	89.8	0	89.8	0.98	**1.07**
Case B3	36.4	54.5	90.9	89.8	0	89.8	1.16	**1.28**
Case B4	18.6	72.7	91.3	89.8	0	89.8	1.52	**1.67**
Case B5	0.9	90.9	91.8	89.8	0	89.8	2.00	**2.18**

In the table, the total active energy absorbed by the network W_{tot} is the sum of the energy W_{tr} delivered at the transformers MV side and the energy W_{PV} produced by the solar plants. Instead, W_{load} is constant and defined just by the base load W_{base}, while the energy W_{EV} absorbed by the EV charging stations is null.

4.3.1 Transformer Loading Factor

Transformer 4 of the simulated network is chosen for the analysis as it experiences medium-to-heavy load conditions. In case A0, transformer 4 has a maximum peak power of 343.9 kVA at hour 22.00. Its power rating is 630 kVA and consequently the maximum power factor reached is 54.6%.

The graph below (*Figure 4-12*) represents the apparent power through the MV side of the substation for each simulation made. Case A0 presents a curve with slow ramps during morning and afternoon, with two peaks at hours 13.00 and 22.00. The midday apparent power peak decreases with case B1 and reaches a minimum with case B2 (104.2 kVA at hour 13.00). Apparent power starts to increase again with case B3, exceeding the starting power peak in case B5. In fact, in the last case two maximum peaks

are observed, but also two deep depressions are present around hours 9.00 and 17.00, with consequent steep power ramps throughout the day.

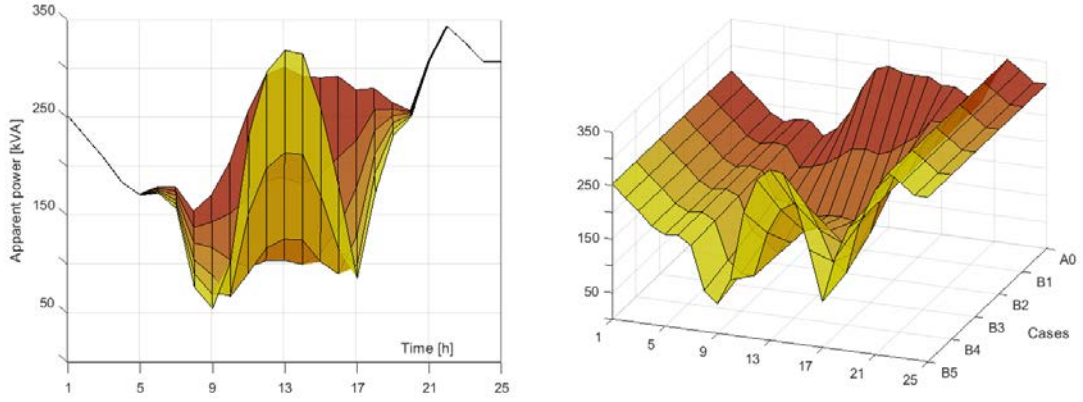

***Figure 4-12**. Apparent power of transformer 4 (MV side) during the day. PV implemented cases.*

The maximum apparent power peak is still at hour 22.00, and the maximum loading factor is unchanged. The apparent power behavior during sunny hours is a direct consequence of the active power inversion described above, resulting in case B2 to be once more the best condition. Note that apparent power values never reach zero because of the reactive power committed by the load, which is not supplied by PV plants. As a matter of fact, reactive power is always supplied by the MV network through the substations.

Figure 4-13 compares the loading factor (and apparent power) of transformer 4 of every case with a box and whiskers plot. As previously discussed, the maximum loading factor value is 54.6%, unaffected by the PV plants. The median value has instead a parabolical trend, with minimum reached in cases B2 and B3 around 28%. Lastly, the minimum loading factor keep decreasing, reaching a value of 8.8% in case B5.

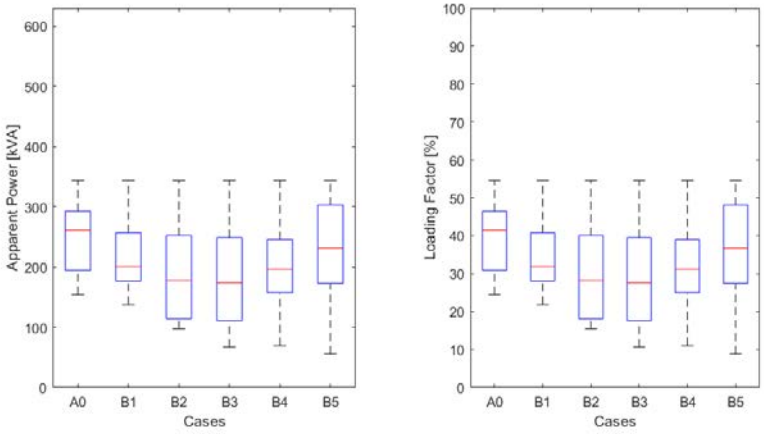

***Figure 4-13**. Apparent power (left) and loading factor (right) of transformer 4 during the day. PV cases.*

Therefore, an average loading factor reduction of transformers can be achieved with a proper PVDG penetration. This can be valuable in order to reduce the daily hours in which a transformer operates in heavy conditions. On the other hand, the difference between the maximum and minimum loading factor values increases with PV penetration, bringing the network towards a less constant power flow, with steeper slopes and sharper peaks. This involves a more complex energy market management that – considered the intrinsic uncertainty of PV technology, as well as other RESs – will have lower predictability and higher need for timely interventions.

4.3.2 Line Voltage Drop

To further analyse the consequences of an incremental PVDG penetration, it has been chosen bus *850* as representative of the possible risks for the network. The bus chosen is part of the grid connected to substation transformer 5, which works on heavy load conditions. The locations of both bus and transformer are shown in *Figure 4-14*, together with the location of transformer 4, previously discussed.

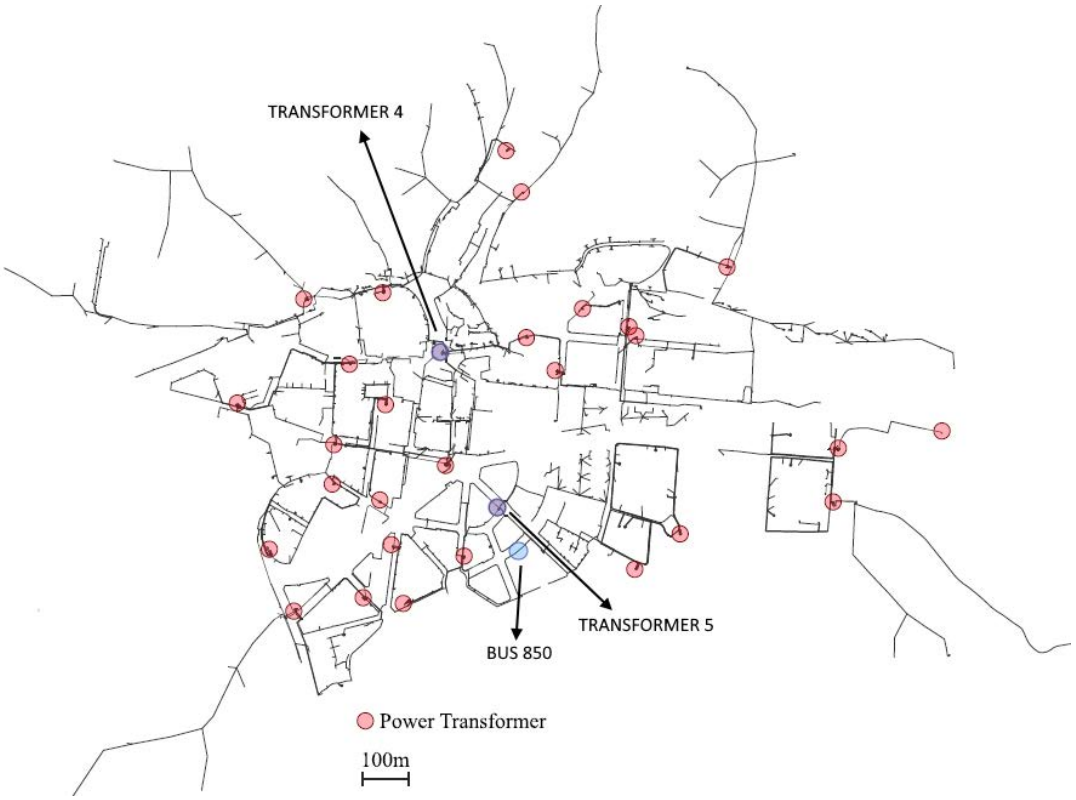

***Figure 4-14**. Locations of transformer 4, transformer 5 and bus 850 in the test system.*

Figure 4-15 represents the voltage behavior of bus *850*: *(a)* compares its phase-to-neutral voltage along the day[15], and *(b)* represents its neutral-to-ground voltage. The profile of case A0 present two soft voltage depressions: one during midday and the other during the evening. In respect to the transformer voltage, which is 240 V, the bus has lower values, but fully within the limits. As the PV penetration increases, the midday voltage depression flattens (cases B1 and B2) and then increases until it exceeds the voltage maximum limit in case B5.

[15] *Figure 4-15 (a)* refers only to phase 1 of bus *850* for clarity, but similar graphs could be made for the other two phases.

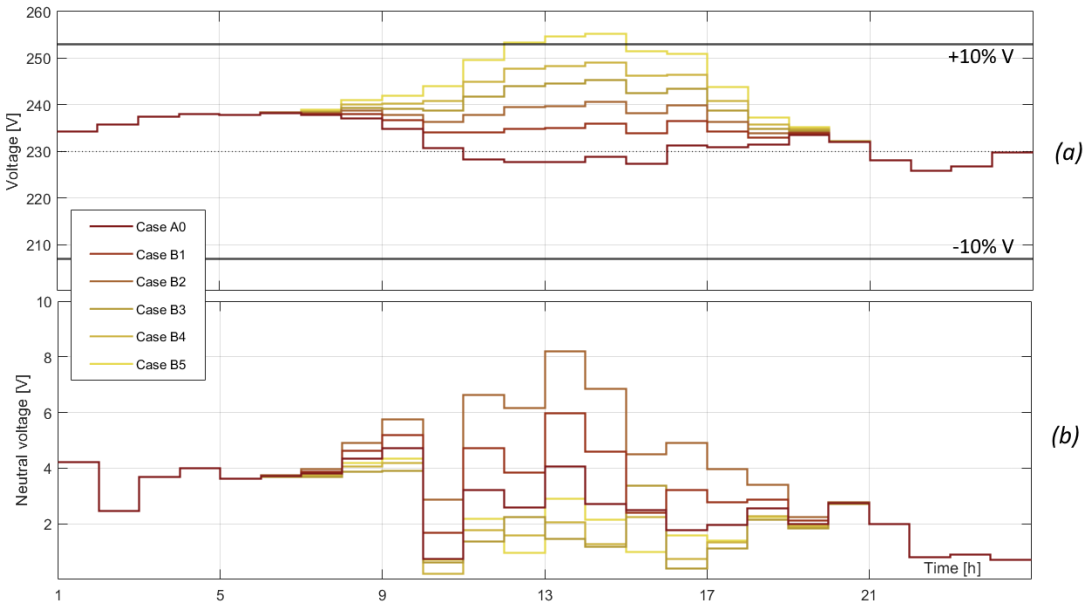

***Figure 4-15**. Bus 850 voltage daily profile on PV implemented cases. (a) phase-to-neutral. (b) neutral-to-ground.*

Decreasing the voltage to 230 V at substation transformers could solve the peak power at high PV penetration rates but would consequently worsen the network voltage condition during high demand hours without PV generation. For the case of this bus, cases B1 and B2 improve the voltage profile, reducing voltage ramps and smoothening the midday depression, but without affecting the evening one.

The neutral-to-ground voltage shows a peculiar behavior with the incrementation of the PV penetration. During the midday hours, the voltage increases in cases with moderated PV generation – which are cases B1 and B2 – but decreases to almost zero in cases B3 to B5, when the PV generation is very high. This seems to be symptomatic of the distribution homogeneity of 1-phase PV plants, which increases with the PV penetration value.[16] For this factor, a highly distributed PVDG network seems to be preferable, rather than a grid with few 1-phase PV plants with high nominal power.

Finally, the voltage against distance profile is represented in *Figure 4-16*. Each graph shows a simulation during hour 13.00 of the day, which is the worst-case scenario in regard to the overvoltage due to PV generation. As before, black, red and blue dotted lines represent respectively conductors 1, 2 and 3 of each LV line. The thicker red axes represent minimum and maximum voltages allowed during normal network conditions, which are 207 V and 253 V.

[16] 1-phase rooftop PV plants increase the voltage asymmetry of the network, with a consequent increase in the neutral-to-ground voltage [62]. Then, a homogeneous DG could, as in this case, reduce the power absorption difference between the three conductors of a LV line, reducing voltage asymmetry and neutral-to-ground voltage.

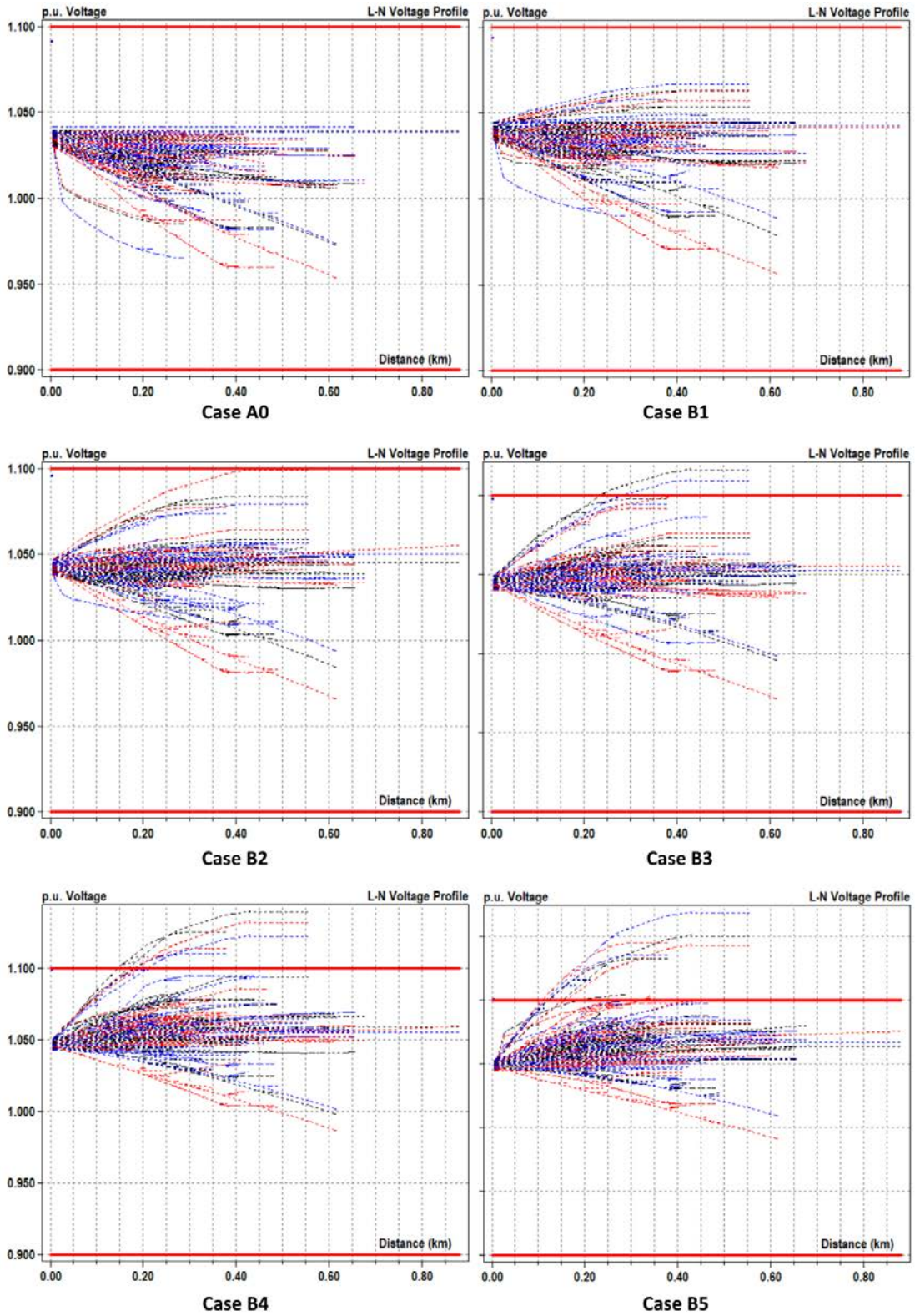

***Figure 4-16**. Voltage against distance profile of the network at hour 13.00 on PV implemented cases.*

As expected, with the increase in PVDG penetration, the voltage profile changes from the typical shape of a passive network – which refers to case A0 – to a more symmetrical one along the voltage axis in cases B2 and B3. Furthermore, in cases B3 to B5 the maximum voltage limit is largely exceeded by a few peculiar LV lines. These lines are connected to transformer 21 that has a great PV generation but

no-load consumption[17]. The case of transformer 21 cannot be considered commensurable to a real grid and consequently its lines are not considered reliable. However, real cases in which a portion of the network is only injecting energy – with low or zero power absorption – could uncommonly happen. Then, this situation should be avoided while networks are designed with high PV penetration.

In cases B4 and B5, other LV lines reach values close or above the maximum voltage limit. To reduce the overvoltage of the lines – and so, to partially solve the problem – voltage at the substations could be reduced with tap changers, bringing it back to around 1.0 pu. This results in a vertical translation of the voltage profile. The operation must however always comply with the network standards – with some safety limit consideration – especially considered the hour of heaviest load, which has already been referred in *Figure 4-10*.

Furthermore, the situation considered refers to a sunny spring/autumn day, which has different generation and load profiles in respect to winter or summer periods. The substations voltage should then be chosen wisely, and a high PVDG penetrated network could need an OLTC (On-Load Tap Changer) transformer to fulfill its needs.

4.4 Cases C1 and C2: Simulations with EV Load Implementation

In simulation cases C1 and C2, loads representing PEV charging stations – both 1-phase (Slow Charge) and 3-phase (Quick Charge) typologies – have been implemented throughout the network. In each of the two cases, a 15% EV penetration on the base energy absorption of the network is implemented, comprehensive of 300 Slow Charge connection points and 40 Quick Charge stations. The criteria whereby the loads are implemented have been discussed in section 4.1.3, while *Table 4-6* summarizes the main characteristics of the two cases.

***Table 4-6**. EV charging stations installed for PV study cases.*

	PV Pen. [%]	EV Pen. [%]	N. of Slow Charge stations	N. of Quick Charge stations
Case C1	**0** (0.00)	**15** (14.96)	300	40
Case C2	**100** (99.97)	**15** (14.96)	300	40

As shown in table, case C1 has no PV generation plants, case C2 instead analyses the EV charging contribution on a network with 100% PV penetration (as for case B5).

No other PV penetrated case have been chosen to be represented with EV loads because the large mismatch between PV and EV daily curves allows to study the two implementations separately. This can be observed in *Figure 4-17*, where the active energy absorbed by the whole network at the MV transformers side is shown. The EV charging causes an increase in the power absorption peak of hour 22.00 and the overall power absorption between hours 18.00 and 7.00. Therefore, it increases the energy consumption daily swing. Instead, the PV generation implemented in case C2 affects only the network power during daylight hours which are not affected by EV charging, except for a circumstantial influence at hours 6.00 and 7.00 during the morning and hours 18.00 to 20.00 during the evening.

[17] In fact, every load connected to that transformer has a null energy absorption, probably because that network branch supplies a new residential area still not commissioned.

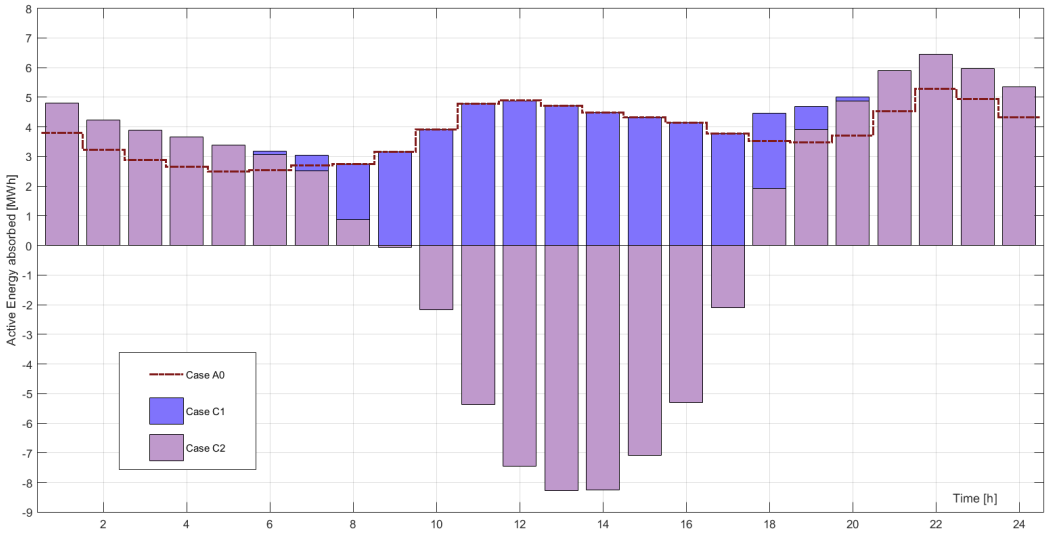

***Figure 4-17**. Aggregated energy consumption of the network during the day on EV implemented cases.*

Following, *Table 4-7* presents the overall power production, absorption, and losses within the grid. As expected, when compared to case A0, case C2 has an increase in power losses of **0.10%**. Instead, it is observable a slight improvement in power losses from case B2 to case C2.

***Table 4-7**. Power production, absorption, and losses for each EV case of study.*

	W_{tr} [MWh]	W_{PV} [MWh]	W_{tot} [MWh]	W_{base} [MWh]	W_{EV} [MWh]	W_{load} [MWh]	W_{loss} [MWh]	$W_{loss\%}$ [%]
Case A0	90.9	0	90.9	89.8	0	89.8	1.16	**1.28**
Case C1	104.8	0	104.8	89.8	13.6	103.4	1.45	**1.38**
Case C2	14.7	90.9	105.6	89.8	13.6	103.4	2.25	**2.13**

4.4.1 Transformer Loading Factor

As before, *Figure 4-18* and *Figure 4-19* show the apparent power flow through transformer 4 and its loading factor during the simulated day.

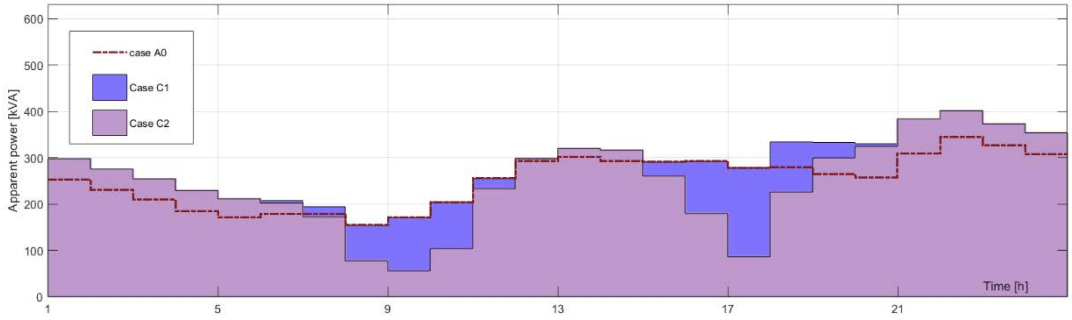

***Figure 4-18**. Apparent power of transformer 4 (MV side) during the day on EV implemented cases.*

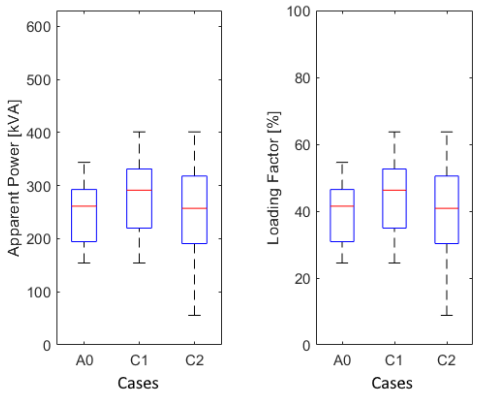

***Figure 4-19**. Apparent power (left) and loading factor (right) of transformer 4 during the day. EV cases.*

The increase of the power peak (at hour 22.00) and the overall increase in the power absorption strongly influence the transformer loading factor. In fact, the maximum loading factor reached by the transformer amount to **63.7%** (401 kVA) for both case C1 and C2, which is **+9.1%** compared to case A0. In regard to the median loading factor, it slightly worsens in case C1 (+4.8%) to drop once again to almost the previous value in case C2.

4.4.2 Line Voltage Drop

Bus *850* is studied again for cases C1 and C2 and its voltage represented in *Figure 4-20*. *(a)* represents its phase-to-neutral voltage and *(b)* its neutral-to-ground voltage through the day.

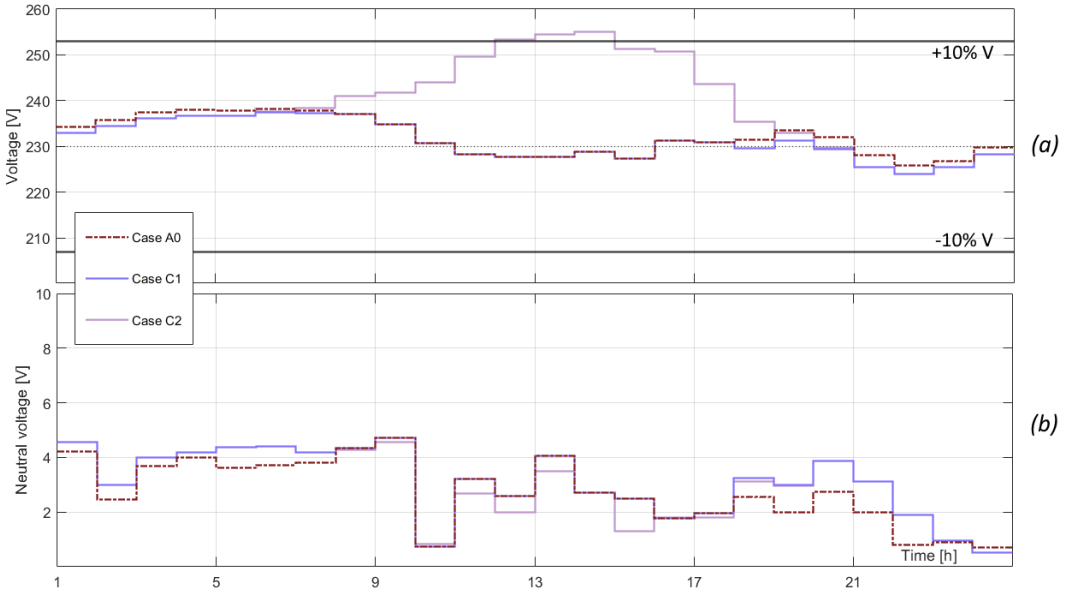

***Figure 4-20**. Bus 850 voltage daily profile on EV implemented cases. (a) phase-to-neutral. (b) neutral-to-ground.*

It can be observed that case C2 is not only affected by the overvoltage caused by PV generation excess, but also by a heavier evening voltage drop. Therefore, with a further increase in EV penetration the action of a Tap Changer could be unpracticable or done with unsafe margin.

A wider analysis of the voltage drop conditions of the network is shown in *Figure 4-21*, where the voltage against distance profiles of cases A0 and C2 are represented for every conductor at hour 22.00[18].

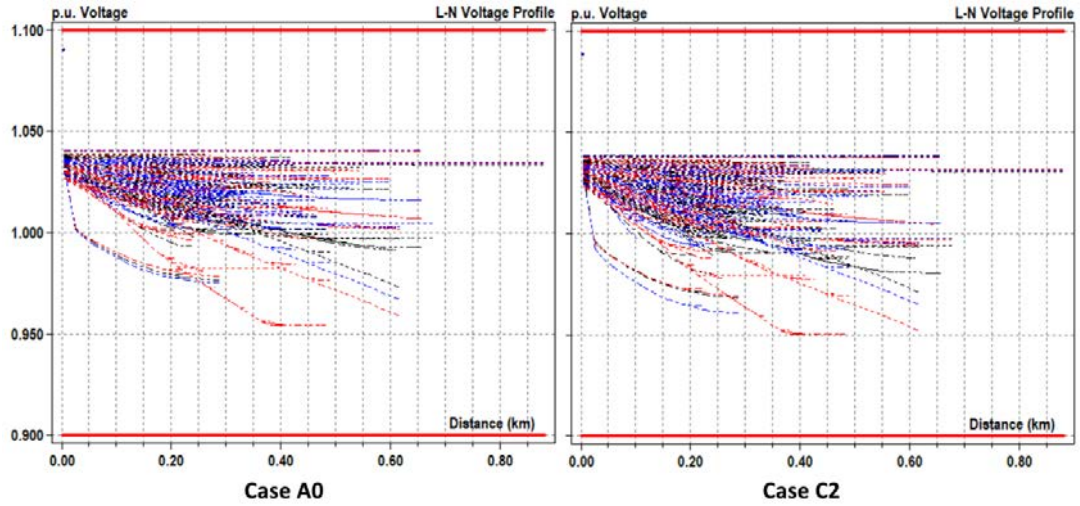

***Figure 4-21**. Voltage against distance profile of the network at hour 22.00 on EV implemented cases.*

Because of the EV loads absorbing energy during the evening, the whole network has increased voltage drops, with a maximum value of **0.95 pu**. These drops are still within the voltage limits. Then, the network can largely hold the implementation of these new EV loads, even with heavier penetrations, provided a not more than moderate PV penetration.

4.5 Results

In conclusion, the behavior of the simulated network – studied at the variation of PV and EV penetrations – widely complies with the literature presented in Chapter 2.

Assuming a moderate power injection, the PV distributed generators implemented in the grid strongly reduces the power flow during midday hours. Case B2 allows an almost zero flow of energy at the transformers from hour 10.00 to 16.00, due to the local energy production-consumption cycle. Consequently, the power losses are reduced by **-0.21%** – which means -190 kW – in respect to the original case A0. Heavier PV penetration cases (B3-B5) cause instead a strong inversion of power which implies a worsening of the loss factor, while further load compensation in the grid is marginal. The mismatch between PV generation and the load curve is accentuated by the implementation of the PEV charging stations, which absorb power during evening and night and increase the maximum evening load peak of hour 22.00.

Therefore, the network daily power flow assumes a 'duck-curve' shown in *Figure 4-22* similar to the one described previously in section 2.3.3. The graph highlights the mismatching phenomenon by representing the daily active power of the following cases:

- case A0, as the baseload,
- case B5, which satisfy the Net Zero Energy condition through PV implementation,
- case C1, which adds EV consumption to the baseload,
- case C2, which adds EV consumption to case B5.

[18] Because of the absence of PV generation at hour 22.00, profiles C1 and C2 are equal and represented with only one graph.

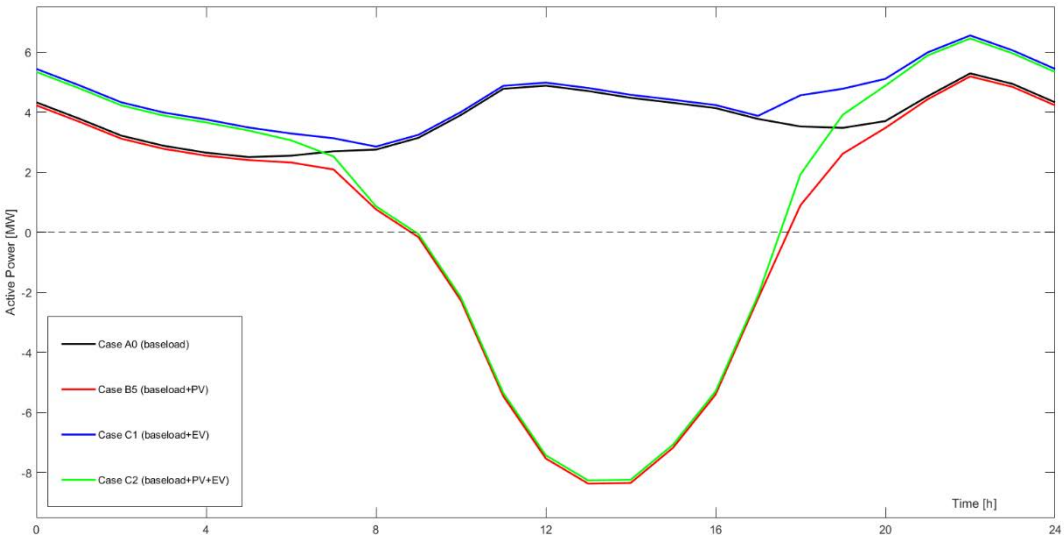

***Figure 4-22**. Load 'duck-curve' due to PV and EV mismatch.*

This power daily curve compels transformers and lines to work on strongly variable conditions, with power flowing in both directions through the network and consequent large voltage ripple. Having a wide voltage daily range increases the risk of exceeding the standard voltage limits, and even if the transformer voltage is properly modified with a tap changer, the network would allow a less safety margin.

In the simulation emerged also the problem of some LV lines which have connected a vast majority of PV plants in relation to their loads. These lines have high generation peaks with voltages that extend much over the standard limit of +10% on the base voltage (230 V). Although not common, these limit cases should also be considered in a high PV penetrated network.

Figure 4-23 shows the two worse voltage conditions of case C2 during the day. The left graph represents hour 13.00 of the day, which is the time of maximum generation, the right one instead represents hour 22.00, which is the time of maximum power absorption.

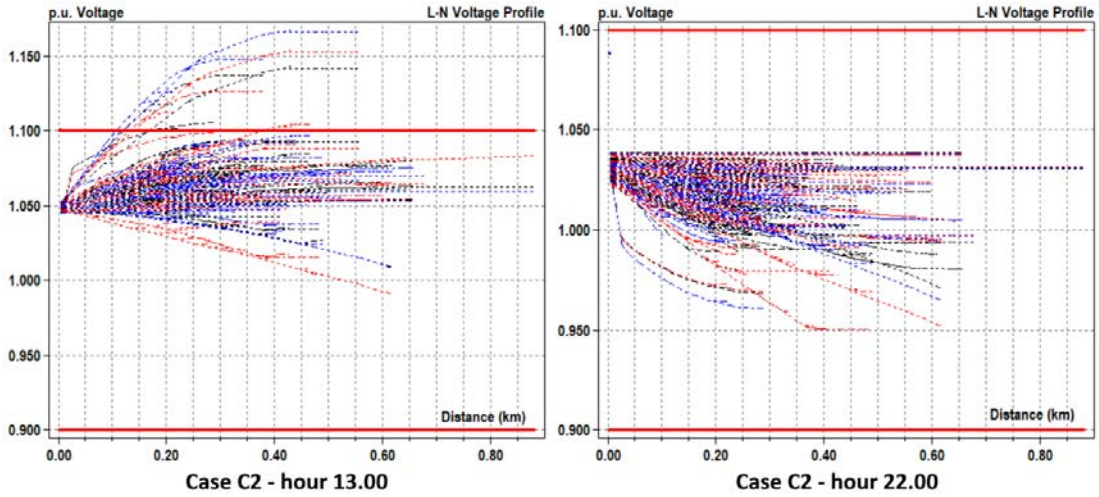

***Figure 4-23**. Voltage against distance profiles of case C2 at hour 13.00 (left) and hour 22.00 (right).*

As discussed above, in the left image are immediately observable the LV lines with heavy PV generation that extend their voltage values much over the limit. In the right graphic the voltage drop fall to 0.95 pu. Then, without a proper control, the network of case C2 is completely unsustainable in regard to the daily voltage variations.

Due to PV generation, the active power at transformers can flow in both direction, depending on the hour, but on the other way, the reactive power is only supplied by the MV network and constantly injected to satisfy lines and loads requests.

Even in heavy conditions scenarios, the transformers seem to handle quite well the flowing of power due to their oversizing. However, in *Figure 4-24* are represented the loading factors of case C1 *(a)* and case C2 *(b)*. Then, it is evident that transformer 8 exceeds its rated power during hours of maximum generation, as well as transformers 5 and 12 which reach critical values. On the contrary, the EV penetration is accepted without any problem by the network.

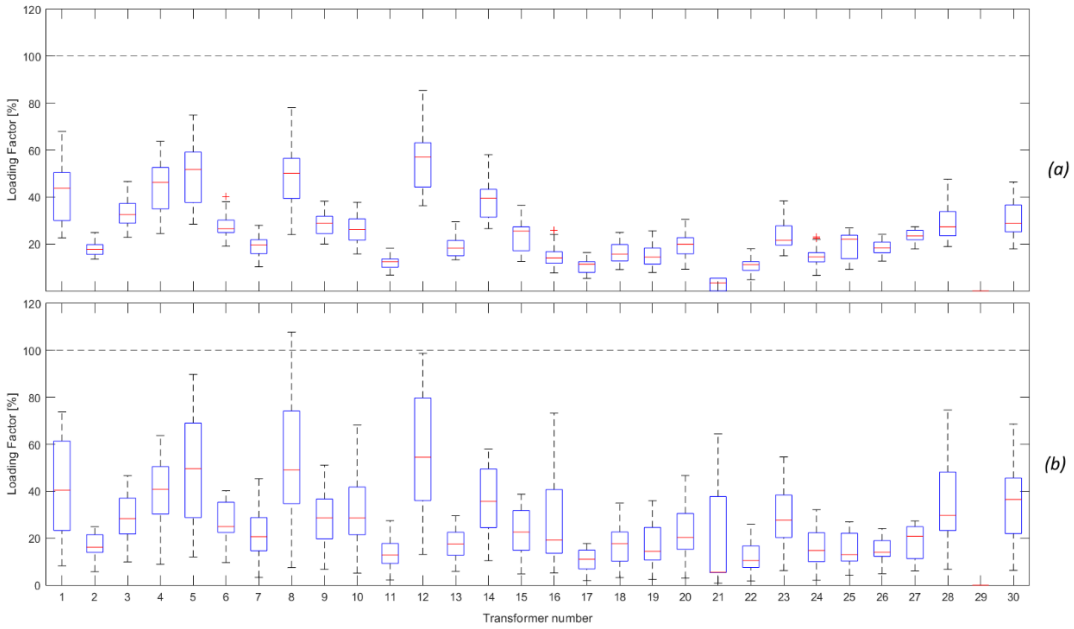

***Figure 4-24**. Loading factor of the substation transformers during the day. (a) case C1. (b) case C2.*

However, the working conditions of substation transformers gets inexorably worse both for high PV penetration (cases B4 and B5) and EV implementation. As seen in figure, maximum loading factor values increase as well as minimum values decrease (in respect to case A0 – *Figure 4-8*), whilst the medians stay about the same. Therefore, lifetime of each transformer could be affected, and the consequences of wider working conditions should be considered. Cases B4 and B5 should then be avoided.

5 Conclusions and Future Works

5.1 Conclusions

The GOCT has proven to be a powerful tool that allows researchers to work on existing networks. Clearly, the test system proposed, is an exceptional product of the GOCT. With an entire understanding of the tool, its modularity facilitates the system modification according to the researchers' needs. Further, the MATLAB interface can subsequently elaborate the OpenDSS network results to achieve (for example) better graphical representations. Furthermore, the tool can also be used to simulate alternative scenarios by implementing synthetic elements, as presented in Chapter 4.

In fact, this work proves once more that a moderated PVDG implementation applied to a residential LV network – up to around 40% penetration on the base energy consumption – widely improves the grid conditions. An evident effect is the reduction in active power energy delivered from the MV network, which causes a consequent reduction in substations average loading factor, as well as a decrease in power losses and a flattening of the voltage depression through LV lines. A higher PV penetration instead causes overvoltage in lines, transformers average and maximum loading factor increases, as well as strong inconstancy of power and voltage throughout the day.

PEV charging stations – both Slow and Quick, with a 15% penetration on the base energy consumption – can be totally implemented without heavy impact on the network. The charging happens concurrently with the evening load peak causing an increment of the maximum power absorption and transformer loading factor. The EV consumption is almost independent from the PV generation due to the strong mismatch between the two curves. Consequently, PVs cannot smooth out EV contribution to the load curve without an electric storage system or a shift in the EV curve through a regulated charging system. Then, a further increase in EV penetration can be accepted only with a different resolutive measure, and which offers an interesting future research topic.

5.2 Future Works

The PV and EV curves employed in this work are plausible synthetic shapes, and their values have been obtained from reliable studies [27, 61]. However, they lack statistical dissimilarity, which is necessary to have realistic curves. For more reliable solutions, more complex and accurate algorithms should then be implemented, or else the curve values could be taken from smart meter sampling, consistent with the approach adopted for consumer loads.

The increase in the MV/LV substation loading factor – brought to 70% at transformer 12 – has been done to reach a more stressful condition, aligned to the typical European network situation and consistent with the approach adopted by Koirala *et al.* in their article. However, the discrepancy between what is stated and what is sampled in the article is strong and further studies concerning the European LV network loading should be carried out.

The following, are some valuable research topics that could be of interest in future works.

First, GOCT should be applied to data packages from other DSOs to verify its versatility and to provide variety of networks. Non-synthetic systems are suitable to test network regulation algorithms, such as regulated PEV charging or PV mitigation methods, whose development is of primary importance for the future grid.

The injection of harmonics due to DC/AC static conversion of PVs and EVs must still be evaluated to verify the network penetrability, before reaching unacceptable THD values. Another significant concern associated with the increase in their penetration, is the rate of change (the slope) associated with power and voltage curves during the day. Understanding the implications and the actual technological restraints is important to define another limit concerning the PVDG and EV penetration within the grid, and possibly overcome it.

At last, more in-depth studies in regard to the European earthing systems should be carried out. In this way, more faithful earthing representations can be built, allowing more reliable studies on the NEV behavior in presence of 1-phase PV plants.

In conclusion, DSOs – which own the electrical and geographical data to exploit the GOCT – will play a very important role in the future grid management. It is expected that this kind of tool will become of significant importance, allowing them a new strategic way to design the grid accordingly to their real installation conditions, and further leading one step closer to the realization of smart grid technology.

Acknowledgement

Thinking about my long university path, I feel astonished by how time seems to be passed in few moments. Our intrinsic ability to narrow down the past years and pack them into a few important moments insinuates me with the desire to thank those who spent these moments with me.

It's been over a year since I spent my (short) experience in Dublin. I would like to infinitely thank Dr. Keith Sunderland who followed the development of my work well after the end date of the Erasmus project. It is thanks to his presence that I feel extremely proud of the results achieved.

I warmly thank Alessandra, who in this same year has always been by my side, allowing me to live this difficult period with more serenity.

Almost 3 years have passed since I met my awesome fellows: Chiara, Alessandro, Noah and finally Chiara again. You have been my pillars during these last university years!

It's been over 5 years since my university life started! And I want to thank Anna with affection, who in turn introduced me to other beautiful people, including dear Silvio, the only loyal who faced the roughness of this electric path from the beginning to the end.

Ten years have passed since I met Lorenzo and Marco thanks to Scouting. Friendships that are now stronger than ever, despite the passing of time. Thinking back to the past my heart tightens, as I would like to thank many people, some still close, others now distant, but for reasons of space it is not possible for me to name all of you.

Finally, I would like to deeply thank my brother and Silvia, my parents, my uncles and aunts, my cousins, and my grandparents for being my wonderful family. Thanks, as I could not wish for better.

Ringraziamenti

Ripensando a questo mio lungo percorso di studi universitari, rimango tutt'oggi sorpreso da come il tempo sembri in realtà trascorso in pochi istanti. La nostra intrinseca capacità di restringere gli anni passati e confezionarli in pochi importanti momenti mi insinua il desiderio di ringraziare chi questi momenti li ha trascorsi con me.

È infatti passato ormai oltre un anno da quando ho trascorso la mia (breve) esperienza a Dublino. Ci tengo infinitamente a ringraziare il Dr. Keith Sunderland che ha seguito lo svolgimento di questo mio lavoro ben oltre la data di conclusione del progetto Erasmus. È grazie alla sua presenza che mi ritengo estremamente fiero dei risultati raggiunti.

Ringrazio con affetto Alessandra, che in questo stesso anno mi è stata sempre accanto, permettendomi di vivere con più serenità questo difficile periodo.

Sono passati quasi 3 anni da quando ho conosciuto i miei fantastici compagni: Chiara, Alessandro, Noah ed infine di nuovo Chiara. Siete stati la mia colonna portante durante questi ultimi anni universitari!

Sono passati oltre 5 anni da quando la mia vita universitaria è iniziata! E voglio con affetto ringraziare Anna, che a sua volta mi ha fatto conoscere altre bellissime persone, tra cui ci tengo a menzionare il carissimo Silvio, unico fedelissimo che ha affrontato con me le intemperie di questo percorso elettrico dall'inizio alla fine.

Dieci anni sono passati da quando ho conosciuto Lorenzo e Marco grazie allo Scautismo. Amicizie che ringrazio siano ora più solide che mai, nonostante il tempo. A ripensare al passato mi si stringe il cuore, poiché vorrei ringraziare moltissime persone, alcune tutt'ora vicine, altre ormai distanti, ma per motivi di spazio non mi è possibile nominarvi tutti e tutte. Grazie.

Infine, vorrei ringraziare profondamente mio fratello e Silvia, i miei genitori, i miei zii e le mie zie, le mie cugine ed i miei nonni per essere la mia stupenda famiglia. Grazie, poiché non potrei desiderare di meglio.

Appendix A

B2_Photovoltaics.m script, implemented in the Chapter 4 simulation, is entirely reported here. In this case, a PV penetration of 40% has been defined by line 1 variable '*PVpen*'.

```
1   -  PVpen=0.40;                              %PV penetration level desired [%]
2
3   -  TOTbaseenergy=90926.0;                   %kWh during day 1
4   -  PVkWh=14.5;                              %PV kWh produced energy
5   -  nPV=floor(PVpen*TOTbaseenergy/PVkWh)     %number of 3kW photovoltaics
6
7      %% PVloadshape_ind
8
9   -  OutDir  = [pwd filesep 'RunDss' filesep];
10  -  MatDir = [pwd filesep 'mat' filesep];
11
12  -  pvshape = fopen([OutDir 'PV_Loadshape.txt'],'w');
13  -  mytext=('New Loadshape.PVshape_3kw npts=481
         minterval=60mult=(file=PVePHEV\\PVshape_3kw.csv) useactual=true\r\n');
14  -  fprintf(pvshape,mytext);
15
16  -  fclose(pvshape);
17
18     %% PV_indexed
19
20  -  GetRandPhase(0);    %Reset random number genrator;
21  -  OutDir  = [pwd filesep 'RunDss' filesep];
22
23  -  pvind1=fopen([OutDir 'PV_indexed.txt'], 'w');
24  -  pvmarker=fopen([OutDir 'PV_BusMarker.txt'], 'w');
25
26  -  pvphaseerror=fopen([OutDir 'PV_error_phasemissing.txt'],'w');
27  -  pvacometidaserror=fopen([OutDir 'PV_ac_error.txt'],'w');
28  -  errortext_phase='%s  %s  phase missing random phase=%d \r\n';
29  -  erracc='%s  %s  acometidasmissing \r\n';
30
31  -  n_load=size(load_loc);
32  -  n_load=n_load(1);
33
34  -  n_loadbus=size(loadbus);
35  -  n_loadbus=n_loadbus(1);
36  -  size_phase_raw=size(phaseraw);
37  -  size_phaseraw=size_phase_raw(1);
38  -  PVbus1=zeros(n_load,1);
39  -  PVbus1_new=zeros(nPV,3);
40  -  myloadtext_1ph='New Generator.PV%d Phases=1 Bus1=%d.%d.4 kV=0.23 kW=1 PF=1
         daily=PVshape_3kw\r\n';
41  -  myloadtext_3ph='New Generator.PV%d Phases=3 Bus1=%d.1.2.3.4 kV=0.4 kW=1 PF=1
         daily=PVshape_3kw\r\n';
42  -  myloadtext_neg='!New Generator.PV%d Phases=1 Bus1=%d.%d.4 kV=0.23 kW=1 PF=1
         daily=PVshape_3kw\r\n';
43  -  myloadtext_3phneg='!New Generator.PV%d Phases=3 Bus1=%d.1.2.3.4 kV=0.4 kW=1 PF=1
         daily=PVshape_3kw\r\n';
44  -  myPVmarker='AddBusMarker Bus=%d code=5 color=Red size=20\r\n';
45  -  load_ind=[];
46
47  -  PVcount=1;
48  -  PVnumb=n_load/nPV;
49  -  conn=[];
50  -  for temp=1:nPV
```

```
51  -      conn=[conn floor(temp*PVnumb)];
52  -  end
53
54  -  for i=1:nPV
55  -      t=conn(i);
56  -      if t==7900||t==8070
57  -      else
58  -          loc=find(any(load_loc(t,1)==loadbus(:,2),2));
59  -          if ~isempty(loc)
60  -              PVbus1(t)=loadbus(loc(1),3);%bus list
61
62  -          else
63  -              PVbus1(t)=0;
64  -              fprintf(pvacometidaserror,erracc,load_loc_raw{t+1,1},load_loc_raw{t+1,18});
65  -          end
66  -          phase=0;
67
68  -          l1=find(any(busindex_new(:,1)==PVbus1(t),2));
69  -          if length(l1)>1
70  -              l1=l1(1);
71  -          end
72              %checking phases of PV
73  -          if load_loc_raw{t+1,11}(1)=='M'
74  -              m=find(strcmp(load_loc_raw{t+1,1},phaseraw));
75  -              if length(m)==1
76  -                  if(phaseraw{m,2}=='R')
77  -                      phase=1;
78  -                  elseif(phaseraw{m,2}=='S')
79  -                      phase=2;
80  -                  elseif(phaseraw{m,2}=='T')
81  -                      phase=3;
82  -                  else
83  -                      phase=GetRandPhase();
84  -                      err = [' PV number ',num2str(t),' has random phase assigned. '];
85                          %disp(err)
86  -                      PVbus1_new(PVcount,4)=phase;
87  -                  end
88  -              elseif length(m)>1
89  -                  for c=1:length(m)
90  -                      if(phaseraw{m(c),2}=='R')
91  -                          phase=1;
92  -                          break;
93  -                      elseif(phaseraw{m(c),2}=='S')
94  -                          phase=2;
95  -                          break;
96  -                      elseif(phaseraw{m(c),2}=='T')
97  -                          phase=3;
98  -                          break;
99  -                      end
100 -                  end
101 -              end
102 -              if phase==0
103 -                  phase = GetRandPhase();
104 -       fprintf(pvphaseerror,errortext_phase,load_loc_raw{t+1,1},load_loc_raw{t+1,20},phase);
105 -                  err = [' PV number ',num2str(t),' has random phase assigned. '];
106                     %disp(err)
107 -                  PVbus1_new(PVcount,4)=phase;
108 -              end
109
110 -              if isempty(l1)
111 -                  fprintf(pvind1,myloadtext_neg,t,0,phase);
112 -              else
113 -                  fprintf(pvind1,myloadtext_1ph,t,busindex_new(l1,5),phase);
```

```
114 -                 fprintf(pvmarker,myPVmarker,busindex_new(l1,5));
115 -                 PVbus1_new(PVcount,1)=t;
116 -                 PVbus1_new(PVcount,2)=busindex_new(l1,5);
117 -                 PVbus1_new(PVcount,3)=1;
118 -             end
119
120 -         else
121 -             if isempty(l1)
122 -                 fprintf(pvind1,myloadtext_3phneg,t,0);
123 -             else
124 -                 fprintf(pvind1,myloadtext_3ph,t,busindex_new(l1,5));
125 -                 fprintf(pvmarker,myPVmarker,busindex_new(l1,5));
126 -                 PVbus1_new(PVcount,1)=t;
127 -                 PVbus1_new(PVcount,2)=busindex_new(l1,5);
128 -                 PVbus1_new(PVcount,3)=3;
129 -             end
130 -         end
131
132 -         PVcount=PVcount+1;
133 -     end
134 - end
135 -
136 - PVcount=PVcount-1
137 - TruePVpen=PVkWh*PVcount/TOTbaseenergy   %real PV penetration level
138 - save([MatDir 'PVbus1_new.mat'], 'PVbus1_new')
139
140 - fclose(pvacometidaserror);
141 - fclose(pvphaseerror);
142 - fclose(pvind1);
143 - fclose(pvmarker);
```

Appendix B

B3_ElectricVehicles.m script was also implemented in Chapter 4 simulation and is reported here. The EV penetration chosen is 15%, as defined by line 1 variable '*EVpen*'.

```
1   -  EVpen=0.15;                        %EV penetration level desired [%]
2
3   -  TOTbaseenergy=90926.0;             %kWh during day-1
4   -  EVkWh=40;                          %EV kWh produced energy
5   -  nEV=floor(EVpen*TOTbaseenergy/EVkWh)%number of 40kWh vehicles
6
7      %% EVloadshape_ind
8
9   -  OutDir  = [pwd filesep 'RunDss' filesep];
10  -  MatDir = [pwd filesep 'mat' filesep];
11
12  -  evshape = fopen([OutDir 'EV_Loadshape.txt'],'w');
13  -  mytext_slow=('New Loadshape.EVshape_slow npts=481 minterval=60
         mult=(file=PVePHEV\\EVshape_slow.csv) useactual=true\r\n');
14  -  mytext_quick=('New Loadshape.EVshape_quick npts=481 minterval=60
         mult=(file=PVePHEV\\EVshape_quick.csv) useactual=true\r\n');
15  -  fprintf(evshape,mytext_slow);
16  -  fprintf(evshape,mytext_quick);
17
18  -  fclose(evshape);
19
20     %% EV_indexed
21
22  -  GetRandPhase(0);    %Reset random number genrator;
23  -  OutDir  = [pwd filesep 'RunDss' filesep];
24
25  -  evind1=fopen([OutDir 'EV_indexed.txt'], 'w');
26  -  evmarker=fopen([OutDir 'EV_BusMarker.txt'], 'w');
27  -  evphaseerror=fopen([OutDir 'EV_error_phasemissing.txt'],'w');
28  -  evacometidaserror=fopen([OutDir 'EV_ac_error.txt'],'w');
29  -  errortext_phase='%s  %s  phase missing random phase=%d \r\n';
30  -  erracc='%s  %s  acometidasmissing \r\n';
31
32  -  n_load=size(load_loc);
33  -  n_load=n_load(1);
34
35  -  n_loadbus=size(loadbus);
36  -  n_loadbus=n_loadbus(1);
37  -  size_phase_raw=size(phaseraw);
38  -  size_phaseraw=size_phase_raw(1);
39  -  EVbus1=zeros(n_load,1);
40  -  EVbus1_new=zeros(nEV,3);
41  -  myloadtext_1ph='New Load.EV%d Phases=1 Bus1=%d.%d.4 kV=0.23 kW=1 PF=0.98
         daily=EVshape_slow\r\n';
42  -  myloadtext_3ph='New Load.EV%d Phases=3 Bus1=%d.1.2.3.4 kV=0.4 kW=1 PF=0.95
         daily=EVshape_quick\r\n';
43  -  myloadtext_neg='!New Load.EV%d Phases=1 Bus1=%d.%d.4 kV=0.23 kW=1 PF=0.98
         daily=EVshape_slow\r\n';
44  -  myloadtext_3phneg='!New Load.EV%d Phases=3 Bus1=%d.1.2.3.4 kV=0.4 kW=1 PF=0.95
         daily=EVshape_quick\r\n';
45  -  myEVmarker='AddBusMarker Bus=%d code=3 color=Blue size=20\r\n';
46  -  load_ind=[];
47
48  -  EVcount=1;
49  -  SLOW=0;
```

```
QUICK=0;
EVnumb=n_load/nEV;
conn=[];
for temp=1:nEV
    conn=[conn floor(temp*EVnumb)];
end

for i=1:nEV
    t=conn(i);
    if t==7900||t==8070
    else
        loc=find(any(load_loc(t,1)==loadbus(:,2),2));
        if ~isempty(loc)
            EVbus1(t)=loadbus(loc(1),3);%bus list

        else
            EVbus1(t)=0;
            fprintf(evacometidaserror,erracc,load_loc_raw{t+1,1},load_loc_raw{t+1,18});
        end
        phase=0;

        l1=find(any(busindex_new(:,1)==EVbus1(t),2));
        if length(l1)>1
            l1=l1(1);
        end
        %checking phases of EV
        if load_loc_raw{t+1,11}(1)=='M'
            m=find(strcmp(load_loc_raw{t+1,1},phaseraw));
            if length(m)==1
                if(phaseraw{m,2}=='R')
                    phase=1;
                elseif(phaseraw{m,2}=='S')
                    phase=2;
                elseif(phaseraw{m,2}=='T')
                    phase=3;
                else
                    phase=GetRandPhase();
                    err = [' PV number ',num2str(t),' has random phase assigned. '];
                    %disp(err)
                    EVbus1_new(EVcount,4)=phase;
                end
            elseif length(m)>1
                for c=1:length(m)
                    if(phaseraw{m(c),2}=='R')
                        phase=1;
                        break;
                    elseif(phaseraw{m(c),2}=='S')
                        phase=2;
                        break;
                    elseif(phaseraw{m(c),2}=='T')
                        phase=3;
                        break;
                    end
                end
            end
            if phase==0
                phase = GetRandPhase();
     fprintf(evphaseerror,errortext_phase,load_loc_raw{t+1,1},load_loc_raw{t+1,20},phase);
                err = [' EV number ',num2str(t),' has random phase assigned. '];
                %disp(err)
                EVbus1_new(EVcount,4)=phase;
            end

```

```
113 -              if isempty(l1)
114 -                  fprintf(evind1,myloadtext_neg,t,0,phase);
115 -              else
116 -                  fprintf(evind1,myloadtext_1ph,t,busindex_new(l1,5),phase);
117 -                  fprintf(evmarker,myEVmarker,busindex_new(l1,5));
118 -                  EVbus1_new(EVcount,1)=t;
119 -                  EVbus1_new(EVcount,2)=busindex_new(l1,5);
120 -                  EVbus1_new(EVcount,3)=1;
121 -                  SLOW=SLOW+1;
122 -              end
123 
124 -          else
125 -              if isempty(l1)
126 -                  fprintf(evind1,myloadtext_3phneg,t,0);
127 -              else
128 -                  fprintf(evind1,myloadtext_3ph,t,busindex_new(l1,5));
129 -                  fprintf(evmarker,myEVmarker,busindex_new(l1,5));
130 -                  EVbus1_new(EVcount,1)=t;
131 -                  EVbus1_new(EVcount,2)=busindex_new(l1,5);
132 -                  EVbus1_new(EVcount,3)=3;
133 -                  QUICK=QUICK+1;
134 -              end
135 
136 -          end
137 -          EVcount=EVcount+1;
138 -      end
139 -  end
140 
141 -  EVcount=EVcount-1
142 -  SLOW                                  %display number of slow charge stations
143 -  QUICK                                 %display number of quick charge stations
144 -  TrueEVpen=EVkWh*EVcount/TOTbaseenergy   %real EV penetration level
145 -  save([MatDir 'EVbus1_new.mat'], 'EVbus1_new')
146 
147 -  fclose(evacometidaserror);
148 -  fclose(evphaseerror);
149 -  fclose(evind1);
150 -  fclose(evmarker);
```

References

[1] R. C. Green, L. Wang, and M. Alam. "The impact of plug-in hybrid electric vehicles on distribution networks: a review and outlook". Energy Society General Meeting. Minneapolis, MN, USA. 25-29 July, 2010.

[2] R. Fachrizal, M. Shepero, D. van der Meer, J. Munkhammar, and J. Widén. "Smart charging of electric vehicles considering photovoltaic power production and electricity consumption: A review". *eTransportation* 4. 2020.

[3] K. N. Nwaigwe, P. Mutabilwa, and E. Dintwa. "An overview of solar power (PV systems) integration into electricity grids". *Materials Science for Energy Technologies* 2, 3. 2019.

[4] B. Parida, S. Iniyan, and R. Goic. "A review of solar photovoltaic technologies". *Renewable and Sustainable Energy Reviews* 15, 3. 2011.

[5] M. Emmanuel, R. Rayudu, and I. Welch. "Grid incremental capacity evaluation with an optimally deployed photovoltaic system in distribution network". IEEE. 2017.

[6] R. Singh, P. Tripathi, and K. Yatendra. "Impact of Solar Photovoltaic Penetration In Distribution Network". 3rd International Conference on Recent Developments in Control, Automation & Power Engineering (RDCAPE). Noida, India. 10-11 October, 2019.

[7] T. Wang, M. Meskin, Y. Zhao, and I. Grinberg. "Optimal power flow in distribution networks with high penetration of photovoltaic units". IEEE Electrical Power and Energy Conference (EPEC). Saskatoon, SK. 22-25 October, 2017.

[8] M. M. Al Shammari and W. Ko. "Photovoltaic-Based Distribution Generation System Integration Effects on the Power Quality Issues on Electrical Distribution Network". IEEE. 2019.

[9] M. E. Khodayar, M. R. Feizi, and A. Vafamehr. "Solar photovoltaic generation: Benefits and operation challenges in distribution networks". *The Electricity Journal* 32, 4. 2019.

[10] A. Orioli and A. Di Gangi. "Load mismatch of grid-connected photovoltaic systems: Review of the effects and analysis in an urban context". *Renewable and Sustainable Energy Reviews* 21. 2013.

[11] D. H. Popović, J. A. Greatbanks, M. Begović, and A. Pregelj. "Placement of distributed generators and reclosers for distribution network security and reliability". *International Journal of Electrical Power & Energy Systems* 27, 5-6. 2005.

[12] M. Mes, G.M.A. Vanalme, J.M.A. Myrzik, M. Bongaerts, G.J.P. Verbong, and W. L. Kling. "Distributed generation in the Dutch LV network - self-supporting residential area -". 43rd International Universities Power Engineering Conference (UPEC). Padova, Italy. 1-4 September, 2008.

[13] C. Debruyne, J. Desmet, J. Vanalme, B. Verhelst, G. Vanalme, and L. Vandevelde. "Maximum power injection acceptance in a residential area". International Conference on Renewable Energies and Power Quality. Granada, Spain. 23 - 25 March, 2010.

[14] P. Prakash and D. K. Khatod. "Optimal sizing and siting techniques for distributed generation in distribution systems: A review". *Renewable and Sustainable Energy Reviews* 57. 2016.

[15] X. Ren, J. Dong, Z. Wang, J. Wang, Y. Xing, R. Wang, and W. Liu. "Simulation method for voltage control and system development of a distribution network with large-scale photovoltaic". IEEE Conference on Energy Internet and Energy System Integration (EI2). Beijing, China. 26-28 November, 2017.

[16] K. Clement-Nyns, E. Haesen, and J. Driesen. "The Impact of Charging Plug-In Hybrid Electric Vehicles on a Residential Distribution Grid". *IEEE Transactions on Power Systems* 25, 1. 2010.

[17] M. R. Khalid, M. S. Alam, A. Sarwar, and M. S. Jamil Asghar. "A Comprehensive review on electric vehicles charging infrastructures and their impacts on power-quality of the utility grid". *eTransportation* 1. 2019.

[18] A. Bosovic, M. Music, and S. Sadovic. "Analysis of the impacts of plug-in electric vehicle charging on the part of a real low voltage distribution network". IEEE Eindhoven PowerTech. Eindhoven, Netherlands. 29 June - 2 July, 2015.

[19] D. Cai, W. Wang, X. Ma, M. Xu, Z. He, Z. Tang, C. Zhou, N. Han, and Y. Wang. "Analysis of Heavy Load and Overload Distribution Transformer in Regional Power Grid". 2nd IEEE Conference on Energy Internet and Energy System Integration (EI2). Beijing, China. 20-22 October, 2018.

[20] K. P. Schneider, B. A. Mather, B. C. Pal, C.-W. Ten, G. J. Shirek, H. Zhu, J. C. Fuller, J. L. R. Pereira, L. F. Ochoa, L. R. de Araujo, R. C. Dugan, S. Matthias, S. Paudyal, T. E. McDermott,

and W. Kersting. “Analytic Considerations and Design Basis for the IEEE Distribution Test Feeders”. *IEEE Transactions on Power Systems* 33, 3. 2018.
[21] R. C. Dugan, W. H. Kersting, S. Carneiro, R. F. Arritt, and T. E. McDermott. “Roadmap for the IEEE PES test feeders”. IEEE/PES Power Systems Conference and Exposition (PSCE). Seattle, WA, USA. 15-18 March, 2009.
[22] A. Koirala, L. Suárez-Ramón, B. Mohamed, and P. Arboleya. “Non-synthetic European low voltage test system”. *International Journal of Electrical Power & Energy Systems* 118. 2020.
[23] D. Geibel, T. Degner, T. Reimann, B. Engel, T. Bülo, J. P. Da Costa, W. Kruschel, B. Sahan, and P. Zacharias. “Active intelligent distribution networks - coordinated voltage regulation methods for networks with high share of decentralised generation”. CIRED Workshop: Integration of Renewables into the Distribution Grid. Lisbon, Portugal. 29-30 May, 2012.
[24] S. Grijalva and M. U. Tariq. “Prosumer-based smart grid architecture enables a flat, sustainable electricity industry”. IEEE PES Innovative Smart Grid Technologies (ISGT). Anaheim, CA, USA. 17-19 January, 2011.
[25] G. Prettico, F. Gangale, A. Mengolini, A. Lucas, and G. Fulli. “Distribution System Operators Observatory”. *JRC Technical Reports*. Joint Research Centre. 2016.
[26] R. Calvas and B. Lacroix. “Earthing systems worldwide and evolutions”. *Cahier Technique* 173. 1995.
[27] S. Papathanassiou, N. Hatziargyriouand, K. Strunz. “A benchmark low voltage microgrid network”. CIGRE Symposium "Power Systems with Dispersed Generation". Athens, Greece. April, 2005.
[28] Wind Energy and Solar. Installed GW Capacity - Worlwide and by Country. http://www.fi-powerweb.com/Renewable-Energy.html. Accessed April 2020.
[29] Y. Amrane, A. A. Ladjici, M. Boudour, and M. Lamari. “Study of Photovoltaic Power Plant Distribution Network Integration: Case of Algeria-Djanet City Distribution Network”. IEEE. 2019.
[30] M. Khaterchi, J. Belhadj, and M. Elleuch. “Integration of Large-Scale Photovoltaic system in the distribution grid under partially shading”. International Conference on Electrical Sciences and Technologies in Maghreb (CISTEM). Tunis, Tunisia. 3-6 November, 2014.
[31] C. Pei, Q. Wang, Y. Zheng, G. Li, Z. Zheng, and J. Hao. “Research on Voltage Exceeding Limits of Active Distribution Network Caused by Distributed Photovoltaic”. 2nd IEEE Conference on Energy Internet and Energy System Integration (EI2). Beijing, China. 20-22 October, 2018.
[32] A. Zahedi. “A review of drivers, benefits, and challenges in integrating renewable energy sources into electricity grid”. *Renewable and Sustainable Energy Reviews* 15, 9. 2011.
[33] R. K. Varma and M. Salama. “Large-scale photovoltaic solar power integration in transmission and distribution networks”. Energy Society General Meeting. Detroit, MI, USA. 24-29 July, 2011.
[34] D. Q. Hung, N. Mithulananthan, and K. Y. Lee. “Determining PV Penetration for Distribution Systems With Time-Varying Load Models”. *IEEE Trans. Power Syst.* 29, 6. 2014.
[35] J. Wang, X. Zhu, D. Lubkeman, N. Lu, N. Samaan, and B. Werts. “Load Aggregation Methods for Quasi-Static Power Flow Analysis on High PV Penetration Feeders”. IEEE/PES Transmission and Distribution Conference and Exposition (T&D). Denver, CO, USA. 16-19 April, 2018.
[36] C. K. Gan, M. Shamshiri, and D. Pudjianto. “Integration of PV system into LV distribution networks with Demand Response application”. IEEE Eindhoven PowerTech. Eindhoven, Netherlands. 29 June - 2 July, 2015.
[37] V. Venizelou, S. Theocharides, G. Makrides, V. Efthymiou, and G. E. Georghiou. “Demand response for the promotion of photovoltaic penetration”. IEEE 44th Photovoltaic Specialists Conference (PVSC). Washington, DC, USA. 25-30 June, 2017.
[38] K. S. Ratnam, K. Palanisamy, and G. Yang. “Future low-inertia power systems: Requirements, issues, and solutions - A review”. *Renewable and Sustainable Energy Reviews* 124. 2020.
[39] J. García-Villalobos, I. Zamora, J. I. San Martín, F. J. Asensio, and V. Aperribay. “Plug-in electric vehicles in electric distribution networks: A review of smart charging approaches”. *Renewable and Sustainable Energy Reviews* 38. 2014.
[40] L. Dickerman and J. Harrison. “A New Car, a New Grid”. *IEEE Power and Energy Mag.* 8, 2. 2010.

[41] S. Habib, M. Kamran, and U. Rashid. “Impact analysis of vehicle-to-grid technology and charging strategies of electric vehicles on distribution networks – A review”. *Journal of Power Sources* 277. 2015.
[42] S. Satarworn and N. Hoonchareon. “Impact of EV home charger on distribution transformer overloading in an urban area”. 14th International Conference on Electrical Engineering/Electronics, Computer, Telecommunications and Information Technology (ECTI-CON). Phuket, Thailand. 27-30 June, 2017.
[43] J. Duan, Z. Li, Y. Zhou, and Z. Wei. “Study on the voltage level sequence of future urban DC distribution network in China: A Review”. *International Journal of Electrical Power & Energy Systems* 117. 2020.
[44] M. Shepero and J. Munkhammar. “Spatial Markov chain model for electric vehicle charging in cities using geographical information system (GIS) data”. *Applied Energy* 231. 2018.
[45] M. R. Islam, H. Lu, M. J. Hossain, and L. Li. “Mitigating unbalance using distributed network reconfiguration techniques in distributed power generation grids with services for electric vehicles: A review”. *Journal of Cleaner Production* 239. 2019.
[46] W. H. Kersting. “Radial distribution test feeders”. Winter Meeting of the IEEE Power Engineering Society. Columbus, OH, USA. 28 January -1 February, 2001.
[47] W. G. Sunderman, R. C. Dugan, and D. S. Dorr. “The neutral-to-earth voltage (NEV) test case and distribution system analysis”. Energy Society General Meeting. Pittsburgh, PA, USA. 20-24 July, 2008.
[48] W. H. Kersting. “A comprehensive distribution test feeder”. IEEE PES T&D. New Orleans, LA, USA. 19-22 April, 2010.
[49] R. F. Arritt and R. C. Dugan. “The IEEE 8500-node test feeder”. IEEE PES T&D. New Orleans, LA, USA. 19-22 April, 2010.
[50] K. Schneider, P. Phanivong, and J.-S. Lacroix. “IEEE 342-node low voltage networked test system”. IEEE Power & Energy Society General Meeting. National Harbor, MD, USA. 27-31 July, 2014.
[51] K. P. Schneider, Y. Chen, D. Engle, and D. Chassin. “A Taxonomy of North American radial distribution feeders”. Energy Society General Meeting (PES). Calgary, Canada. 26-30 July, 2009.
[52] Distributed PV Monitoring and Feeder Analysis. Electric Power Research Institute. https://dpv.epri.com/index.html. Accessed May 2020.
[53] EPRI Test Circuits. Electric Power Research Institute. http://svn.code.sf.net/p/electricdss/code/trunk/Distrib/EPRITestCircuits/. Accessed May 2020.
[54] IEEE PES Resources. IEEE PES AMPS DSAS Test Feeder Working Group. https://site.ieee.org/pes-testfeeders/resources/. Accessed May 2020.
[55] Y. Li and P. J. Wolfs. “Taxonomic description for western Australian distribution medium-voltage and low-voltage feeders”. *IET Generation, Transmission & Distribution* 8, 1. 2014.
[56] V. Rigoni, L. F. Ochoa, G. Chicco, A. Navarro-Espinosa, and T. Gozel. “Representative Residential LV Feeders: A Case Study for the North West of England”. *IEEE Trans. Power Syst.* 31, 1. 2016.
[57] F. Bu, Y. Yuan, Z. Wang, K. Dehghanpour, and A. Kimber. “A Time-Series Distribution Test System Based on Real Utility Data”. North American Power Symposium (NAPS). Wichita, KS, USA. 13-15 October, 2019.
[58] C. Mateo, G. Prettico, T. Gómez, R. Cossent, F. Gangale, P. Frías, and G. Fulli. “European representative electricity distribution networks”. *International Journal of Electrical Power & Energy Systems* 99. 2018.
[59] T. van Cutsem, J. A. Dos Santos, B. Tamimi, G. Taranto, C. Vournas, M. Glavic, W. Rosehart, C. Canizares, M. Kanatas, L. Lima, F. Milano, L. Papangelis, and R. A. Ramos. “Test Systems for Voltage Stability Studies: IEEE Task Force on Test Systems for Voltage Stability Analysis and Security Assessment”. *IEEE Trans. Power Syst.* 2020.
[60] OpenDSS User Manual. R. C. Dugan, D. Montenegro, and Electric Power Research Institute. http://svn.code.sf.net/p/electricdss/code/trunk/Distrib/Doc/. Accessed July 2020.
[61] J. Mies, J. Helmus, and R. van den Hoed. “Estimating the Charging Profile of Individual Charge Sessions of Electric Vehicles in The Netherlands”. *WEVJ* 9, 2. 2018.
[62] M. J. Alam, K. Muttaqi, and D. Sutanto. “Alleviation of neutral-to-ground potential rise under unbalanced allocation of rooftop pv using distributed energy storage”. *IEEE Transactions on Sustainable Energy* 6, 3. 2015.